CRANFIELD INSTITUTE OF TECHNOLOGY

School of Industrial and Manufacturing Science

PhD Thesis

Author : N.J.Tyler

INVESTIGATION OF A PIEZO-POLYMER ARRAY TRANSDUCER FOR PULSE-ECHO ULTRASONIC MATERIAL EXAMINATIONS

Supervisor: M.W.B.Lock

July 1992

BEST COPY

AVAILABLE

Variable print quality

To the Memory of my Father.

ACKNOWLEDGEMENTS

Many people have assisted me in the course of this research, and it therefore seems appropriate to acknowledge at least some of them.

I would particularly like to thank Dr. Mike Lock, who provided the initial concept of the array transducer, and whose continued interest and encouragement were invaluable at every stage of the project. I would also like to thank my colleague, Mick Smith, for many interesting and helpful discussions and suggestions on signal processing algorithms, and for allowing me to use his C-Scan equipment.

Thanks are also due to my colleagues at Nene College, especially Paul Richardson for his expert assistance in the chemistry laboratory.

The wide variety of PVdF materials provided by Atochem (prev. Pennwalt Piezo Films) formed an important part of the research, and thanks are also due to Flextronic (prev. Dowty Flexible Circuits) for allowing access to details of their laminating processes.

Finally, I would like to congratulate my wife, Wendy, for putting up with me while this thesis was being written.

ABSTRACT

The aim of this investigation was to make a flexible array of pulse-echo ultrasound transducers by etching two orthogonal linear arrays of conducting elements into the metallisation of either side of a sheet of PVdF. These would then be multiplexed under computer control in an X-Y raster, thereby forming an image of subsurface defects in a material specimen.

A potential source model was used to predict the sensitivity of a single element air-backed transducer far from resonance. Initial investigations confirmed the predictions, and reaffirmed the results of previous workers.

In making a prototype array, it was found necessary to use a bi-laminar arrangement with a central ground plane, due to difficulties with crosstalk and charge leakage into the specimen materials. The radiation pattern of this array was tested and found to agree with the predictions for Fraunhofer (Far-Field) radiation.

A 10 MHz analogue to digital converter was constructed to interface with the IBM-PC clone as a transient recorder, through a data capture program written in 'C'. However, the electrical noise generated by the PC was found to interfere strongly with the signal from the array transducer.

A wide-band amplifier and full-wave rectifier was then added to the multiplexer and A/D converter, and the system enclosed in an electrically isolated environment, which made it possible to obtain clear signal data from the transducer.

Non-linear regression was implemented in the software, to smooth the data and locate echo peaks, and the most frequently occurring peak separation was used to indicate sample thickness at that location in a false-colour mapping on the screen of the PC.

CONTENTS

CHAPTER 1 - INTRODUCTION 1

1.1 Ultrasound in Non-Destructive Testing. 1

1.2 Piezo-Electric Transducers. 12

1.3 Piezoelectric Transducers in Non Destructive Testing 18

1.4 Piezoelectricity in Poly-Vinylidene Fluoride . . . 22

1.5 Conclusions. 27

CHAPTER 2 - THE PROPOSED ARRAY TRANSDUCER 29

2.1 General Proposals. 29

2.2 Theoretical Considerations. 30

2.3 Limits of Spatial Resolution. 31

2.4 Anticipated Sensitivity of a PVdF Transducer. 36

CHAPTER 3 - PRELIMINARY EXPERIMENTS 45

3.1 Determination of Signal Levels. 45

3.2 The 2 x 2 Matrix Prototype 48

3.3 The 8x8 Matrix Prototype and Differential Amplifier. 49

3.4 Summary of Preliminary Results. 52

CHAPTER 4 - THE 7x7 ARRAY TRANSDUCER 54

4.1 Construction of the Bi-Laminar Prototype Array. 54

4.2 Measured Sensitivity. 55

4.3 Determination of Lateral Resolution. 56

4.4 Experiments with an Aluminium Test Block. . . 63

4.5 Summary of Results from the 7x7 Array Transducer. 66

CHAPTER 5 - DESIGN OF A DATA CAPTURE SYSTEM 67
5.1 Overview. 67
5.2 Central Processing Unit and Display 68
5.3 Digital Interface to the PC 69
5.4 Analogue to Digital Converter. 70
5.5 Multiplexers. 72
5.6 Pre-Amplifier. 73
5.7 Program 1 - Transient Recorder. 74

CHAPTER 6 - THE ISOLATED SYSTEM 78
6.1 Overview. 78
6.2 I/O Port Allocation. 80
6.3 Transmit Pulse Multiplexers 81
6.4 The Analogue Board 81
6.5 Isolated System Power Supply. 84
6.6 Results with the isolated system: Program 2 . . . 85

CHAPTER 7 - NON-LINEAR REGRESSION ALGORITHM 88
7.1 Overview. 88
7.2 First Trials. 89
7.3 Non-Linear Regression. 90
7.4 Software Implementation 93
7.5 Peak Indications in the Algorithm. 94
7.6 Example Program and Test Data. 95

CHAPTER 8 - RESULTS WITH THE ISOLATED SYSTEM 97
8.1 Peak detection and Depth indication 97
8.2 Array Transducer Imaging Experiments 99
8.3 Array Transducer Sensitivity Variations 101

CHAPTER 9 - ADDITIONAL ARRAY TRANSDUCERS 103
9.1 Overview. 103
9.2 16 x 16 Array from Pennwalt 104
9.3 6 x 6 Array Transducer. 106
9.4 First Rigid Transducer. 108
9.5 Second Rigid Transducer. 115

CHAPTER 10 - CONCLUSIONS 128
10.1 Validity of the Array Transducer Concept . . . 128
10.2 Theoretical Limitations 130
10.3 Data Capture and Display Routines. 133
10.4 Critical Factors in Array Transducer Construction 135
10.5 Suggestions for Further Work 137

REFERENCES 139

BIBLIOGRAPHY 141

APPENDIX 1: CIRCUIT DIAGRAMS OF TRANSIENT RECORDER 143

APPENDIX 2: TRANSIENT RECORDER PROGRAM 150

APPENDIX 3: CIRCUIT DIAGRAMS OF ISOLATED SYSTEM . 154

APPENDIX 4: TRANSIENT RECORDER PROGRAM FOR ISOLATED SYSTEM 164

APPENDIX 5: FINAL C PROGRAM 169

LIST OF FIGURES.

1: Incident, Transmitted and Reflected waves at a water-steel interface. (The three waves are separated for clarity) 3

2: Incident, reflected and transmitted waves at an oblique angle to an interface. 5

3: Typical applications of pulse-echo ultrasonic NDT in a steel sample. 8

4: A-Scan display produced by the compression wave transducer of Figure 3. 9

5: C-Scan of bond-line defects in a Perspex sample. 10

6: Axis Orientations in a Cubic Unit Cell and a Piezo-Ceramic Disc. 13

7: Construction Details of a Typical Piezo-Ceramic Compression-Wave Transducer. 19

8: Configuration of the Proposed Array Transducer. 29

9: Calculation of the Spatial Resolution of two adjacent Array Elements. 33

10: KLM Model of a Piezoelectric Thickness Expander Plate. 36

11: Estimation of Receiver Sensitivity for Piezoelectric Thin Films. 40

12: Simplified Transducer Configuration Showing Stray Capacitances in the Circuit. 43

13: Construction of a Simple Air-Backed PVdF Transducer. 45

14: Back-Wall Echo Transmitted and Received by a PZT Probe coupled into 25 mm Steel. (Gain Setting: 0dB) . . 47

15: Back-Wall Echo Transmitted by the same PZT Probe, Received by the PVdF Probe. (Gain Setting: 30dB) 47

16: Back-Wall echo Transmitted and received by the PVdF Transducer (25mm Steel at 5MHz. Gain Setting: 70dB) 48
17: Method of Testing the 8 x 8 Array Transducer. 50
18: Construction Details of the 7x7 Array Transducer. 54
19: C-Scan Beam Plot of 7x7 PVdF Array Element (Top Surface). 57
20: C-Scan Beam Plot of 7x7 PVdF Array Element (Bottom Surface). 57
21: Vertical Cross Section of Beam Plot in Figure 19. 59
22: Vertical Cross Section of Beam Plot in Figure 20. 60
23: C-Scan Beam Plot of 7x7 PVdF Array Transducer (TX/RX mode). 61
24: Vertical Cross-Section of Beam Plot in Figure 23. 62
25: Dimensions of the Aluminium Test Block 63
26: Back-Wall Echoes from the Test Block Using the 7x7 Array Transducer. (Scale 3 mm / horizontal division) . . . 64
27: Back-Wall Echoes from the Test Block Machined area, using the 7x7 PVdF Array Transducer.(Scale 3mm / horizontal division). 64
28: Back-Wall Echoes from the Test Block Machining Edge Using the 7x7 Array Transducer.(Scale 3mm/division). . 65
29: General Outline of the Proposed System. 67
30: Digitised A-Scan of the Test Block Using a commercial 5MHz PZT Transducer. 75
31: Digitised A-Scan of the Test Block Using the 7x7 PVdF Array Transducer. 76
32: Control/Status Port 308H 80
33: FET Switch Pulse-Suppression Technique. 82

34: Measured Voltage Drop and Phase Shift across a 1kΩ resistor in series with an Array Element from the first Rigid Transducer. 84
35: Implementation of "least squares fit" algorithm. 93
36: Demonstration of the Signal-Smoothing and Peak-Detection Ability of the Regression Algorithm. 95
37: A-Scan Output from the Regression and Peak Detection Algorithm. 97
38: Flaw Map of the Aluminium Test Block Produced by the Data Capture and Display System, using a PZT Transducer for the Generation and Detection of U-S. . . . 99
39: Flaw-Map of the Aluminium Test Block, using the Multiplexed PVdF Array Transducer. 100
40: Sensitivity Map of the 6x6 Gold Sputtered PVdF Transducer. 107
41: Cross-Section of the Construction of the first rigid Transducer, showing the number of bond-lines required. 110
42: Sensitivity Map of the Lower Layer of the 15x15 Rigid Transducer. 112
43: Sensitivity Map of the Upper layer of the 15x15 Rigid Transducer. 113
44: Sensitivity Map of the 15x15 Transducer in Combined Tx/Rx mode. 114
45: Bottom Layer Sensitivity Map of Final Rigid Transducer, During Construction. 117
46: Smoothed and Processed Image from the Data of Figure 45 118
47: Bottom Layer Sensitivity Map of Final Rigid Transducer. 123

48: Second Layer Sensitivity Map of Final Rigid Transducer. 124
49: Sensitivity Map of the Second Rigid Transducer in Combined Tx/Rx mode. 125
50: Flaw map of the Aluminium Test Block Produced by the 16 x 16 system using a PZT Transducer. 126
51: Flaw Map of the Aluminium Test Block Produced by the Final Rigid Transducer 127

NOTATION

A	Area of Parallel Plates
A_m	Amplitude of Wave Mode 'm'
c_o	Parallel Plate Capacitance (Clamped)
C	Elastic Modulus
$d_{i,j}$	Piezoelectric Stress Coefficient
d	Diameter of Transducer
D_i	Electric Displacement
$e_{i,j}$	Piezoelectric Coefficient
E_i	Electric Field
f	Frequency
$g_{i,j}$	Piezoelectric Coefficient
$h_{i,j}$	Piezoelectric Strain Coefficient
I	Acoustic Intensity
k	Array Element Separation
L	Return Trip Distance
M	Electro-Mechanical Equivalence Term (in KLM)
Q	Charge Density
R	Acoustic Reflectance
t	Thickness of Transducer Element
T	Acoustic Transmittance
v_m	Velocity of Wave Mode 'm'
$V_{i,j}$	Piezoelectric Voltage
X_3	Electromechanical Impedance Term (in KLM)
X	Stress
ε	Dielectric Permittivity
θ	Incident Angle
λ	Wavelength
ρ	Density
σ	Poisson's Ratio

CHAPTER 1 - INTRODUCTION

1.1 Ultrasound in Non-Destructive Testing.

The Non-Destructive Testing and Evaluation (NDT and NDE) of materials and products is often concerned with the detection, location and sizing of material or bonding defects. Many of these do not appear on the material's surface, or may be internal to structures that cannot easily be examined such as pressure vessels and pipelines. Methods have therefore been developed to examine the integrity of these structures, and one of the most widely used of these is ultrasonics.

Ultrasonic testing relies on the properties of elastic waves both within the bulk material and also at flaws and material boundaries. There are, of course many different types, or modes, of wave motion in solids, but of these, only the compression (primary) wave, and the shear wave are of widespread interest to NDT. Rayleigh, Lamb, and other wave modes occur almost exclusively in thin plates or within one or two wavelengths of the material surface. Other NDT techniques, (such as electromagnetic eddy current analysis) are generally more appropriate for defect detection in samples of this type.

The velocities of the compression and shear modes in bulk materials are given by the equations

$$V_c = \sqrt{\frac{C(1-\sigma)}{\rho(1+\sigma)(1-2\sigma)}} \qquad (1.1)$$

and

$$V_s = \sqrt{\frac{C}{2\rho(1+\sigma)}} \qquad (1.2)$$

where C is the Elastic Modulus
ρ is the Density
and σ is Poisson's ratio

In aluminium and mild steel, for example, these velocities are in the region of 6000 m/s for compression waves, and 3000 m/s for shear waves. (This difference has important implications in determining the relevant wave mode for the required NDT application.)

Consider, however, a compression wave crossing an interface perpendicular to the wave motion, between a steel mass and another material with different acoustic properties such as water, (Figure 1). A portion of the wave will be reflected with inverse phase to the incident wave, and a further portion will be transmitted.

The ratios of incident (A_i), reflected (A_r) and transmitted (A_t) amplitudes are called the Reflectance (R) and Transmittance (T) respectively, and depend on the product of the density and the velocity of the wave mode in the two materials.

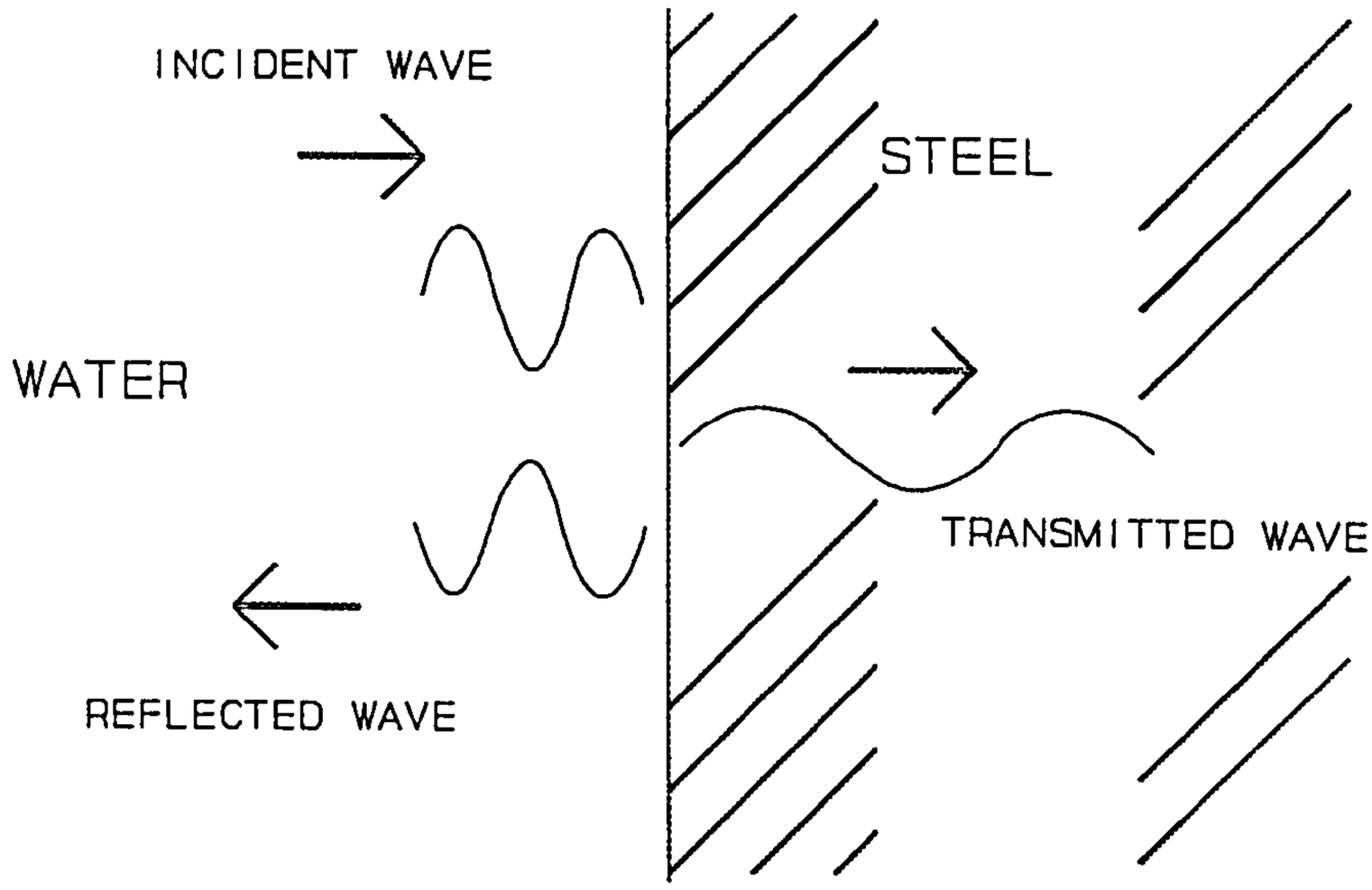

Figure 1: Incident, Transmitted and Reflected waves at a water-steel interface. (The three waves are separated for clarity)

This product is called the Acoustic Impedance, (Z) and is given for a range of materials in Table 1. Using this terminology, we can write (for an orthogonal interface)

$$T = \frac{A_t}{A_i} = \frac{2\,Z_2}{(Z_1+Z_2)} \qquad (1.3)$$

and

$$R = \frac{A_r}{A_i} = \frac{(Z_1-Z_2)}{(Z_1+Z_2)} \qquad (1.4)$$

where

$$Z = \rho * V \qquad (1.5)$$

Equations 1.3 and 1.4 are of fundamental importance in the use of ultrasound in NDT, since they imply that any discontinuity in the material will reflect acoustic waves. By introducing an acoustic wave into a bulk material and detecting the reflected waves, it is therefore possible to infer internal details of the material under test.

These equations hold good both for shear waves and compression waves where the material on both sides of the interface is capable of transmitting them, and where the interface is orthogonal to the direction of propagation of the wave. (It should be noted that liquids cannot in general transmit shear, and that therefore a solid liquid interface will reflect shear waves completely.)

PROPERTY MATERIAL	DENSITY (ρ) ($x10^3$ kg/m^3)	COMPRESSION WAVE VEL. V_c (m/s)	ACOUSTIC IMPEDANCE Z ($x10^6$ kg/m^2.sec)
WATER	1.0	1509	1.509
STEEL	7.8	5900	46.0
ALUMINIUM	2.7	6300	17.0
PZT	7.43	4440	33.0
PERSPEX	1.15	2700	3.1
PVdF	1.78	2200	3.9

Table 1: Acoustic Properties of Selected Materials.

For example, taking the values for a water-steel interface from the table of acoustic properties of selected materials, (Table 1), we find that Z(water)=1.509 and Z(mild steel)=46.0 . This means that the transmitted wave in the steel has only 35% of the incident amplitude, and the reflected wave in the water has 94% of the incident amplitude. This argument is valid for an interface perpendicular to the wave motion, and for the most part remains valid for small angles of incidence, where the wave energy stays in the same mode.

For the case of an interface at an oblique angle to the wave-motion, we can use Snell's Law to derive the reflected and transmitted angles, ie.

$$\theta_{reflected} = \theta_{incident} \tag{1.6}$$

and

$$\frac{\sin(\theta_i)}{V_{c(i)}} = \frac{\sin(\theta_i)}{V_{c(i)}} \tag{1.7}$$

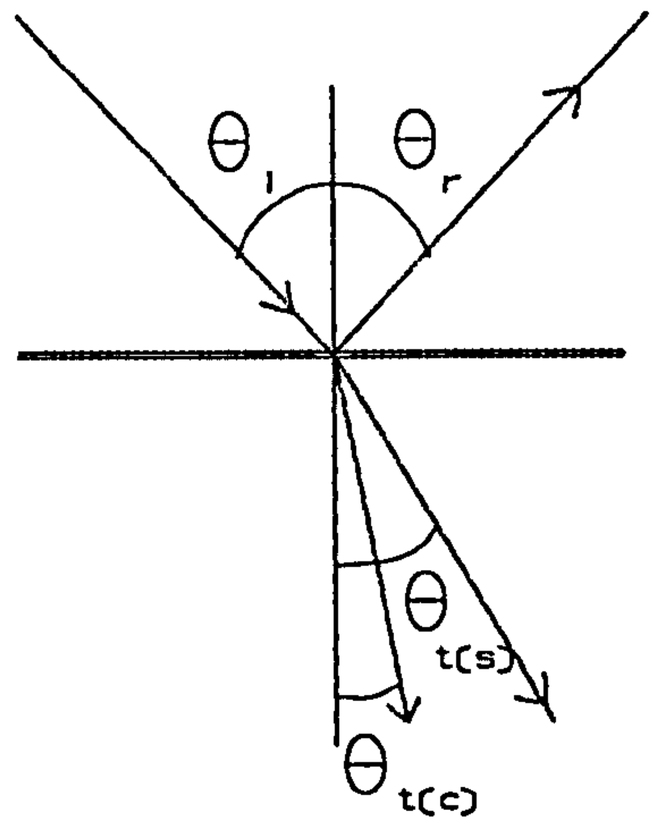

Figure 2: Incident, reflected and transmitted waves at an oblique angle to an interface.

The relative amplitudes of the wave are further modified, however, by the conversion from compression mode to shear mode (or vice versa) which takes place at an angled interface. A unit cell under the influence of a compression wave will distort in all possible directions. Where there is a discontinuity at an angle to the unit cell, however, this distortion will leak energy into other wave modes. In metals, such as mild steel or aluminium, there is no unit cell of dimensions appreciable to the wave energy, and mode conversion only occurs at the boundaries of the specimen. In crystalline materials, however, mode conversion occurs at the crystal boundaries. The ultrasonic examination of materials such as austenitic steels is severely hampered by this effect, as the poly-crystalline structure randomly re-orientates the direction and mode of the incident ultrasonic energy.

It can also be shown that when the velocity of the incident wave is greater than the velocity of the transmitted wave, there is a critical angle of incidence beyond which no wave energy in that mode can be transmitted into the material. For a steel/water interface this is about 15 degrees for compression waves, and about 35 degrees for shear waves. For this reason, material examinations which require a relatively large angle of incidence, (such as butt welds in pipelines,) use transducers designed to generate shear waves.

It is clear, therefore, that the reflected acoustic waves in a material specimen carry a great deal of information about the internal structure of that material. A great deal of research has been done to quantify this information so as to define defect shapes, surface roughness, or the extent and severity of bond line defects. Developments in this field are reported in the "Annual Review of Progress in Quantitative Non-Destructive Testing" published by

Plenum Press, but in general this kind of research is limited by the practical difficulties of generating consistent reproducible acoustic waves in a wide variety of materials and structures.

The quantifiable information most used for defect location and sizing is the intensity of the reflected acoustic signal (which is obtained electronically by rectifying and integrating the signal over a small number of wavelengths). The time elapsed between the transmission and reception of the acoustic wave defines the depth at which the echo was generated and the intensity is used to determine the extent of the defect.

The available resolution of defects is of the same order of magnitude as the wavelength of the ultrasound in the material. Not only because the wave energy does not interact with interfaces very much smaller than a wavelength, but also because the radiation pattern of a transducer is dominated by diffraction effects which depend on the transducer diameter and the wavelength of the ultrasound. It would be expected from these arguments that the accurate location of defects in steel to within +/- 1mm will require a frequency of around 6 MHz. In fact, for the inspection of metal structures, frequencies in the range 1-10 MHz, and transducer diameters from 5-20 mm are commonly used.

The attenuation of the acoustic energy also increases with frequency, however, and for lossy materials with much lower acoustic velocities, such as polymers, or fibre reinforced plastics, frequencies as low as 100 kHz may be required.

Figure 3 illustrates the way these conclusions are generally put into practice.

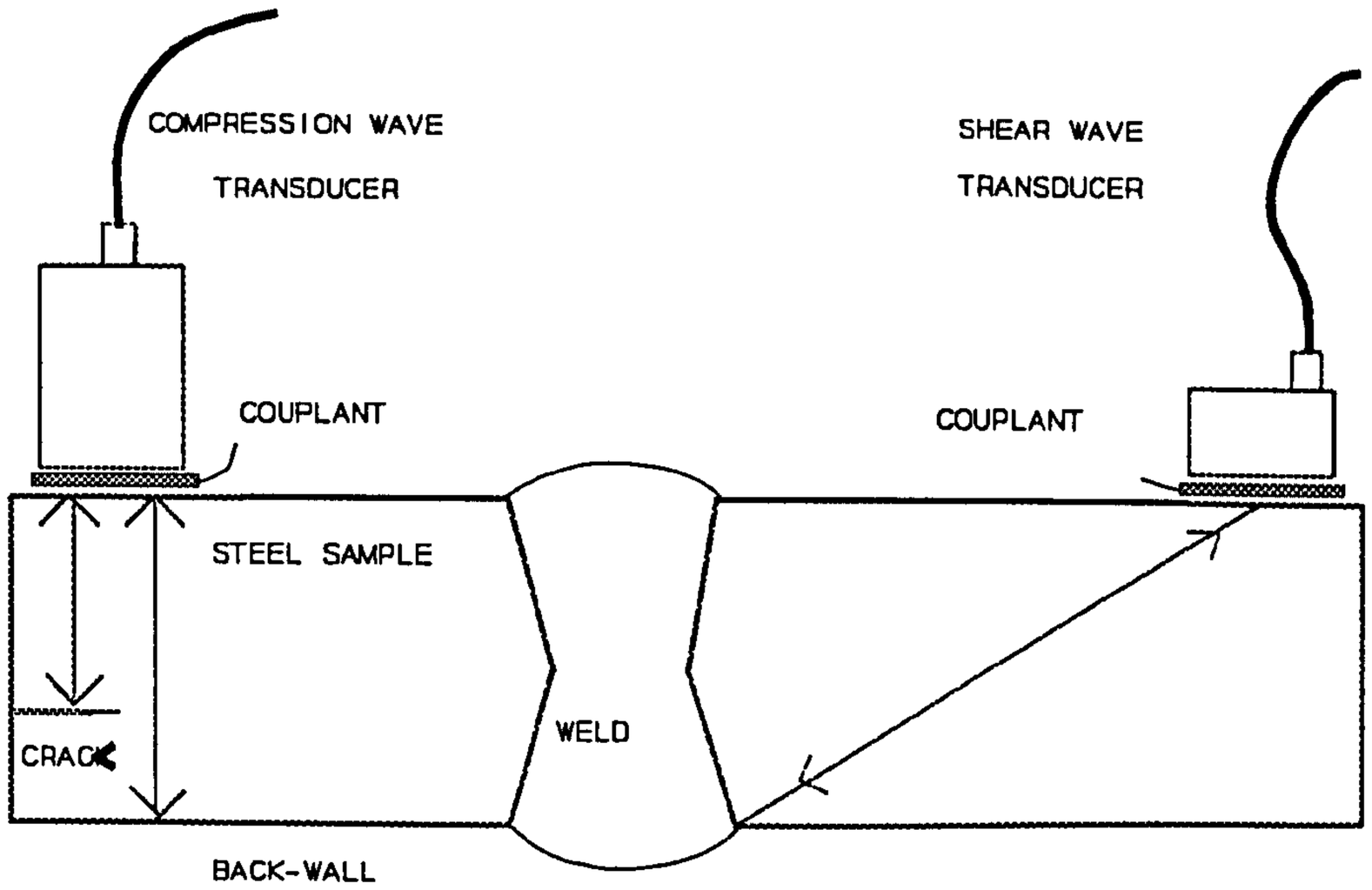

Figure 3: Typical applications of pulse-echo ultrasonic NDT in a steel sample.

A short pulse (preferably a single cycle) of ultrasound (either compression waves, or shear waves,) is generated by an electroacoustic transducer and coupled into the sample by a thin fluid layer. The reflected waves are detected by this transducer, amplified and passed to a display.

Defects which will reflect ultrasound perpendicular to the surface are investigated with compression waves, but if the flaw line is at an angle, as in the weld in Figure 3, a probe designed to generate shear waves may be used. These reflect off the back wall of the steel, to approach the weld line from the necessary orientation. Reflections from defects in the weld line will traverse the same path, and can be detected by the same transducer.

Typically, the time elapsed between the transmitted pulse and the received echoes can be displayed as the X-axis of an oscilloscope trace, while the amplitude of the ultrasound echo, either as an RF signal, or (more usually,) rectified and smoothed, will be displayed as the Y-axis. This produces what is known as an A-scan.(figure 4)

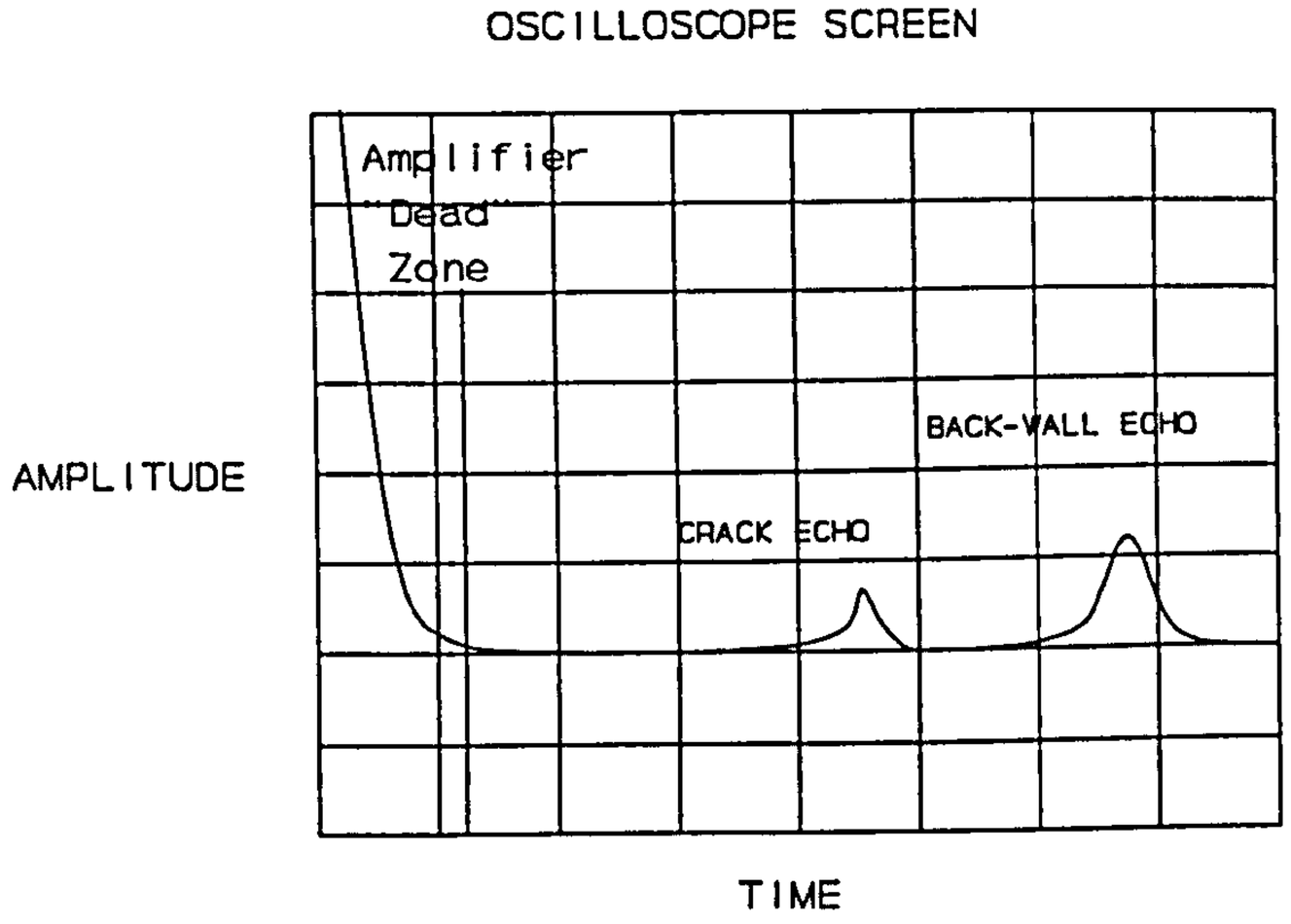

Figure 4: A-Scan display produced by the compression wave transducer of Figure 3.

The A-Scan is by far the most commonly used display technique for ultrasonic NDT, and in recent equipment can be automated or provided with amplitude thresholds at given depths to warn operators of the likely failure of components.

Medical ultrasonics makes much use of the B-scan technique, in which the x-y locations of individual pixels on a video screen represent the location (in cross section) of the echo source within the patient, and the intensity of the echo from that location is represented by the brightness of that pixel. The focused ultrasound beam is continually scanned, (either mechanically, or electronically

using phase-shifted arrays of transmitting elements,) and the video image is updated in 'real-time'. This B-scan technique gives very good cross sectional images of organic material, but is not generally used in NDT.

Another technique in common use involves mechanically scanning a transducer in an X-Y raster pattern at a set distance from a sample (which is frequently held in a water bath). The amplitude of the echo at a given depth (or time elapsed) is displayed on a computer screen, either as a grey-scale or as a false-colour map against the X-Y coordinates of the transducer.

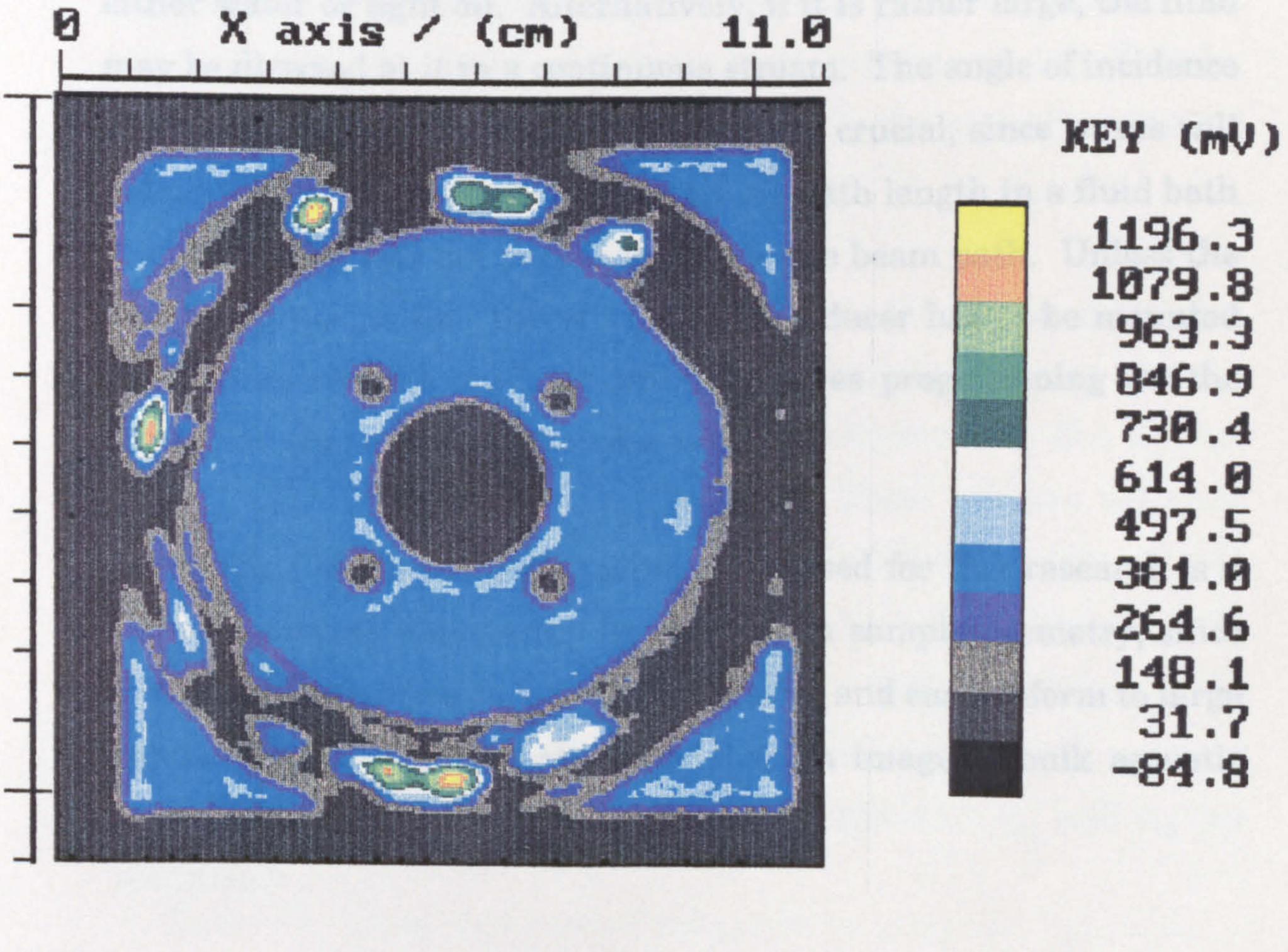

Figure 5: C-Scan of bond-line defects in a Perspex sample.

This technique, (called a C-scan) is of great interest to many industries requiring NDT, as it gives visual indications of the size, location and severity of defects, and can be automated to make repeatable checks of batches of products.

Figure 5 shows a typical C-Scan, of the joint between a perspex cylinder and a flat plate. Disbonded areas within the circular joint are clearly visible.

In order to produce this sort of image however, a means has to be found to couple the ultrasound between the stationary sample and a moving transducer. The sample may be immersed in a bath of either water or light oil. Alternatively, if it is rather large, the fluid may be directed at it in a continuous stream. The angle of incidence of the beam on the surface of the sample is crucial, since waves will only return to the transducer over a long path length in a fluid bath if all the interfaces are perpendicular to the beam path. Unless the sample surface is flat, therefore, the transducer has to be mounted on a multi-axis manipulator which requires programming for the particular shape of sample under test.

The flexible array transducer proposed for this research is a way of removing these strict limitations on sample geometry, since it will be placed in contact with the surface, and can conform to large radius curvature, whilst still providing an image of bulk acoustic properties.

1.2 Piezo-Electric Transducers.

It has long been known (Ref. 1) that certain materials with asymmetric crystalline structure will generate an electric charge on their surfaces when deformed. The inverse of this effect is also true, that the materials will deform under the presence of an electric field. The amount of charge generated is related to the applied stress by the relationship

$$Q = d_{ij} * X_j * A \qquad (1.8)$$

where the coefficient $d_{i,j}$ is a tensor quantity relating the orientations of the charge and stress to the crystal unit cell, X_j is the component of stress in the j direction and A is the area of the crystal surface.

Typically, the d_{33} coefficient relates to the charge generated across a thin film or disk under compression, whereas the d_{31} coefficient describes the charge generated across a thin film or disk which is being stressed along its length. These two are the most important coefficients for ultrasound transducers, describing the generation and detection of compression and shear waves respectively. The materials used are generally arranged to be symmetrical in two of their axes, and have their dipole moment oriented across the third. (So that the coefficients d_{31} and d_{32} are identical.)

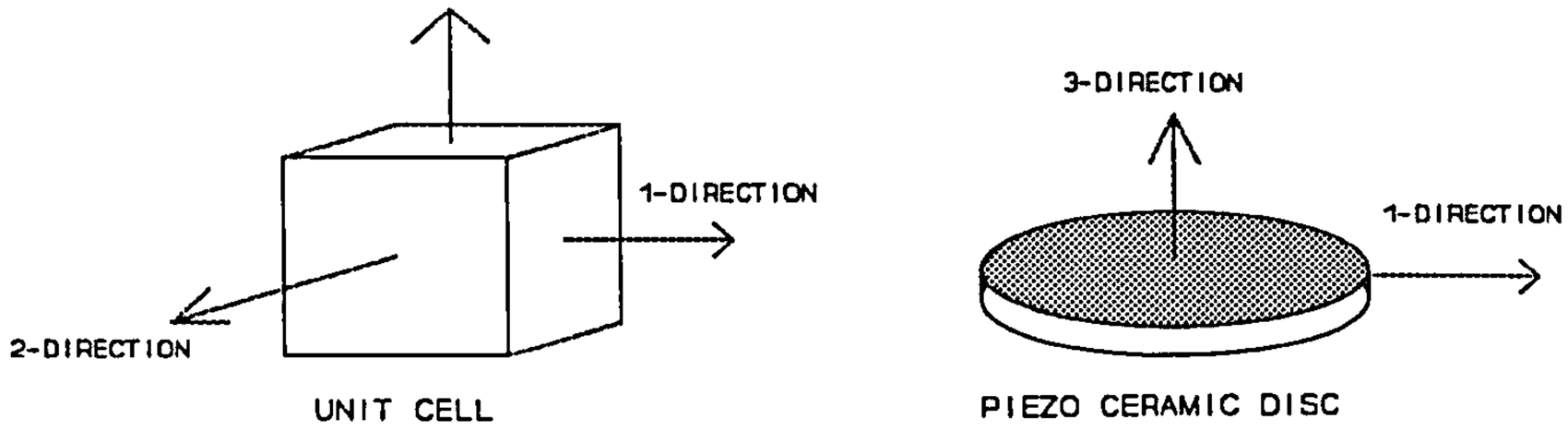

Figure 6: Axis Orientations in a Cubic Unit Cell and a Piezo-Ceramic Disc.

The inverse effect can be described by the relationship,

$$V_i = h_{ij} * \delta t_j \qquad (1.9)$$

and again the coefficients h_{ij} relate the voltage generated (V_i) with the deformation (δt) in the axes related to the unit cell.

The earliest known piezoelectric materials had d_{33} coefficients between 2×10^{-12} meters/Volt (for quartz) and 275×10^{-12} (for Rochelle salt). Later discoveries included a number of ferro-electric ceramics, such as Barium Titanate and Lead Zirconium Titanate (PZT), with much higher coefficients, and better coupling factors, especially in the important thickness-extension mode. (See Table 2). Sintered ceramics like these have no net piezoelectric moment, but they can be "poled" by aligning the ferroelectric domains under an electric field at an elevated temperature.

Material	Quartz (X-cut)	$BaTiO_3$	PZT-5H
Dielectric Constant ε_r	4.5	1200	3400
Coupling Factor k_{33}	0.10	0.48	0.75
Stress Constant d_{33} (10^{-12}m/V)	2.3	149	593
Acoustic Impedance Z (10^6 N.m/s^3)	15.2	29.4	33.0

Table 2: Properties of Common Piezoelectric Materials

PZT in particular has proved very popular, and the properties of the basic material have been improved by doping it with other elements. The variant listed in Table 2 is proprietary, and known as PZT-5H.

The electromechanical coupling factor k_{ij} can be understood by imagining two identical piezo discs rigidly clamped together. All of the deformation induced in one will be experienced by the other, and from equations 1.8 and 1.9 (or their equivalents) we can obtain

$$\frac{V_r}{V_t} = \frac{h_{33} * \delta t_b}{(\frac{1}{d_{33}}) * \delta t_a} \qquad (1.10)$$

which simplifies to

$$\frac{V_r}{V_t} = d_{33} * h_{33} \qquad (1.11)$$

This latter is a measure of how much of the acoustic energy translates into electrical energy (and vice versa) and is often quoted in manufacturers data as k_{ij} where

$$k_{ij}^2 = h_{ij} * d_{ij} \qquad (1.12)$$

Two other coefficients may be taken into account when specifying the piezoelectricity of a material. For completeness, the relationships which define all four are given here in the same format.(Eqs 1.13 to 1.16)

$$\left(\frac{\partial D_i}{\partial X_j}\right)_{E=0} = d_{ij} \qquad (1.13)$$

$$\left(\frac{\partial E_i}{\partial X_j}\right)_{D=0} = g_{ij} \qquad (1.14)$$

$$\left(\frac{\partial D_i}{\partial t_j}\right)_{E=0} = e_{ij} \qquad (1.15)$$

and

$$\left(\frac{\partial E_i}{\partial t_j}\right)_{D=0} = h_{ij} \qquad (1.16)$$

Where D is electric displacement (Q/m^2)

E is electric field (V / m)

X is Applied Stress (N / m^2)

and t is strain ($\delta t/t$)

Obviously, these coefficients are not directly determinable, but must be measured by some other method. They are not independent, however, and are related by the fundamental material properties ε_r and the elastic constant C.

That is:

$$\frac{d}{g} = \frac{e}{h} = \varepsilon_r \varepsilon_0 \qquad (1.17)$$

and

$$\frac{e}{d} = \frac{h}{g} = C \qquad (1.18)$$

In conclusion, any piezoelectric material may be used to generate and detect pressure waves in a material, simply by exciting it across the relevant orientation with a waveform from a voltage source, and connecting charge-collecting metallisation on either side of the material to an electronic amplifier.

The applied field excites deformation in all possible modes, and acoustic reflections from the material boundaries generate back-emf with a complex waveform. The electrical impedance of a transducer is thus strongly dependent on the specific dimensions of the piezoelectric element and the acoustic properties of the materials surrounding it in construction. Typically, a PZT disk will have a

number of resonant frequencies at which the input impedance rises to near infinity, and the acoustic wave amplitude is a maximum.

The amplitude of the applied electric field is related to the amplitude of deformation under static conditions by the piezoelectric coefficient $d_{i,j}$, and typically 400 volt pulses are used, giving electric field strengths of the order of 10^5 V/m. Field strengths greater than this are not generally used, since the ferro-electric properties of the transducer would then weaken after prolonged use. (An effect known as "De-poling".)

Transducer materials are principally characterised therefore, by the values of the $d_{i,j}$, $h_{i,j}$ and $k_{i,j}$ coefficients, (which should be high) and a close match of acoustic impedance between the transducer material and the range of materials which the transducer is proposed to examine.

1.3 Piezoelectric Transducers in Non Destructive Testing

As discussed previously, the amplitude of the acoustic wave is a maximum at specific resonant frequencies. At these frequencies, the narrow-band reponse of the electrical impedance causes 'ringing', which stretches the pulse train over an envelope of several cycles. In other words, a simple transducer designed for high-amplitude acoustic waves loses depth resolution in echo detection. Furthermore, the applied electric field generates all possible modes of acoustic wave, and since these modes travel at different velocities, confusion over echo location could arise.

The special characteristics required for NDT transducers are conflicting therefore, in that the ideal is a short pulse with a large amplitude, with all the energy in a known mode.

A number of equivalent circuit models and computer programs have been developed over the years, to predict transducer performance and improve reliability, and these are discussed in detail a little later. Use of the equivalent circuit models has enabled designers to trade-off these factors and produce piezoelectric transducers with much better (and more reproducible) characteristics for pulse-echo NDT, and transducer construction is now reasonably standardised. Figure 7 shows a typical NDT compression wave transducer in cross-section.

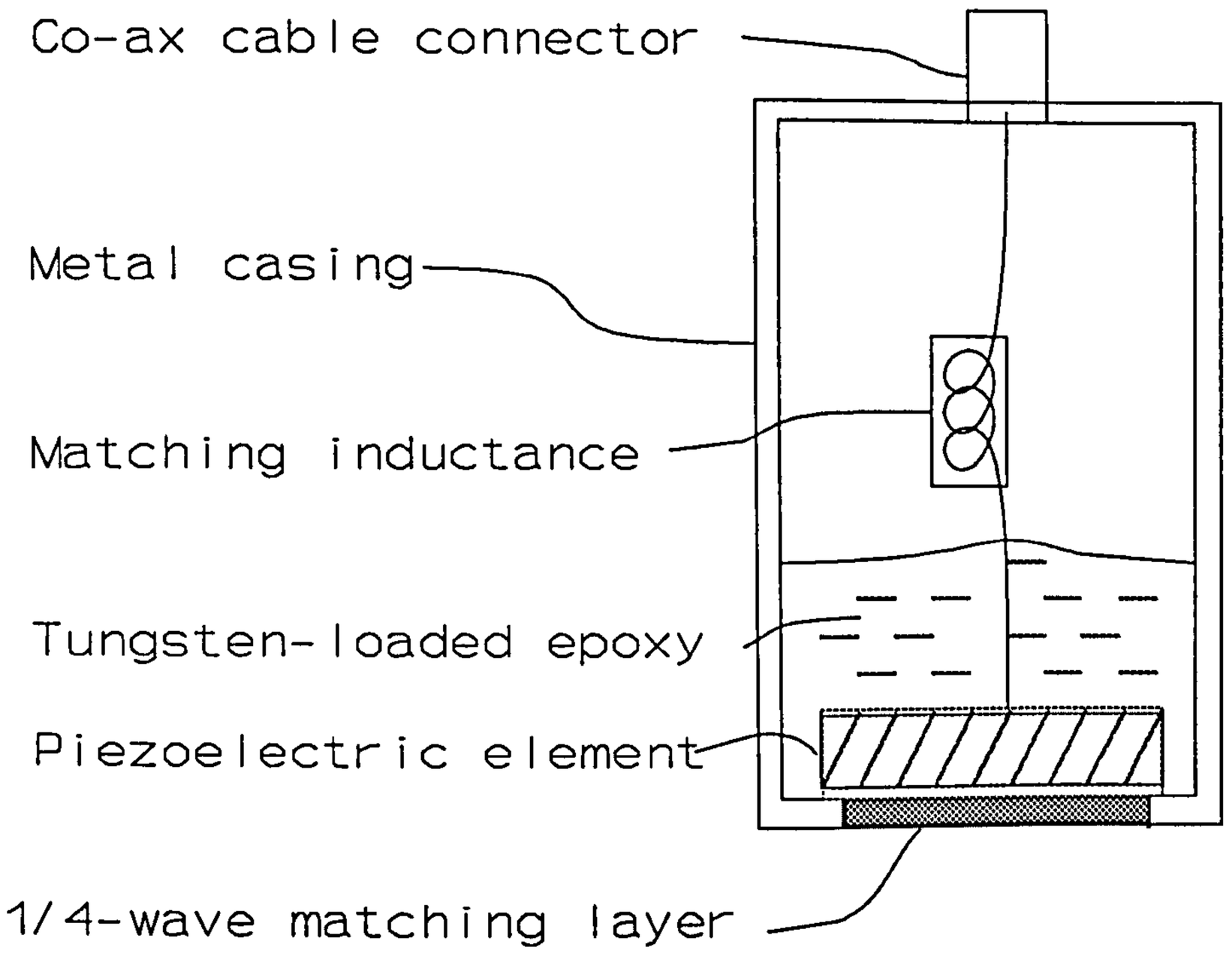

Figure 7: Construction Details of a Typical Piezo-Ceramic Compression-Wave Transducer.

The ceramic element itself is a disc, typically 5-25 millimetres in diameter, of ferroelectric material poled to give the orientation described in Figure 6. It is nominally half-wave resonant in its thickness-extension mode, giving a centre frequency of

$$f = \frac{v_t}{2*t} \qquad \textbf{(1.19)}$$

As an example, the ceramic disc of a PZT probe which is nominally tuned to 5 MHz is 0.5 mm thick. It is not difficult to produce discs of brittle ceramic to these sorts of dimensions, and within acceptable tolerances. However, much greater diameters, or frequencies above 15-20MHz are impractical to manufacture reproducibly.

As already outlined, a half-wave resonant disc with a large acoustic impedance mismatch at its boundaries, and low absorption, 'rings' for several cycles when driven with an applied voltage pulse. It will also exhibit a number of resonances in different wave-modes besides its nominal thickness-extension mode frequency.

In order to prevent these undesirable effects, the rear face of the ceramic disc is bonded to an acoustic absorbing material.

This tungsten-loaded epoxy backing, effectively loads the rear face of the disc with a highly attenuating material of comparable acoustic impedance (around $10*10^6$ N.m/s^3) and helps to suppress spurious wave-modes. The tungsten inclusions both add to the density of the epoxy, and provide grain boundaries to disperse the acoustic wave within the material.

One other effect of this backing is to reduce the resonant frequency from that of the pure half-wave resonance, so that a nominal 5 MHz probe may now have its resonant peak as low as 4.2 MHz. The Q of the mechanical resonance is also lowered as a natural by-product of the loading, and thus the energy of the acoustic wave generated will be decreased.

On the outer face of the probe between the element and the material under test a hard wearing layer is bonded. Again the thickness of this is designed to match the probe's centre frequency, but there is another important factor in the choice of material for this layer. The energy reflected from an interface is, as we have seen, related to the acoustic impedances of the two materials. It can be shown that to maximise the energy coupled through a thin layer between two dissimilar materials, the acoustic impedance of the coupling layer should be calculated from

$$Z_{layer} = \sqrt{Z_a * Z_b} \qquad (1.20)$$

where Z_a is the acoustic impedance of the transducer material, and Z_b is the acoustic impedance of the material under test.

Since the value of Z_b differs for each type of material the probe is used on, different materials ought to be used for the matching layer, depending on the prospective use of the probe. Eg. for Medical applications, where the majority of sample materials have Z close to that of water, the material used for the matching layer should have a Z of around $7 * 10^6$ kg/sec-m^2. For examining metals, however, Z should be around $40 * 10^6$ kg/sec-m^2.

From all of the above, it is clear that ferroelectric ceramics are widely applicable to the piezoelectric generation of ultrasound for NDT and medical applications. However, they do exhibit certain limitations in some circumstances, which are summarised here.

In those applications where the material has an acoustic impedance close to that of water, such as medical examinations, the high impedance of the ceramic material prevents the optimum signal/noise ratio being obtained. Tissue-type materials are highly attenuating at ultrasonic frequencies, and significant improvements could be made if a transducer with a closer matching Z could be manufactured.

Also, as mentioned previously, the ceramic elements are both small in diameter, and brittle. The examination of curved structures presents particular problems in this area because the probe must be held so that the wave motion is perpendicular to the surface at all

times, especially if there is a substantial water-path between the probe and the sample, (as in C-scan equipment). Furthermore, the probe's small diameter requires quite long scan-times to cover larger structures, even if the defect tolerance is large.

Finally, these ceramic materials are difficult to lap accurately to thicknesses below 0.2 mm, and the effective frequency range has an upper limit, therefore at around 20-25 MHz. There are a number of techniques, such as ultrasonic-microscopy, and the examination of thin coating layers or bond lines, that require frequencies from 50 MHz to more than 100MHz.

1.4 Piezoelectricity in Poly-Vinylidene Fluoride

In addition to the ceramic materials outlined above, several organic materials had been known to be piezoelectric. However, their piezo coefficients were several orders of magnitude lower than the crystalline or ceramic materials. But in 1969, the discovery of an organic polymer with coefficients comparable to the crystalline inorganic materials was announced by H. Kawai (2). This material was poly-vinylidene fluoride (or PVdF). It is a homopolymer of the basic cell

$$-(CH_2\text{-}CF_2)-$$

Polymerisation occurs by addition or condensation, in the presence of free radicals, and may take place in gaseous, emulsion or liquid phases. The resultant polymer exists in two forms. Most of the product of polymerisation takes the alpha form, in which, due to

the orientation of the chains, no net piezoelectric moment exists. However, the chains can be realigned by a number of methods into the beta form. This was the material reported by Kawai. In his experiments, the PVdF had been formed as a film, which was then uniaxially stretched, heated to >100°C and a strong electric field applied while the temperature was reduced to ambient. Similar poling techniques were applied to the commercial PVdF film which was used in the experiments described in this thesis.

The resultant film of material is chemically inert, dimensionally stable and highly flexible. It also exhibits a very low surface bonding energy. The commercial PVdF treated in this way and used throughout this research is reported to have a d_{31} coefficient of around $23 * 10^{-12}$ m/V and a d_{33} coefficient of $33 * 10^{-12}$ m/V. There is no measurable d_{32} coefficient and the material is not symmetrical in the axes of the sheet because of the uniaxial stretching used in the manufacture. (See Appendix 6)

Electrodes may be either vapour deposited, sputtered, or sprayed in a solvent base onto the surface of the material. If this is done after poling, (as is usual) strict temperature controls are required, since the ferroelectric properties weaken at around 70°C and disappear altogether above about 80°C. This effective T_c sets an upper limit on the process temperature to which poled PVdF can be subjected.

The connection of flexible wires to the deposited electrodes remains a problem for all researchers.. Techniques ranging from silver-loaded epoxy to punch-through crimping have been reported. Any of these techniques may be satisfactory in situations where the

PVdF will be attached to a rigid substrate, but there is no known satisfactory technique for flexible transducers. The author contacted a major supplier of flexible printed circuits regarding this problem, but the elevated temperatures (between 170 and 220°C) used in the polyimide curing processes would require the PVdF film to be re-poled, for which facilities were not available. This may still be the most reliable way of producing flexible PVdF transducers, but it was not possible to pursue this within the limitations of this project.

Although the reported piezoelectric coefficients are around an order of magnitude lower than comparable ceramics, the relatively low acoustic impedance, low ε_r and high electromechanical coupling coefficient prompted a number of researchers to consider PVdF as an ultrasound transducer for those applications where ceramic materials were limited.

Several researchers, including Shotton (3), DeReggi (4), and Lewin (5) have used thin film PVdF as a hydrophone sensor. Most of these used a single element, either needle type or flexural disc with a small active area, and the requirement for a pre-amplifier mounted in close proximity to the sensor was described by most of these workers, due to the high electrical impedance and small signal levels generated by the piezoelectric element.

Latterly, the ease of manufacture and reproducibility of these transducers has led to an interest in hydrophone arrays of various configurations. (6,7)

Some early efforts were made to produce useful electro-acoustic transducers for use at audio frequencies. Headphones (8) and telephone earpieces (9) have been attempted, and various forms of

microphone are now commercially available (10) . The flat frequency response and wide bandwidth of PVDF across the audio range are the main attractions in these applications, but the low output level compared to other techniques requires comprehensive screening to reduce interference.

The good acoustic impedance match between organic materials and PVDF has also prompted a good deal of research into probes for medical applications. Hunt (11) in an excellent review, describes the requirements, equivalent circuit models and manufacturing techniques of diagnostic medical ultrasound transducers using both PZT-5H and PVdF. Commercial single element transducers made from PVdF have been manufactured by Toray, and show imaging resolution which is comparable with currently available PZT transducers. No significant improvement was shown for these probes however, and they have not gained widespread acceptance.

One area of research for which PVdF is particularly well suited is in producing ultrasound with frequencies above 100 MHz. As discussed earlier, the limitations on manufacture of conventional ceramics place an upper limit of about 20 MHz on PZT and lead metaniobate transducers. Although usable acoustic output has been obtained from thin films of cadmium sulphide, much stronger signals can be induced in a thin layer of PVdF, which can be made to resonate at up to several hundred MHz. Furthermore, because of the low Q of the resonance, it is possible to get usable output at frequencies much higher than this. In one notable application (12), the transducer element was made by dissolving PVdF in an organic solvent. A drop of this solvent was placed on a spinning brass disk, and the PVdF re-crystallised from solution to a very thin film. Poling

was achieved without temperature cycling, under a field strength of 0.1 MV/mm. The resultant transducer had a demonstrated bandwidth of several GHz.

Bui,Shaw and Zitelli (13) were among the first to report the use of PVdF (or PVF2 as it was known then) for generating ultrasonic waves in the frequency range of most interest to NDT techniques (from 100kHz to 10MHz.) They report that transducers made by attaching the poled sheet to the front face of a brass rod exhibit the same sensitivity coupled into water as an equivalent PZT probe at its resonance. They also reported that the PVdF probe had a flat frequency spectrum from 0.1 to 20MHz and that the clean single cycle pulse indicated the broad bandwidth of the arrangement.

Bainton and Silk (14) presented a more rigorous approach to the design of a PVdF pulse-echo probe using the computer modelling developed at the NDT centre of the AERE at Harwell. Although details of the model are not presented, they state that it is based on the KLM model outlined later. The arrangement used in their studies was a backing block of poly-methyl methacrylate (Perspex), and a stand-off or delay-line block of polystyrene with the PVdF clamped firmly between them. They reported a predicted insertion loss of just 6dB less than an equivalent PZT probe and a measured figure of 15dB, attributing the discrepancy to over-optimistic data supplied by the manufacturer of the PVdF. The sample material which the probe was being used to examine, was not stated, however.

Work has also been done in this frequency range by Platte (15) using PVdF as a transmission transducer as well as a receiver. Here

the pulse was generated by a step voltage (rather than the usual pulse) and relied on the natural resonance of the 50μm PVdF film to generate an ultrasound pulse of 50ns duration with no subsequent ringing.

1.5 Conclusions.

The general conclusion of these workers seems to be that PVdF can be used as a wide-band pulse-echo ultrasound transducer for examining a range of materials, since the sensitivity (with careful probe design) can be made to approach that of commercial ceramic probes.

Furthermore, subsequent research has improved on the basic material by either altering the manufacturing process, or introducing other compounds into the polymer matrix. Other poling methods have been described, which have included bi-axial stretching, and the application of corona fields or electron beams, with or without temperature cycling.

Stretching of thick-film material to the voided state has also been utilised to make a much lower frequency transducer material which has proved especially valuable in SONAR hydrophone arrays. In the area of modified chemical composition, the greatest attention recently has focused on the copolymer of Vinylidene Fluoride with Trifluoroethylene. Samples of this copolymer are said to have coefficients up to five times those of the original material. Unfortunately, the highly crystalline structure of this copolymer restricts its use to arrangements in which it can be mechanically clamped, since it has been found to be very brittle. The measured

piezoelectric properties also vary appreciably from the stated figures due to inhomogeneity in the chemical composition of the sheet.

PVdF can be seen to have been used in single element and array transducers, for a wide range of electroacoustic applications. Reported sensitivities are reasonably similar to those achieved with commercial ceramic transducers, and there have been no reports of de-poling through mechanical or electrical strain. It appeared therefore, that there were no constraints on the application of PVdF for the design of an array transducer aimed at NDT applications.

CHAPTER 2 - THE PROPOSED ARRAY TRANSDUCER

2.1 General Proposals.

From the discussions and considerations outlined above, the proposal was made that a sheet of PVDF could be constructed with an x-y matrix of conducting elements acting as active areas (Figure 8). If these elements were accessed by digital switching, the crossing points of the array elements would act as individual pulse-echo transducers. A high speed scanning technique would therefore be made available for defect location and sizing in a variety of materials.

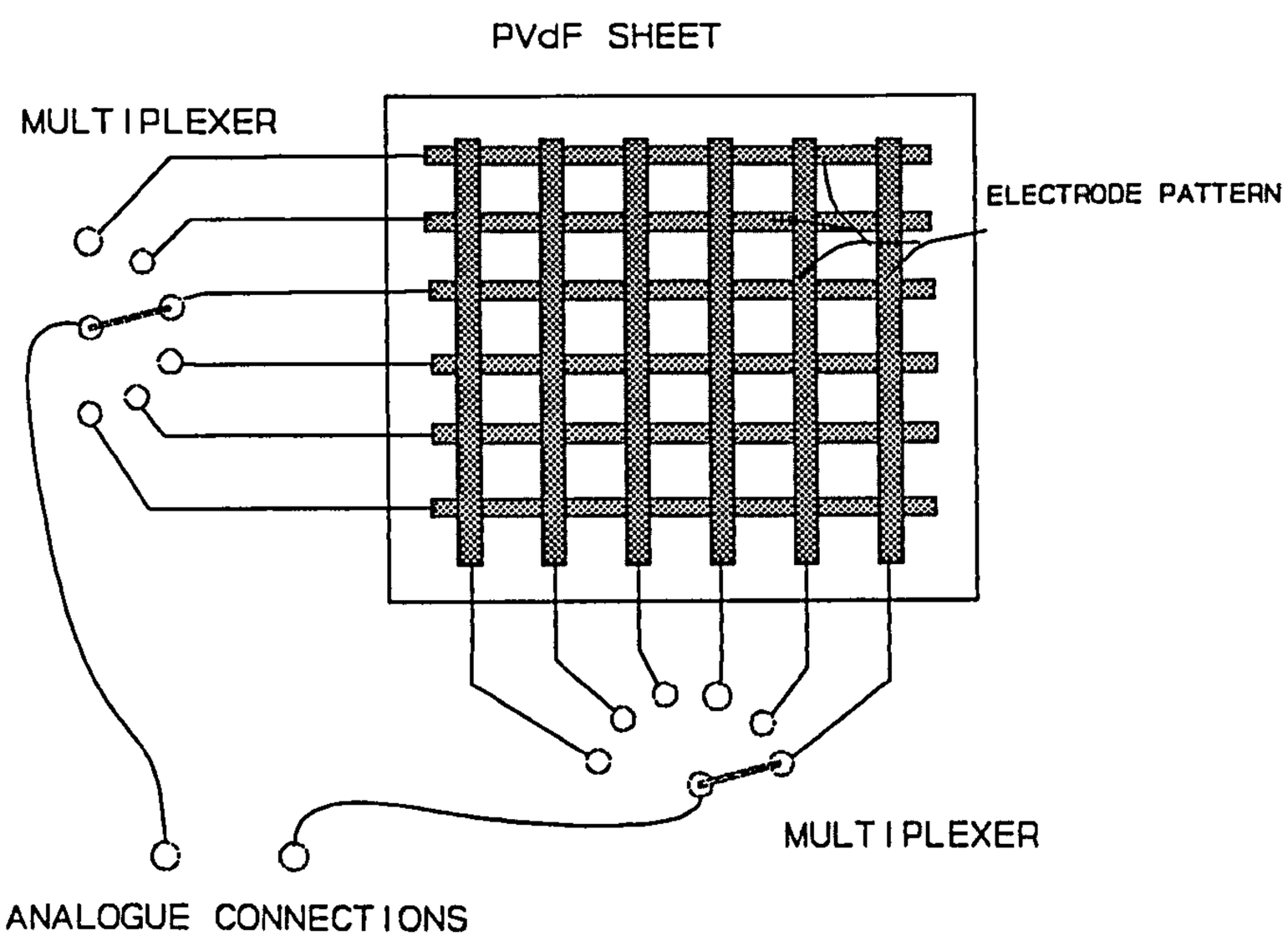

Figure 8: Configuration of the Proposed Array Transducer.

Because of the inherent flexibility of PVdF, it was envisaged that this sheet could be coupled onto curved surfaces directly, without the need for a water path and multi-axis manipulator. Also,

because of the low acoustic impedance and clean pulse shape, the proposed mat probe should be of use in detecting delaminations in GRP and carbon fibre composites. An advantage would also be offered in the time taken to complete a scan, since the probe itself does not need to be re-located during the operation.

2.2 Theoretical Considerations.

From the discussions outlined in the introduction, it was clear that a flexible probe, without any rigid backing material would exhibit a reduced efficiency of electroacoustic conversion compared to the published results mentioned above. The earlier workers had all used clamped or backed PVdF elements. It was hoped, therefore, to model the insertion loss from an air-backed PVdF probe coupling into various materials to determine the likely sensitivity of the arrangement. However, it was considered likely that the sensitivity would be sufficiently low as to require a purpose built pre-amplifier exhibiting wide bandwidth, low noise and a high input impedance.

One other obvious consideration was that of maintaining consistency over a relatively large area. This applies both to the laminating of protective layers on the probe surface, and the eventual coupling of the probe onto the samples. There is no simple method for calculating the effect of variations in these parameters, but work by Silk and others (Ultrasonic Transducers for Non-destructive Testing. Adam Hilger Ltd. Bristol. (1984).) hints at a critical thickness for coupling layers of 10 microns. It was anticipated therefore that bond thicknesses, protective coatings and probe-surface couplant layers should be made smaller than this where practicable.

It was also anticipated that the transducer and leads would require comprehensive screening from electrical noise, due to the pre-amplifier's high input impedance. However, it was first deemed necessary to obtain some realistic signal/noise ratios in the laboratory.

2.3 Limits of Spatial Resolution.

The angular resolution of a transducer array is strongly dependent on the way in which it is utilised. Phased array scanners exist, (and are used daily in hospitals around the world) which focus, and steer a beam of ultrasound, by transmitting phase-shifted signals from a group of regularly spaced sources. The beam width in the focused zone is less than 1mm, for ultrasound frequencies between 3.5 and 10 MHz propagating in organic material with assumed velocity 1540 m/s. It is possible that the phased array technique could be applied to an X-Y matrix transducer to produce similar resolutions at specified depths.

However, in typical NDT applications, the depth of a defect will not be known, and focused probe arrangements are not widely utilised. Under circumstances when only one element of an array is energised at a time, a worst-case approximation for angular resolution can be readily obtained from the diffraction equations for a single rectangular slit.

Consider each element to be a slit of width d, whose length is much greater than its width, so that effects from the ends of the slit can be ignored. Through the slit passes continuous radiation of wavelength λ.

Then at a distance L which is large compared with d or λ, the variation of intensity with angle is given by the Fraunhofer diffraction equation

$$I(\theta) = \left(\frac{\sin(u(\theta))}{u(\theta)}\right)^2 \qquad (2.1)$$

where

$$u(\theta) = \frac{\pi d}{\lambda}\sin(\theta) \qquad (2.2)$$

The first diffraction minima occur at +/- values of θ for which

$$\sin(\theta) = \frac{\lambda}{2d} \qquad (2.3)$$

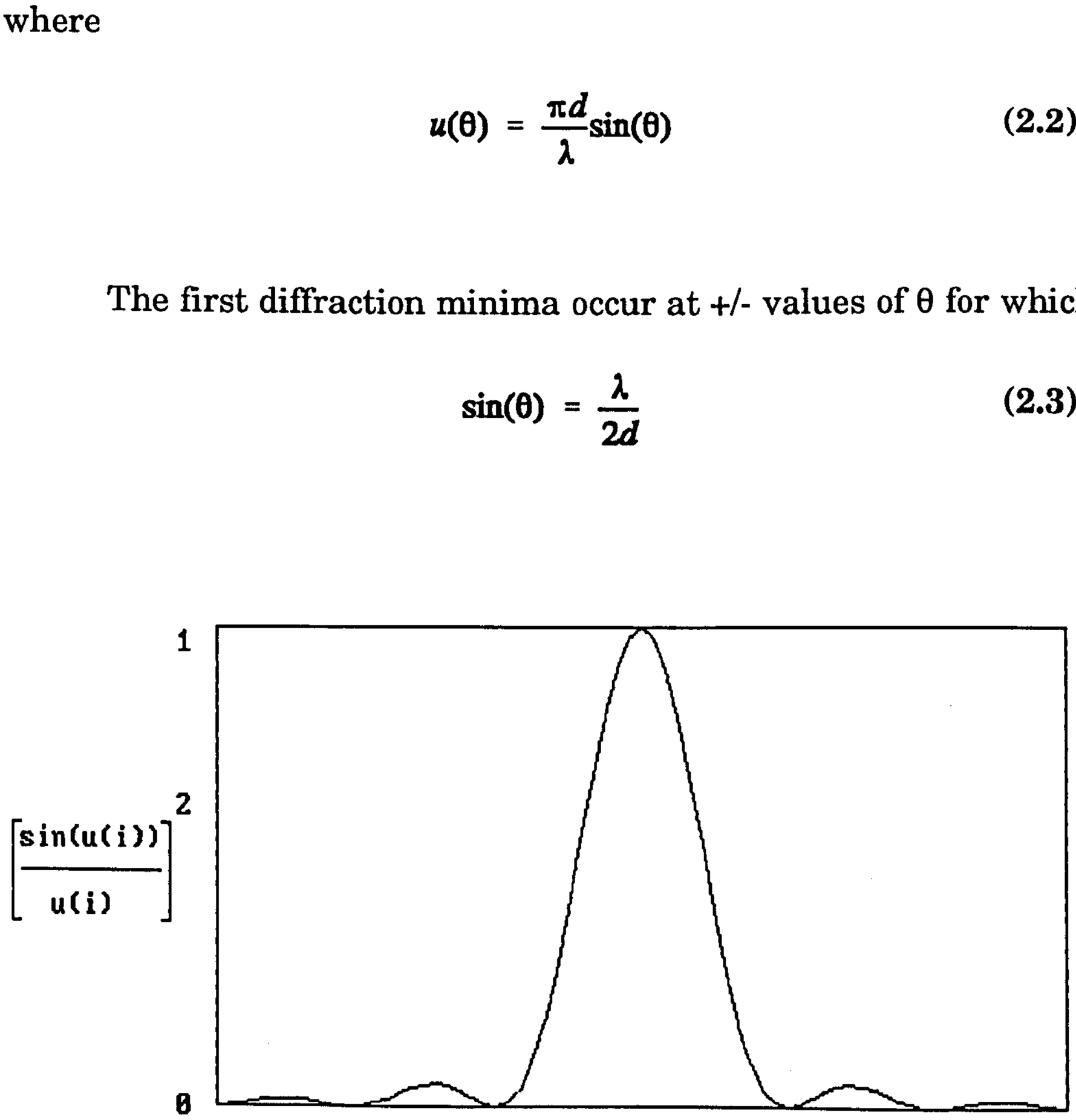

The graph of intensity against incident angle clearly shows the rapid loss of sensitivity off-axis. For a 5MHz, 5mm diameter transducer in water, the beam width is around 5°, but the intensity is 6dB down at only 1° either side of centre.

Looking at Figure 9, it is clear that the limit of resolution of a number of these elements depends on the separation between them (k), and the round trip return distance (2L), such that

$$\frac{\lambda}{d} \textit{ must be less than } \frac{k}{L} \qquad (2.4)$$

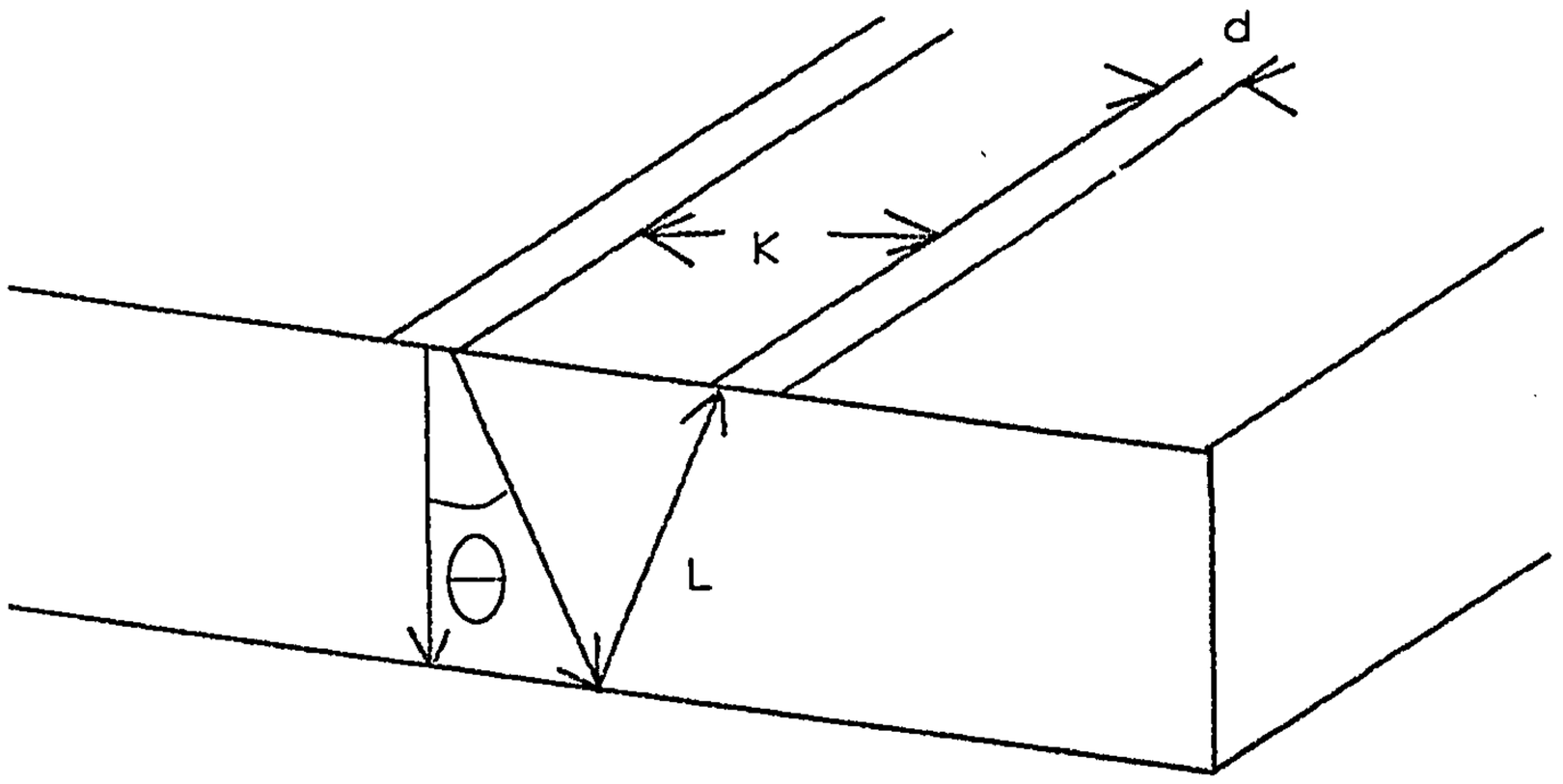

Figure 9: Calculation of the Spatial Resolution of two adjacent Array Elements.

However, to keep θ small, the width of the element d should be made as much greater than the wavelength λ as possible.

As an example, a 5MHz compression wave in 5940m/s steel has a wavelength λ of 1.2mm.

In order to resolve defects in steel up to a depth of 10 mm therefore, equations 2.3 and 2.4 give the requirement that

$$k > \frac{12}{d} \qquad (2.5)$$

The diameter of the transducer needs to be optimised for the depth range over which the transducer is expected to operate, since d should be as large as possible to keep θ small, and as small as possible for the best linear resolution. Setting $d = 4*\lambda$ (approx 5mm) gives a reasonable compromise up to 50mm in steel, where θ is about 7°.

This also sets the minimum separation between elements at 2.5mm, and adding the width of the elements (5 mm) the best possible lateral resolution for this array is 7.5 mm.

For sample thicknesses comparable with d and λ the situation improves. This is an area known as the "Near-Field", in which the variation of intensity within the beam obeys Fresnel, rather than Fraunhofer diffraction, and the beam does not begin to diverge appreciably. The length over which the near field is considered to extend is given by

$$L \leq \frac{d^2-\lambda^2}{4*\lambda} \qquad (2.6)$$

For a (circular) 5 MHz probe with a diameter of 5 mm, this gives a near-field depth which is typically of the order of 5 mm in metals, and around 20 mm in water. This means that a transducer for the

examination of thin sheets of material could be made with much smaller element widths, and consequently greater resolution.

The transducers constructed during this research had element widths based on the Fraunhofer resolution limit, however, since the electrical connection to the elements was one of the more difficult aspects of transducer manufacture in the laboratory. Also it was not clear whether the electronics could be designed with a short enough dead-zone to image in the near field. These difficulties are discussed later, but it was clear at this stage that 5mm elements would give a good idea of the success or otherwise of the array transducer technique, which could perhaps be followed up in a later study to include high-resolution near-field array imaging.

Some further improvement in these figures might also be expected theoretically for a PVdF transducer, since the clean single cycle pulse has a frequency spectrum with much of its energy in the higher frequency components. The expectation is, therefore, of a slightly narrower beam profile than the Fraunhofer prediction, which is based on a continuous wave source.

Overall however, there seems little to be gained by reducing element widths below 5mm, or separations below 2.5mm for the inspection of metals, unless either much higher frequencies, or phased array methods will be used. This result agrees with the consensus of transducer manufacturers, since the smallest commonly available 5 and 10 MHz transducers have diameters of 5 mm.

2.4 Anticipated Sensitivity of a PVdF Transducer.

The electrical and mechanical impedances of a piezoelectric transducer are complex and interrelated, and various models of equivalent circuits have been proposed in attempts to predict probe characteristics. Arguably the most popular of these is the lumped equivalent circuit model proposed by Mason in 1948 (Ref 16). However, the use of a negative capacitance in this model gave rise to some considerable confusion as to the relationship between the physical components of the transducer and their equivalents.

An alternative model was proposed by Krimholtz, Leedom and Matthaei in 1970 (Ref 17).

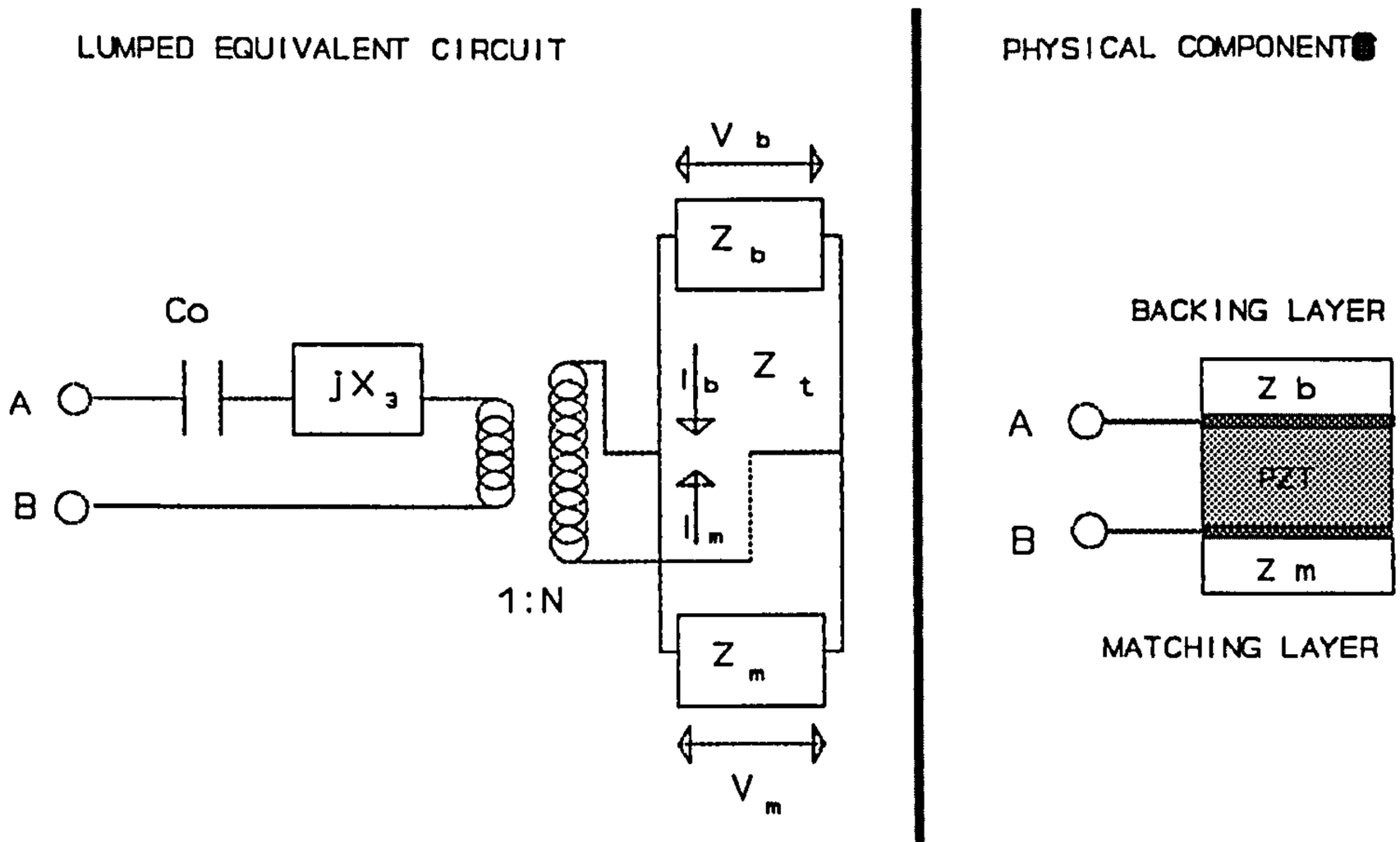

Figure 10: KLM Model of a Piezoelectric Thickness Expander Plate.

This KLM model, as it is now known, proposes that the acoustic branch of the circuit be modelled as a transmission line terminated at each end by the impedances of the materials bounding the transducer. The transmission line is driven at its midpoint by the electrical branch of the circuit, acting through a frequency dependent "transformer".

The terms involved in the circuit are as follows;

c_0 (the clamped capacitance) is derived from the parallel-plate capacitor equation

$$c_0 = \frac{A * e_{33} e_0}{t} \qquad (2.7)$$

where A is the area of the metallized surface

t is the plate thickness

and ε is the dielectric permittivity

$$X_3 = Z_t * (M^2) * \sin\left(\frac{t\omega}{V_t}\right) \qquad (2.8)$$

where Z_t is $A*Z_0$ (the specific acoustic impedance of the probe material)

M is defined as $h_{33}/\omega * Z_t$

V_t is the speed of thickness-mode waves

The turns ratio of the transformer is frequency dependent, and is given by

$$N = \left(\frac{1}{2M}\right) * \mathrm{cosec}\left(\frac{t\omega}{2V_t}\right) \qquad (2.9)$$

As mentioned in Chapter 1, Silk and Bainton (Ref 14) have developed an iterative computer algorithm based on the KLM model to predict the frequency dependent impedance of piezoelectric transducers, but have not published details of the algorithm itself.

For this study, it was considered important to obtain a predicted sensitivity for the proposed array transducer, compared with a manufactured ceramic transducer, at the frequency of interest (i.e. 5 MHz.) An intuitive understanding of the terms in the KLM model was therefore sought, in order to examine its appropriateness to the problem.

As an equivalent electric circuit, the KLM model contains a number of impedance terms. Each of these can also be considered as energy either stored, wasted or radiated. A piezoelectric transducer will involve all these different terms, in electrical forms and mechanical forms.

Each of the terms in the KLM model therefore has a physical counterpart in electrical or mechanical energy. In fact the model simplifies this somewhat, by assuming all the electrical losses to be contained in the driving circuitry, (Typically a nominal 50 Ω resistor in series with a voltage source) and neglecting mechanical losses within the transducer material (i.e. the Loss-less transmission line).

Considering each of the terms independently, we have therefore;

C_0, the clamped capacitance, a store of electrical energy

jX_3, the back emf generated by the reflection of the acoustic wave from the faces of the transducer. This is phase shifted by the ratio of input frequency to resonant frequency.

Z_t, is the specific acoustic impedance of the probe material, and is required to equate electrical to mechanical impedances.

The transformer, of course, converts the electrical impulse into an acoustic wave. This section of the circuit also contains the piezoelectric coefficient h_{33}, and is frequency dependent, since typically the transducer will have a strong resonance.

A PVdF transducer with a thickness of 40μm will have a nominal resonance of approximately 30 MHz, but this is not a strong resonance, due to the high ultrasonic attenuation in PVdF.

The lack of a strong resonance and the fact that the PVdF in this project will be operating a long way from resonance, make the assumption of a loss-less transmission line, and the infinite reflections in the jX and transformer impedances much less valid in this study, than in a ceramic transducer. Since it is possible to obtain a comparative estimate of transducer sensitivity in this situation by a much simpler analysis, it was considered unnecessary to proceed further with the KLM model, unless the predictions of the simpler model were innaccurate.

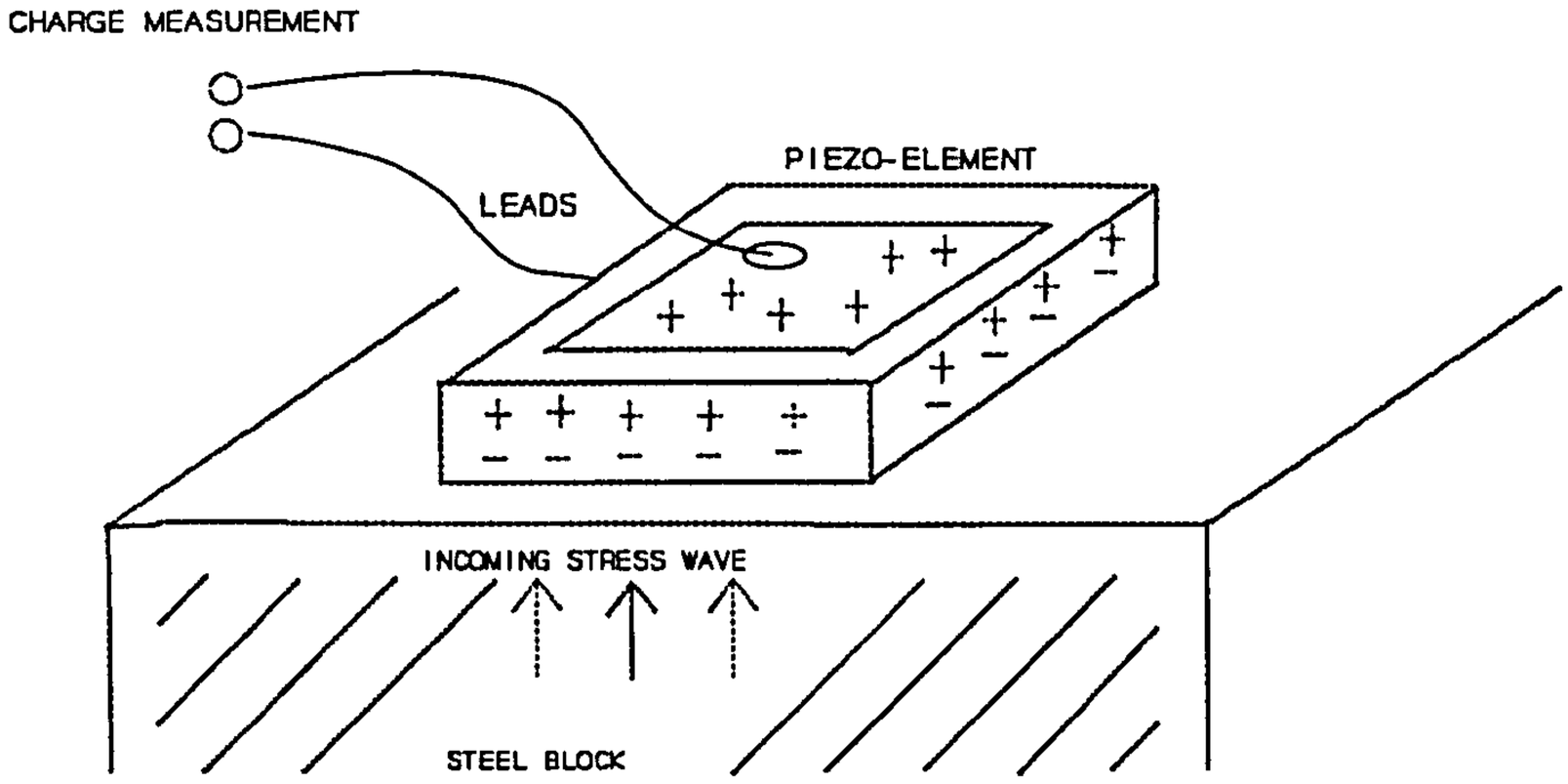

Figure 11: Estimation of Receiver Sensitivity for Piezoelectric Thin Films.

The sensitivity of a thin film transducer may be estimated by considering a pressure wave in a material, (steel, for example) as it is passed to a piezoelectric element on the surface of the material and converted into a charge density.

The plane pressure wave, considered to extend beyond the lateral dimensions of the transducer, is passed to the transducer material according to the Transmittance discussed in Chapter 1.

That is,

$$T = \frac{2\,Z_2}{Z_1+Z_2} \qquad (1.4)$$

For example,

Steel has $Z_1 = 47 * 10^6$ kg/m^2-sec

PZT has $Z_2 = 30 * 10^6$ kg/m^2-sec

and PVdF has $Z_2 = 2.7 * 10^6$ kg/m^2-sec

So $T_{steel/PZT} = 98\%$

and $T_{steel/PVdF} = 29\%$

Furthermore, as the stress wave travels through the transducer material, it generates charge on the electrodes according to the difference in pressure across the thickness of the transducer. Typically, a PZT disk which has generated the pressure wave, will be 1/2 λ thick. The whole peak to peak amplitude is therefore available across the transducer. However, with thin film PVdF transducers,not all of the peak to peak amplitude of the stress wave appears across the transducer.

Assuming the incident wave to be sinusoidal, then at an instant in time, the stress (X) at a position s is given by;

$$X(s) = A*\sin\left(2\pi\frac{s}{\lambda}\right) \tag{2.6}$$

The differential of this is the cosine function, which implies that the difference in stress across a thin sheet will be a maximum if the sheet is centred on s=0, $\lambda/2$ etc. That is, the response of the transducer is $\pi/2$ radians out of phase with the incoming stress wave.

By symmetry arguments, the centre-line of the transducer can be set at s=0, and the variation of the available amplitude with the thickness (t) of a transducer is then,

$$X(t) = 2*A*\left(\sin\pi\left(\frac{t}{\lambda}\right)\right) \tag{2.7}$$

For a transducer made of PVdF sheet (which is typically 50 microns thick,) the wavelength of a 5 MHz compression wave at 2200 m/s is 440 microns.

This gives,

$$X(t) = 0.7 * A \tag{2.8}$$

or

$$\frac{X(t)}{X(p-p)} = 35\% \tag{2.9}$$

For a given stress wave in a metal such as steel, it is clear that a 50 micron PVdF transducer will be receiving only 29% of the acoustic energy in the wave, and will be responding to only 35% of the wave amplitude at 5 MHz. That is, the PVdF transducer could, at best, only be one tenth as sensitive in this application, as a half-wave resonant PZT transducer.

In addition, the piezoelectric stress coefficient d_{33} for PZT-5H is given as $520 * 10^{-12}$ C/N (Table 1) whereas for the commercial PVdF the figure quoted is around $33 * 10^{-12}$ C/N which implies a further reduction in sensitivity by a factor of roughly 15.

The charge generated is usually measured by a voltage amplifier, relying on the capacitance of the transducer element to convert charge to voltage. This "Clamped Capacitance" can be calculated using the parallel plate capacitance equation (2.6).
Using the same comparison as before, a 5mm disk of PZT, 0.6mm thick with ε_r of 1200, will exhibit a clamped capacitance of 1400pF. A 5mm PVdF disk with $\varepsilon_r = 12$, and a thickness of 50 microns, however, has a clamped capacitance of 170pF. That is, for the same charge generated, the PVdF will exhibit roughly 8 times the output voltage as the PZT transducer.

Combining the results from these simple calculations predicts that a typical PVdF transducer 50 microns thick will be roughly 20 times (or 26 dB) less sensitive to an incoming pressure wave than an equivalent PZT transducer, although stray capacitance in the leads and pre-amplifier may affect this figure strongly.

The proposed array transducer may have to include areas of opposing metallisation which are not being affected by the stress wave however, and it is clear that these will act as capacitors in parallel with the transducer's active area, reducing the voltage sensitivity still further. (Figure 12.)

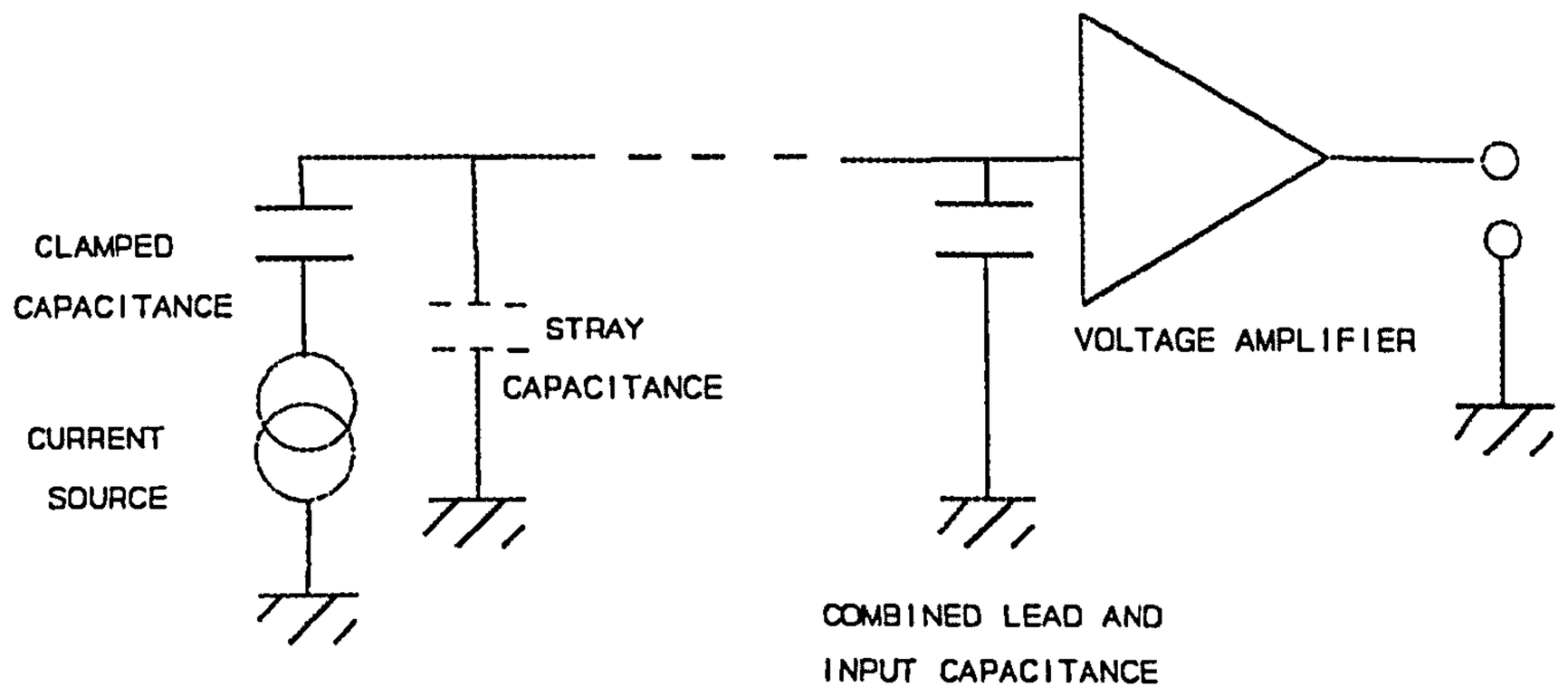

Figure 12: Simplified Transducer Configuration Showing Stray Capacitances in the Circuit.

It is not possible to avoid this, so consideration was given to the use of a high frequency charge amplifier. However, the shielding requirements of these sorts of amplifiers would be hard to implement in the laboratory. Also, each element would need an individual amplifier mounted as close to the transducer as possible, reducing the flexibility of the array transducer below acceptable limits for the proposed use. Consequently, voltage amplifiers were used throughout these investigations.

Modelling the amplitude of stress waves generated from either material is considerably more complex, and requires the pulse generator circuitry and the physical configuration of the transducer being known in detail.

It is reasonable to assume, with a 50 Ω driving impedance, that at frequencies much less than the nominal half-wave resonance, the voltage across a PVdF transducer will follow the input pulse voltage accurately. However, because of the presence of matching networks, loaded backing materials and front-face matching layers, this assumption is not valid when applied to a commercial half-wave resonant PZT transducer. It is unlikely therefore, that the simple calculations used above would yield accurate comparisons of the stress wave amplitude generated by the two types of materials.

As a very rough first estimate, the difference in piezo-coefficients, the much smaller amount of electrical energy stored in the clamped capacitance of the PVdF, and the acoustic impedance mismatch outlined earlier, imply that PVdF will be considerably less effective as a transmitter than the PZT.

Allowing 6dB drop for the stray capacitance in receive mode, and assuming the piezoelectric effect to be perfectly reversible, it is not expected at this stage to obtain better sensitivity than around 60dB less than a PZT transducer in this application.

Acknowledging the simplicity of these calculations, and the number of unknown variables and assumptions made, the earliest experiments performed in this study were designed to obtain realistic figures for the sensitivity of an air-backed PVdF transducer. This was required to determine the impulse voltage levels and pre-amplifier arrangements necessary for the proposed array transducer.

CHAPTER 3 - PRELIMINARY EXPERIMENTS

3.1 Determination of Signal Levels.

As mentioned in chapter two, it was decided that the first investigation should be to determine signal levels in a realistic, simple air-backed PVdF transducer configuration. The simplest possible configuration was chosen and is shown in detail in Figure 13.

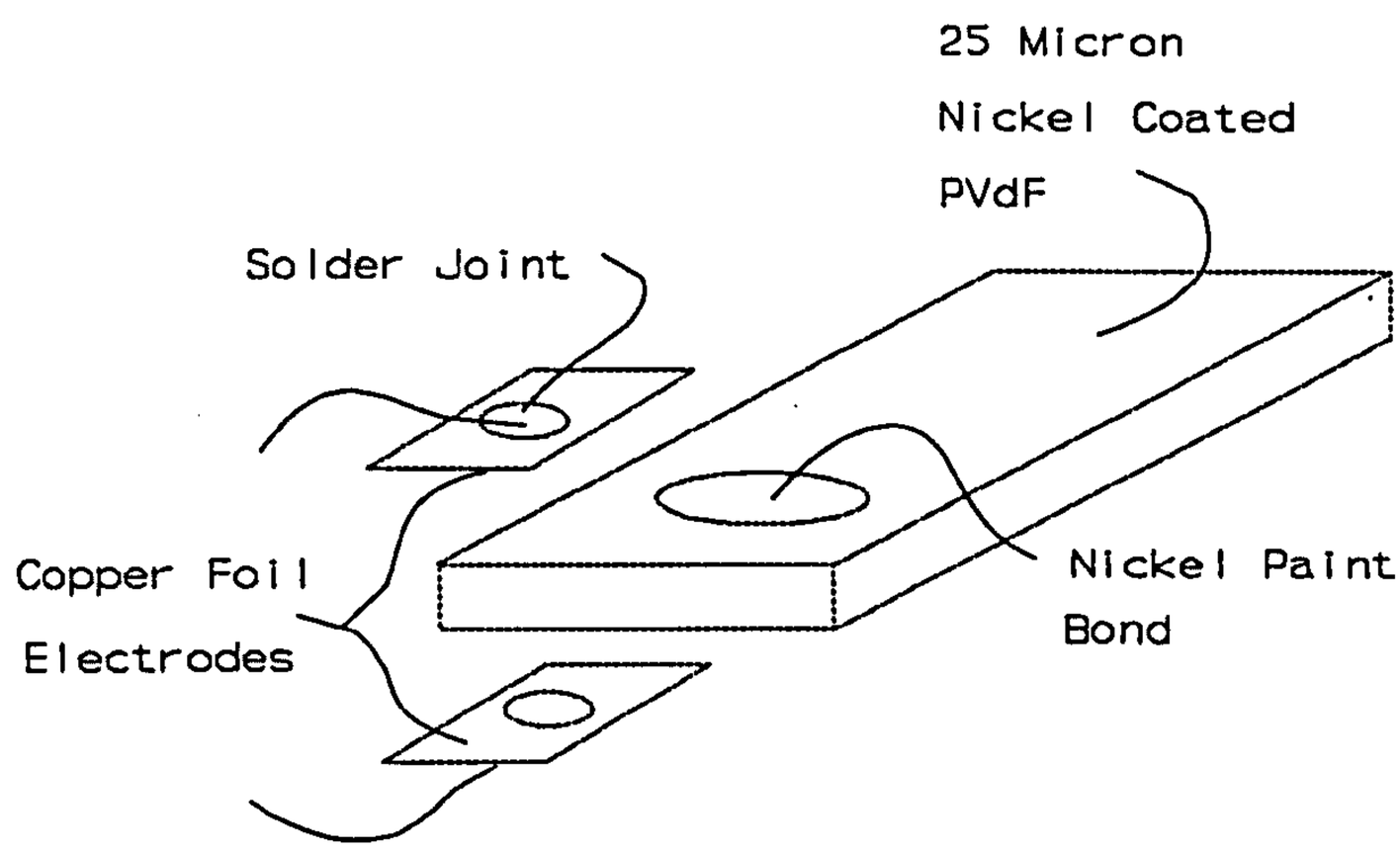

Figure 13: Construction of a Simple Air-Backed PVdF Transducer.

A number of these transducers were made from nickel coated 40 micron PVdF sheet, and the experiments repeated with each, to eliminate some of the uncontrollable variables such as contact resistance or local variability of the piezo-coefficients. The active area was 10mm square, and the wire connections were made by soldering to a small piece of copper foil which was attached to the vapour deposited nickel coating by conductive paint. The PVdF surfaces were then coated with a self-adhesive laminate

approximately 1 micron thick. This coating had previously been applied to the front faces of several PZT transducers of different frequencies, and had been shown to have a negligible effect on sensitivity or bandwidth.

Using the Nortec NDT-150 test set, the pulse shape and comparative sensitivity generated by these probes was determined for compression wave transduction into a standard 25 mm steel test block.

Photographs of the traces obtained are shown in Figures 14 to 16 and the pulse shape for the PVdF transducer in TX/RX mode can be seen to agree overall with the general characteristics of a wide bandwidth transducer. The peak-to-peak amplitude of the echo signal was restored by the application of 30dB gain on the test set for the PVdF receiving the acoustic wave, 40dB for transmitting and 70dB for transmitting and receiving, referred to an average figure derived from three nominally identical commercial PZT probes, 10mm in diameter and tuned to 5 MHz.

None of the PVdF transducers made in this way varied by more than 6dB from the average result, although the probe construction was fragile, and under a combination of handling and electromechanical stress, the electrical connections tended to break down after a short while.

Further experiments with varying pulse widths and amplitudes obtained the anticipated results in that the received peak-to-peak signal level varied linearly with transmit pulse voltage between 5 and 400 volts, and the PVdF showed less than 3dB variation in sensitivity for pulses between 100nS and 20 μS duration.

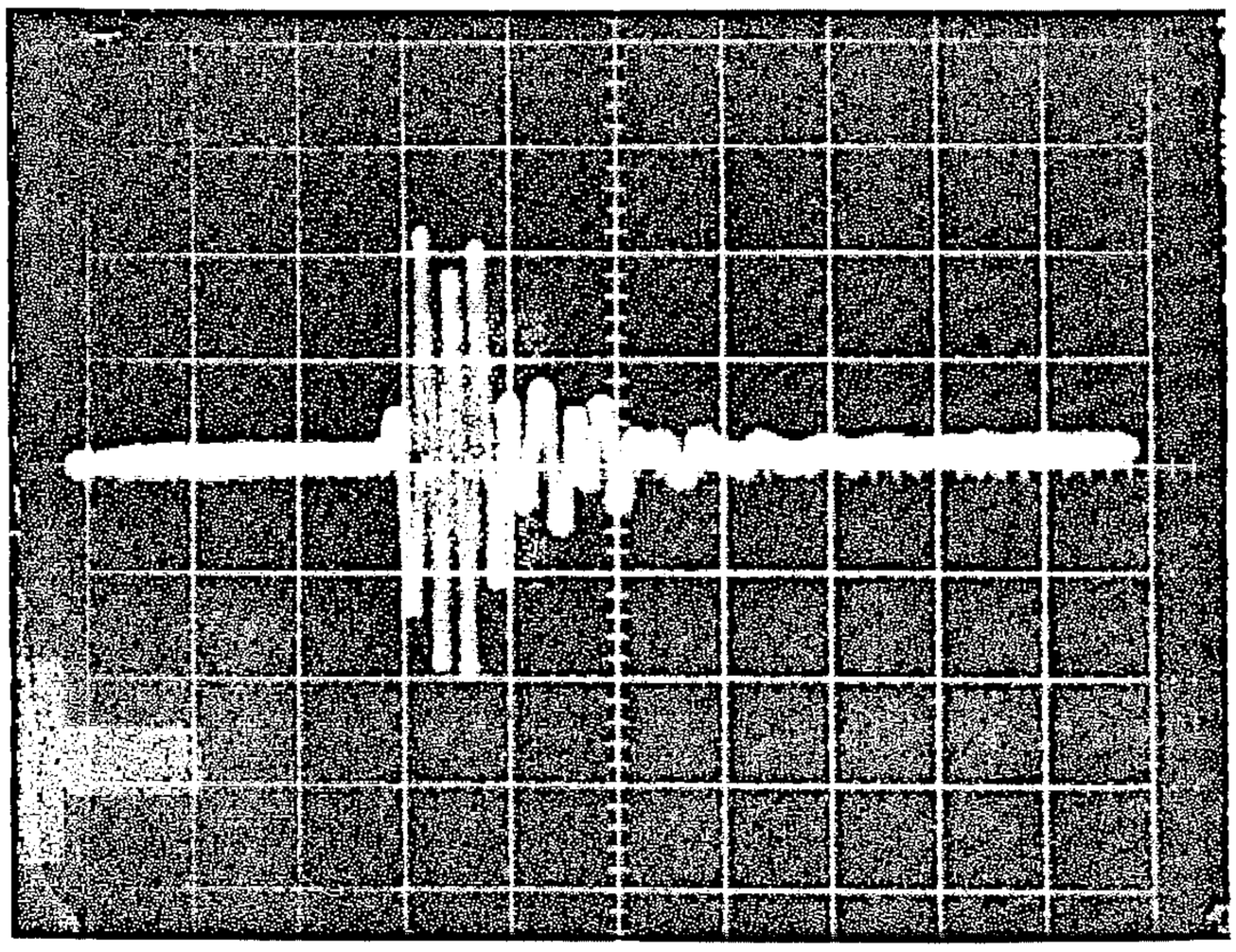

Figure 14: Back-Wall Echo Transmitted and Received by a PZT Probe coupled into 25 mm Steel. (Gain Setting: 0dB)

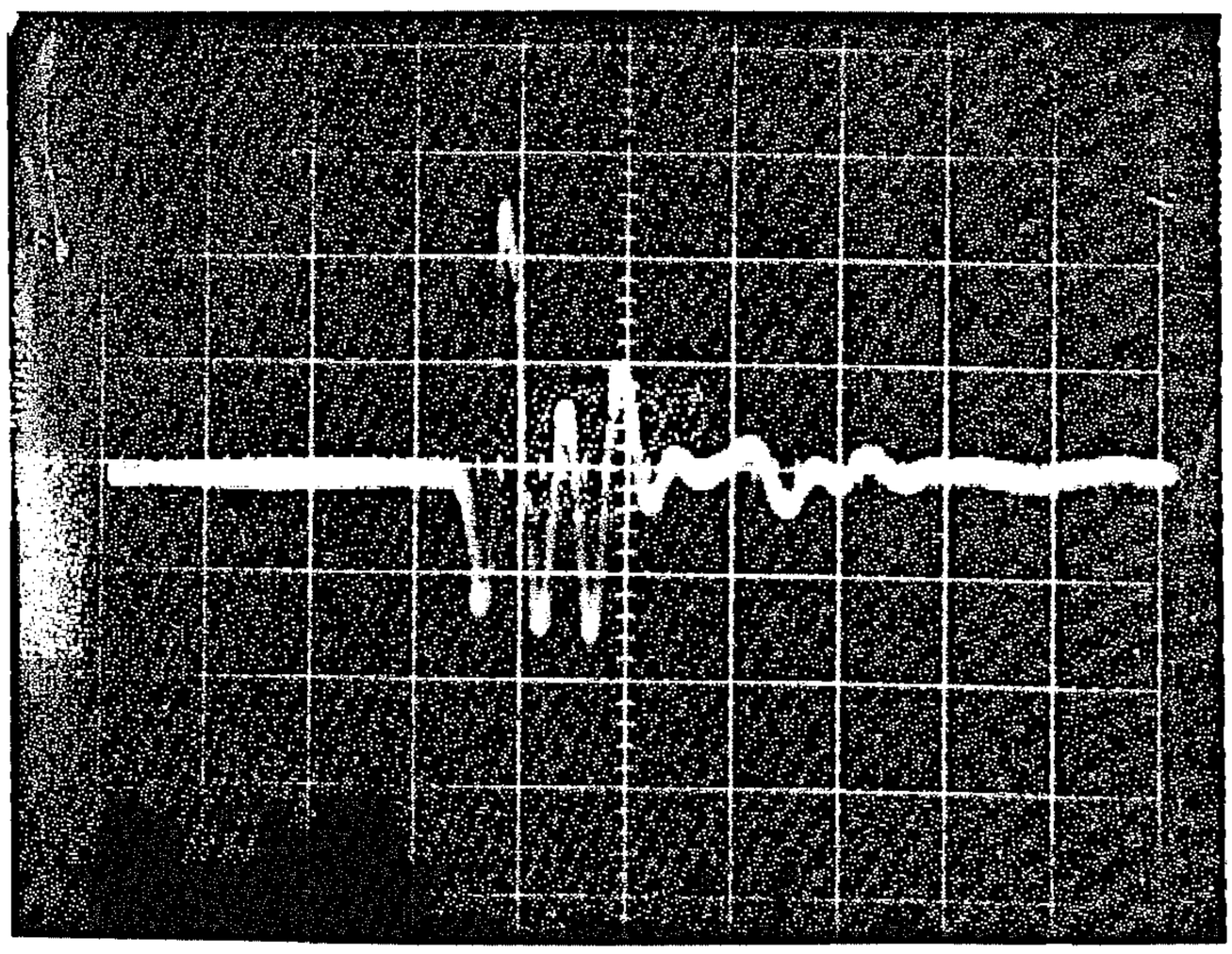

Figure 15: Back-Wall Echo Transmitted by the same PZT Probe, Received by the PVdF Probe. (Gain Setting: 30dB)

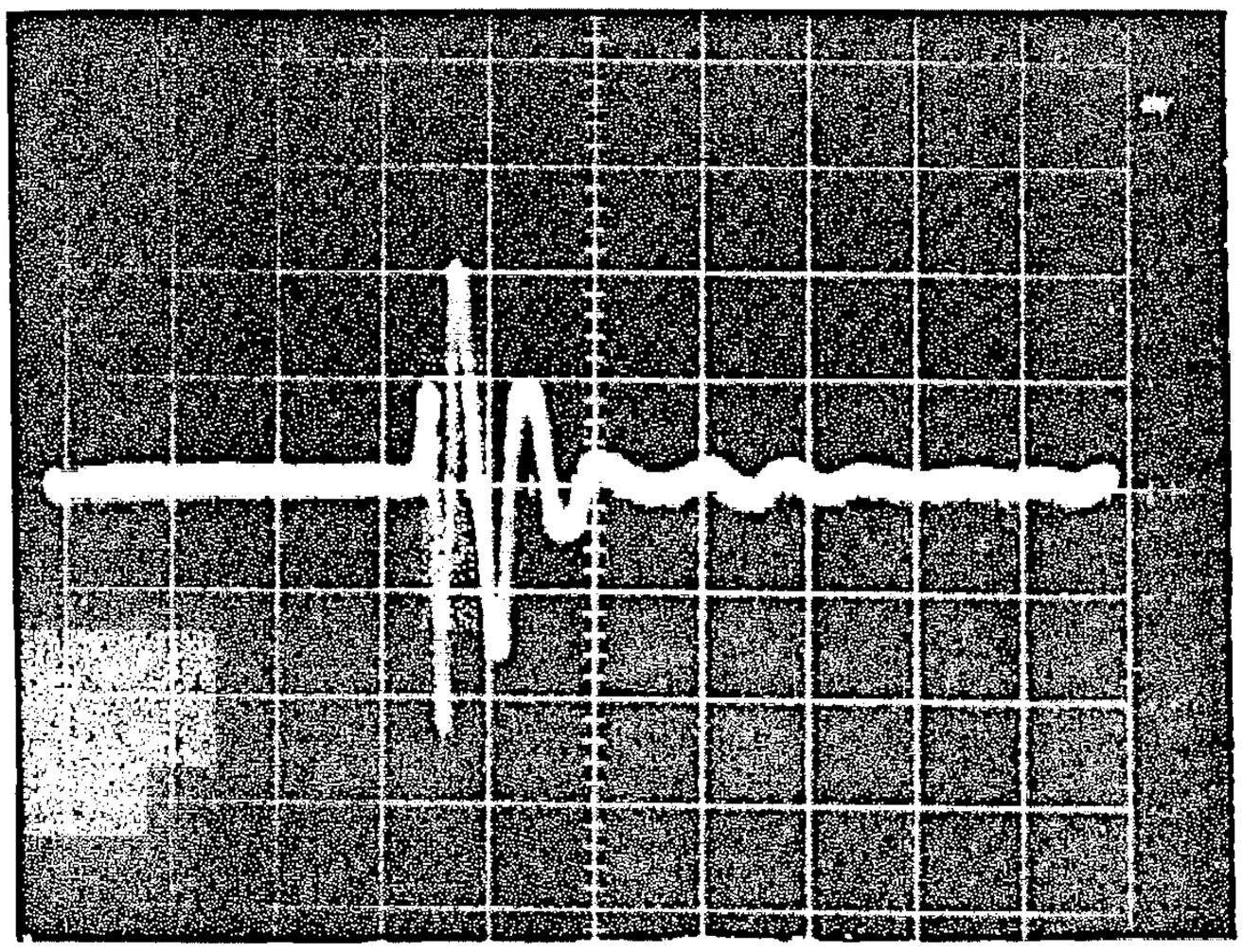

Figure 16: Back-Wall echo Transmitted and received by the PVdF Transducer (25mm Steel at 5MHz. Gain Setting: 70dB)

3.2 The 2 x 2 Matrix Prototype

A number of issues arose through the experiences with the initial configuration. Among these was the requirement for a good electro-mechanical bond between the connecting wires and the areas of metallisation. The copper foil came away from the nickel plating after an average of 30 minutes' use, and had to be re-connected.

A supply of self adhesive copper foil was available, and the question arose whether, if the wires could first be soldered to this, it would be possible to rely on capacitive coupling between this foil and a sample of un-plated PVdF on which it could then be laid.

It was expected that the adhesive layer, being considerably less than 1 micron thick, might have little or no effect on the amount of charge induced in the copper foil, and that therefore the high input impedance of the pre-amplifier should detect the same piezoelectric voltage sensitivity as for a vapour-deposited metallisation. This technique was used to make a 2 x 2 array on a sheet of PVdF which had no metal coating.

The quasi-static loads applied to check that the PVdF was acting as a piezoelectric element showed that, to a first approximation, these assumptions were valid, and the 2 x 2 array proved to be far more robust than the earlier prototypes.

However, two effects obscured the array's sensitivity at ultrasound frequencies. One was the 15 micron thickness of the self-adhesive copper foil, and the other more serious problem was a wideband crosstalk effect which masked any possibility of determining the input pulse location. In effect, the signal appeared on either copper element with equal amplitude, regardless of the location of the transmitting transducer.

3.3 The 8x8 Matrix Prototype and Differential Amplifier.

On the basis of these results, an 8 x 8 array was commissioned from Fulmer Yarsley, one of the two main suppliers of PVdF in Britain. This array was produced with 3mm wide gold contacts at 3mm spacing, sputtered through a stainless steel mask onto 40 μm PVdF film.

After delivery, wires were attached to the linear array elements by silver-loaded epoxy, and the active areas were coated in the self-adhesive insulating layer mentioned earlier. The wires were connected through a manual switch box into a differential amplifier. One switched element from each face of the transducer was connected to either input of the differential amplifier, to reject the common-mode crosstalk and provide X-Y location.

The wideband differential amplifier was constructed to a proven design (Horowitz & Hill, The Art of Electronics, p560), and the 8 x 8 array was tested in this configuration by being coupled onto the face of the steel test block, and scanning a small diameter ceramic probe transmitter over the array area. (See Figure 17).

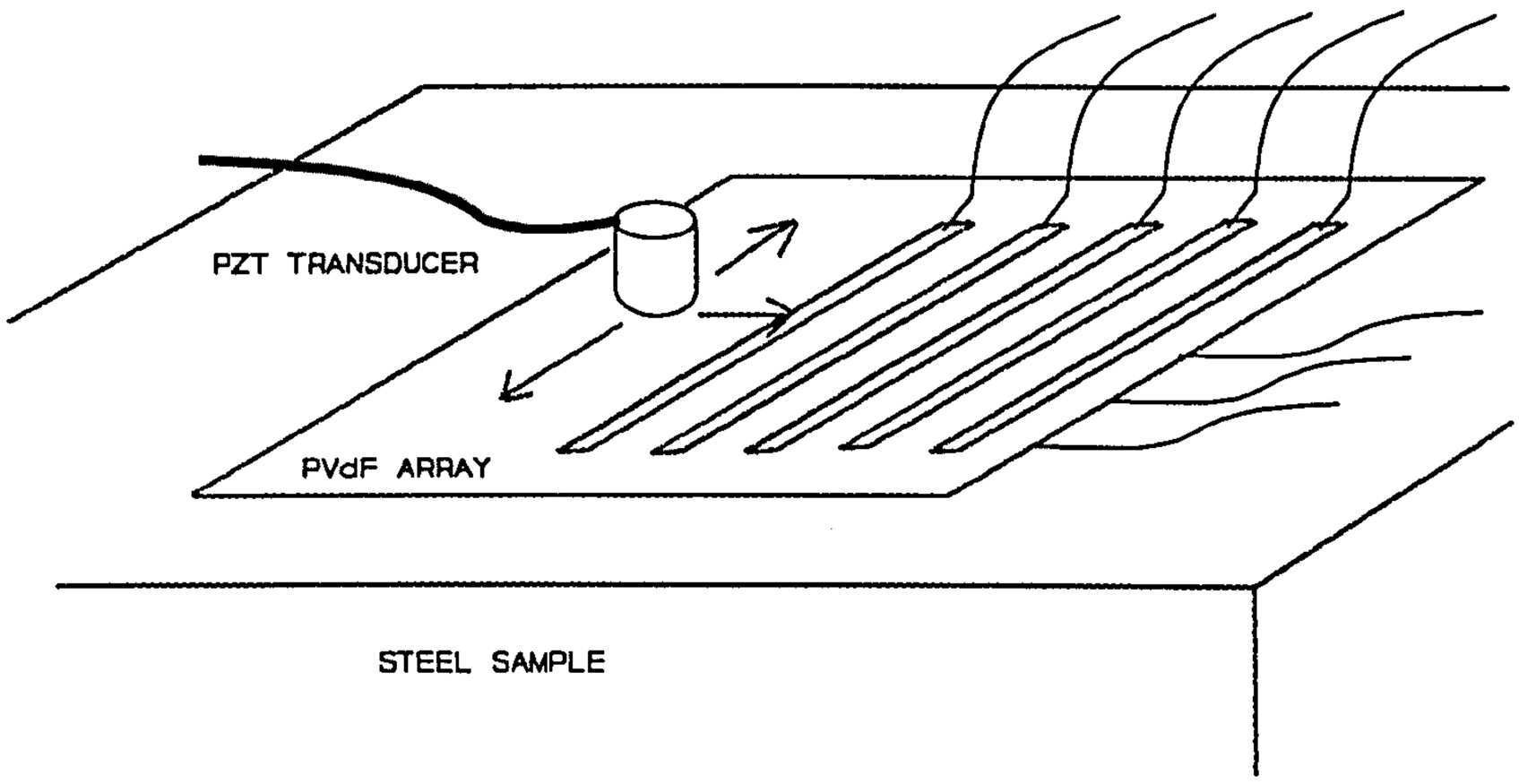

Figure 17: Method of Testing the 8 x 8 Array Transducer.

The most important result of this investigation was unexpected in that the upper surface of the array showed good sensitivity along the entire length of the switched element, while the lower surface of the array was giving no signal at all. This was verified by grounding the inputs to the amplifier in turn. When the array was inverted,

the same result was achieved, with the set of linear elements from the previously active face of the transducer now appearing to give no signal. This proved that it was the geometrical arrangement of array transducer and test block that had this effect. That is, that the transducer surface adjacent to the array was not able to generate any electric field relative to the upper surface.

After substantiating this result in a number of tests, it was further discovered that the elements adjacent to the test block could be disconnected completely, without affecting the sensitivity of the upper surface. That is, strong ultrasonic echo signals were obtained with the transducer attached to the test-set with a single wire.

These investigations led to the conclusion that the steel sample was acting as an effective electrical ground, whether it was connected to the circuit or not, and that the charge generated by that side of the PVdF nearest to the sample, was being 'leaked' into the sample.

Since most of the materials of interest to NDT applications are metals, the results posed a real problem for the feasibility of the simple array transducer as it had been first conceived.

The application of a ground plane was considered, but the way the multiplexing worked at this stage was to reference the charge generated between two points on the PVdF array. A ground plane would allow stray capacitance, and acoustic sensitivity along the length of any switched element. Obviously, if X-Y positional switching were to be maintained, another technique would have to be adopted for driving the transducer.

The format which was decided on was to produce the array transducer from two sheets of PVdF, bonded together over a central ground-plane. The linear elements were arranged orthogonally on the outer faces of the transducer. One element from the surface nearest the sample would be connected to an amplifier through a multiplexer, and would receive along its length. The transmit pulse would be connected to a single element orthogonal to the receiver, on the outer face of the transducer. In this way, X-Y location of the echo source could be obtained. While it is accepted that this is only true for a flaw or back wall which is parallel to the top surface of the specimen, the same constraint also applies to conventional scanning techniques.

3.4 Summary of Preliminary Results.

Investigations have shown that an air backed PVdF transducer of the type proposed for this study is 30dB less sensitive in receive mode, and 40dB less sensitive in transmit than an equivalent commercial PZT transducer tuned to a nominal 5MHz. This figure is likely to be worse in an array, due to the stray capacitance of the areas of linear element not directly affected by the acoustic wave, and varies roughly linearly with the number of elements in the array.

Various array configurations have been tried, and the overall conclusion was that a bi-laminar array, consisting of a central ground plane sandwiched between two sheets of PVdF was required. One set of linear elements would be energised with the transmit voltage pulse, and the other set of elements, at right angles to the first, would act as receivers. This arrangement avoids the need to switch the amplifier out of circuit for the duration of the transmit pulse, and

it was hoped that it should lead to much reduced 'Dead-time' and therefore better near field or thin film resolution.

The pre-amplifier itself needs careful design, as the DC impedance of PVdF is very high, and the 50 Ω input impedance of the usual test-set will not give the best signal/noise figure. A purpose built pre-amplifier was therefore proposed to interface the PVdF transducer to the test-set, as an impedance converter and first gain stage.

Making reliable electrical connections to the conducting elements of the surface of the PVdF remained a problem. The most reliable method so far discovered was to use silver loaded paint, and tack the insulation of the wire to the surface of the PVdF with cyano-acrylate adhesive.

CHAPTER 4 - THE 7x7 ARRAY TRANSDUCER

4.1 Construction of the Bi-Laminar Prototype Array.

The results of the preliminary investigations had shown that it was not feasible to construct a working array transducer from a single sheet of PVdF, and so a prototype bi-laminar array now had to be constructed.

As indicated earlier in Chapter 2, there is a relationship between element width and angular resolution. For the steel test block, a required depth of 30 mm was chosen, and the calculations indicated that an array with 3mm width spaced at 6mm centres would be suitable for locating flaws, without ambiguity, so these dimensions were used for this array.

A source of aluminium foil with a thickness of 0.75 micron had been located and a prototype bi-laminar array transducer was constructed as in Figure 18.

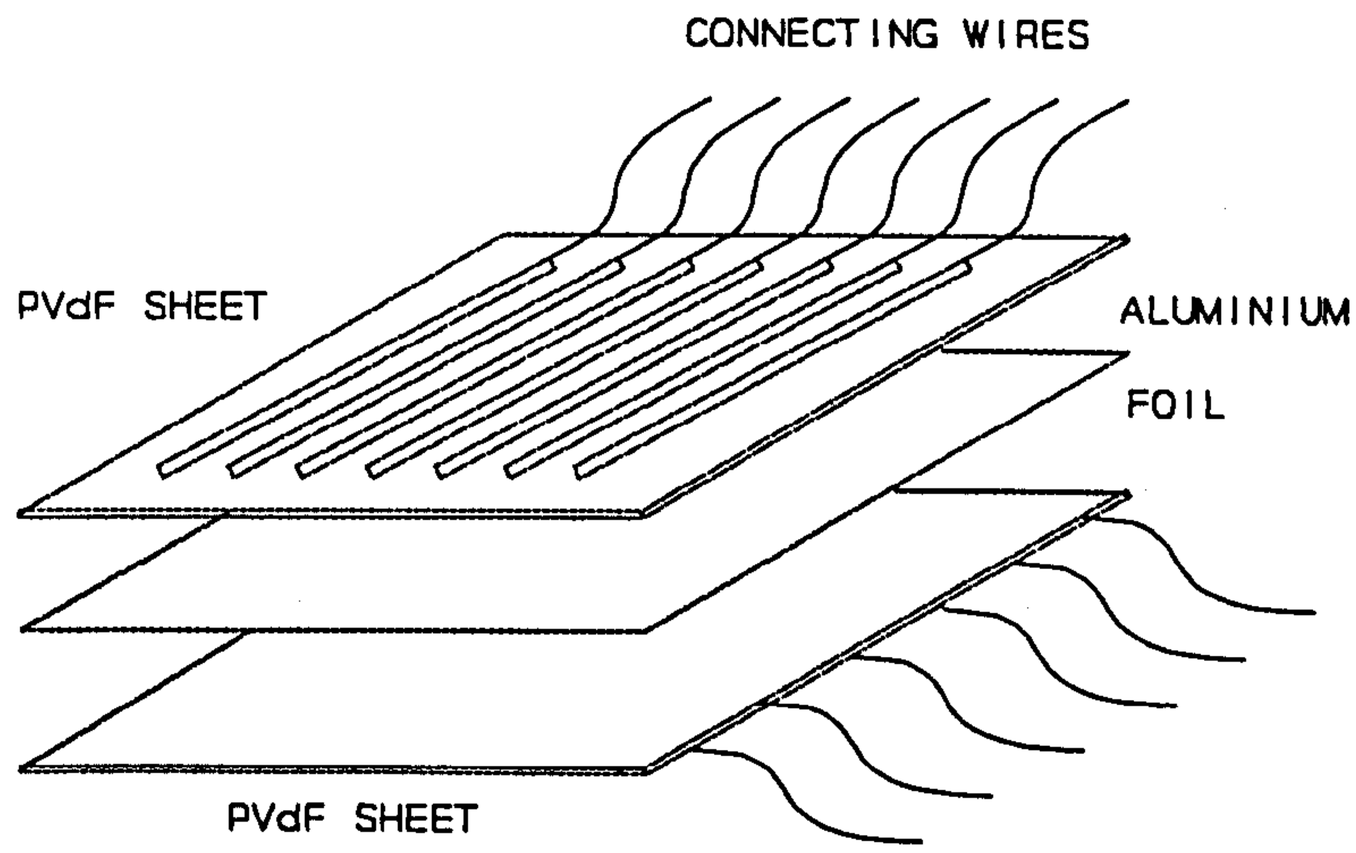

Figure 18: Construction Details of the 7x7 Array Transducer.

Two sheets of PVdF, 40 microns thick, were cut to size and cleaned with propanol. Then a sheet of aluminium foil was cut to size and laminated to one of the PVdF sheets using cyanoacrylate. A pressure of about 10 kN/m^2 was applied to this assembly while the cyanoacrylate set. The other sheet of PVdF was bonded in the same way, to the other side of the aluminium foil, leaving sufficient of the foil exposed for electrical connection. Each side of the laminate was then masked off, in the pattern of the elements, and a xylene based conductive paint sprayed onto the PVdF. The active areas of the elements were given a self adhesive protective coat, as described for the preliminary experiments.

The electrical connection to the elements was made by conductive paint. However, this was mechanically frail, and so the wires were first tacked to the surface with cyanoacrylate (As mentioned in the conclusions to Chapter 3). After the electrical connections had been made and tested, the connection area was 'potted' under araldite. This produced a 7 x 7 array transducer which was flexible, robust, and substantially waterproof (except along the edges.)

4.2 Measured Sensitivity.

Using the Nortec test-set in dual-probe mode, the transmit pulse was connected to each element in turn on one side of the transducer array, while the receive amplifier was connected to each element in turn on the other. The roles of each side were then reversed, and the experiments repeated. This was also done with the geometry of the probe and sample block reversed, as a further check. The initial results from the 25mm steel block were encouraging,

although the signal was now rather weak, and 85dB of gain had to be applied to obtain clear echo indications.

Possible reasons for the loss of sensitivity included the new, thicker electrode materials, and the complexity of the bi-laminar arrangement, but it is likely that most of the problem comes from the areas of the array that are not in the sound field, which, as explained, act as stray capacitors across the transducer. For the dimensions given, the active area has a capacitance of only 24pF, whereas the whole receiving element has a capacitance of 400pF. This would reduce the expected voltage sensitivity by a factor of 16, or about 25dB.

4.3 Determination of Lateral Resolution.

The lateral resolution of the elements in the mat was checked with a series of C-Scans. These were performed in a water bath, at a probe-to-target distance of 35 mm. During these experiments the array transducer was lightly taped to a steel backing plate. The purpose of the plate was to align the flexible array transducer with the C-scanning rig. Also, to simulate a real NDT examination, it was considered necessary to have a metal mass in proximity to the transducer for the reasons discussed in Chapter 3.

The first series of scans were made with a 5mm 5MHz PZT probe as the receiving transducer in the scanning arm, 20 mm above the array transducer. A single element of the array transducer was connected to the transmit pulse generator in the test set. Elements from the top and bottom surfaces of the transducer were scanned, and produced consistent results, as in Figures 19 and 20.

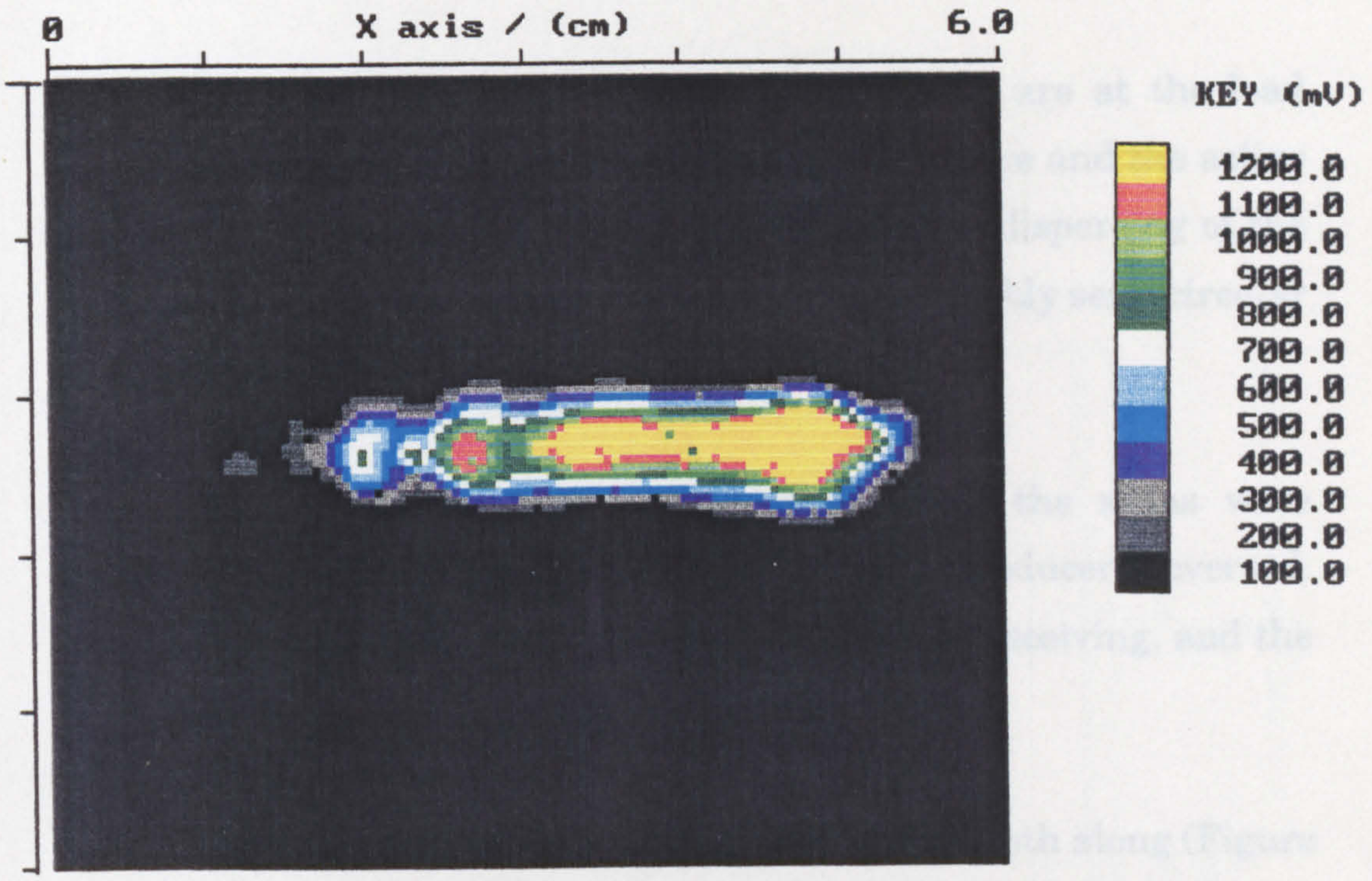

Figure 19: C-Scan Beam Plot of 7x7 PVdF Array Element (Top Surface).

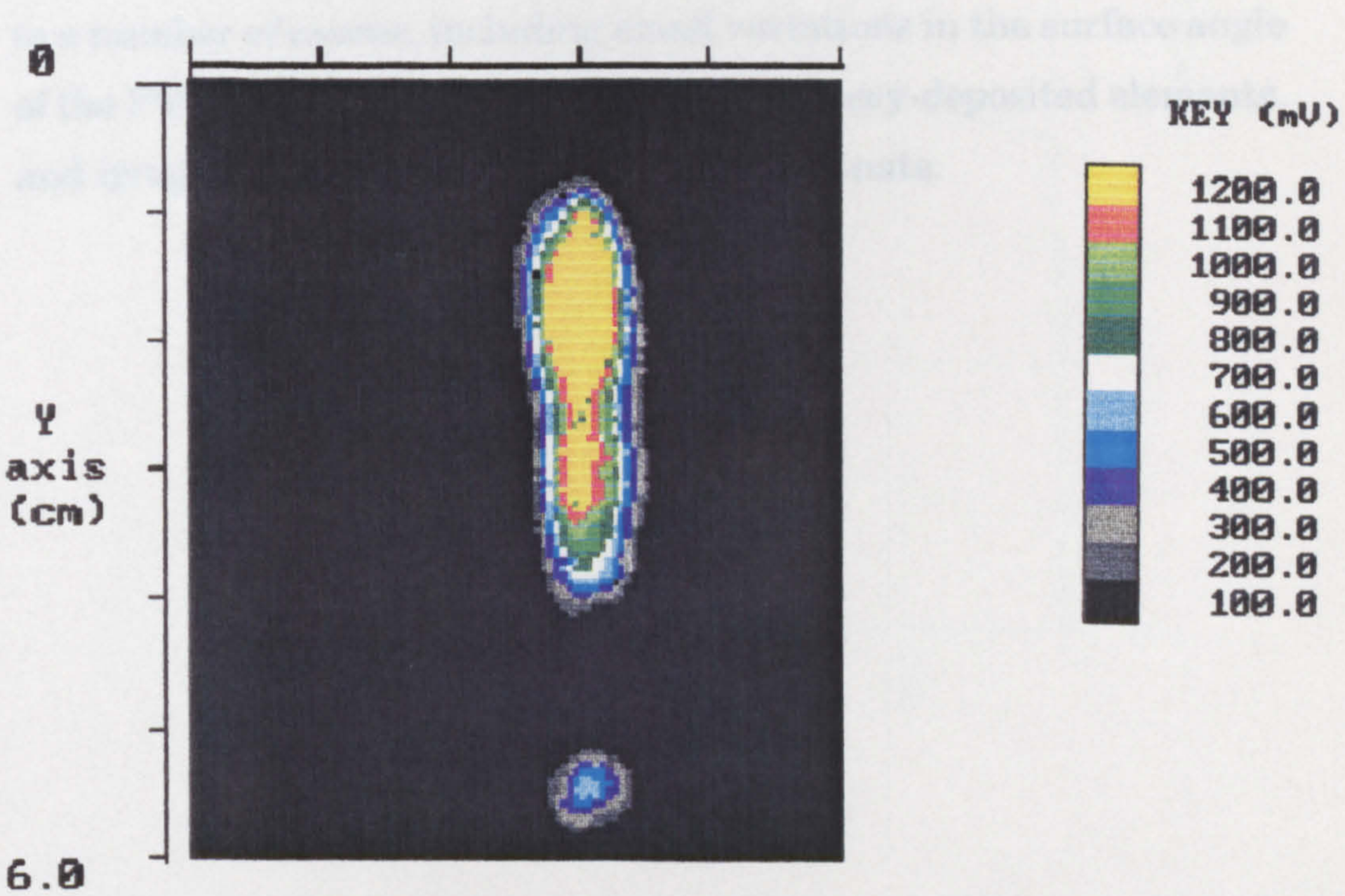

Figure 20: C-Scan Beam Plot of 7x7 PVdF Array Element (Bottom Surface).

The separated areas showing in each scan are at the lead attachment points, and the blank area between there and the active area of the element is considered to be due to the dispersing of the ultrasound by the epoxy potting layer, which is roughly semi-circular in cross section.

Similar results were also obtained when the scans were repeated, with the roles of the PZT and PVdF transducers reversed. That is, with the element of the array transducer receiving, and the PZT transducer transmitting the pressure wave.

The sensitivity of the elements was plotted both along (Figure 21), and across (Figure 22) the elements. Although the consistency along the elements was not particularly good, this could be attributed to a number of causes, including small variations in the surface angle of the PVdF array, poor conductivity of the spray-deposited elements, and irregularities in the bonding of the laminate.

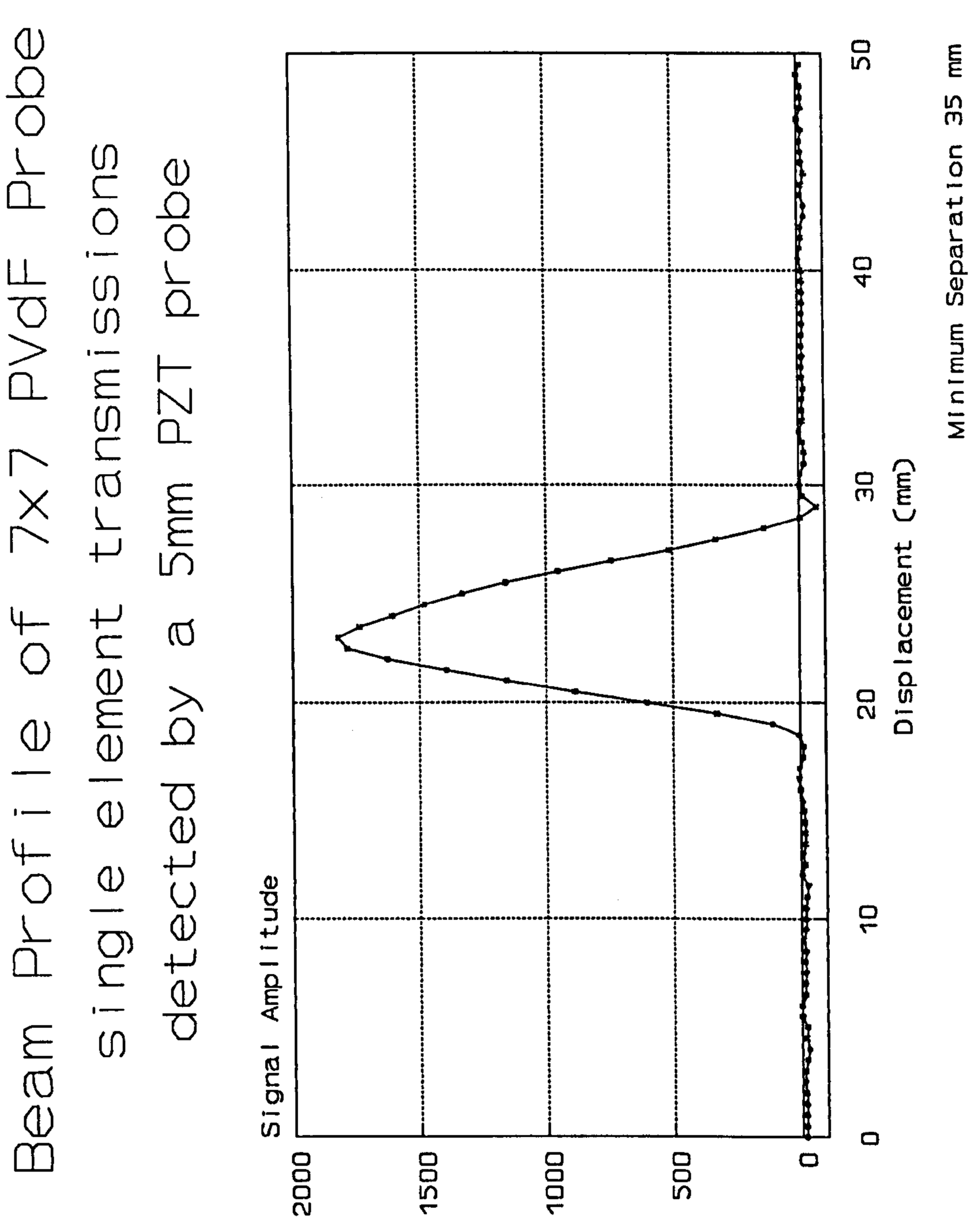

Figure 21: Vertical Cross Section of Beam Plot in Figure 19.

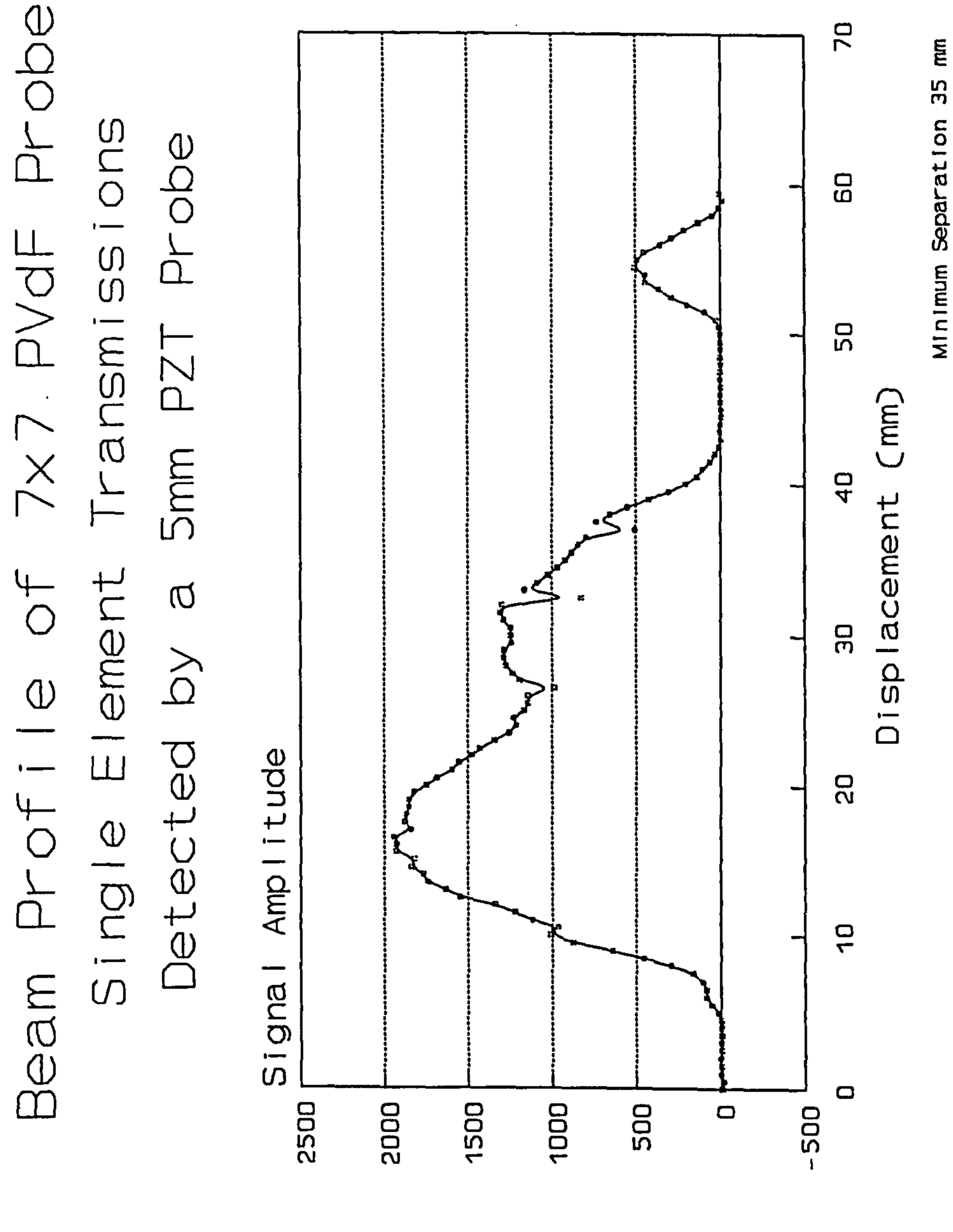

Figure 22: Vertical Cross Section of Beam Plot in Figure 20.

Finally, the PZT transducer was replaced in the scanning arm by a 5mm diameter ball-bearing. An element from each side of the array transducer was connected to the transmitter and receiver respectively, and with a higher gain setting, the scan pattern of Figure 23 was obtained.

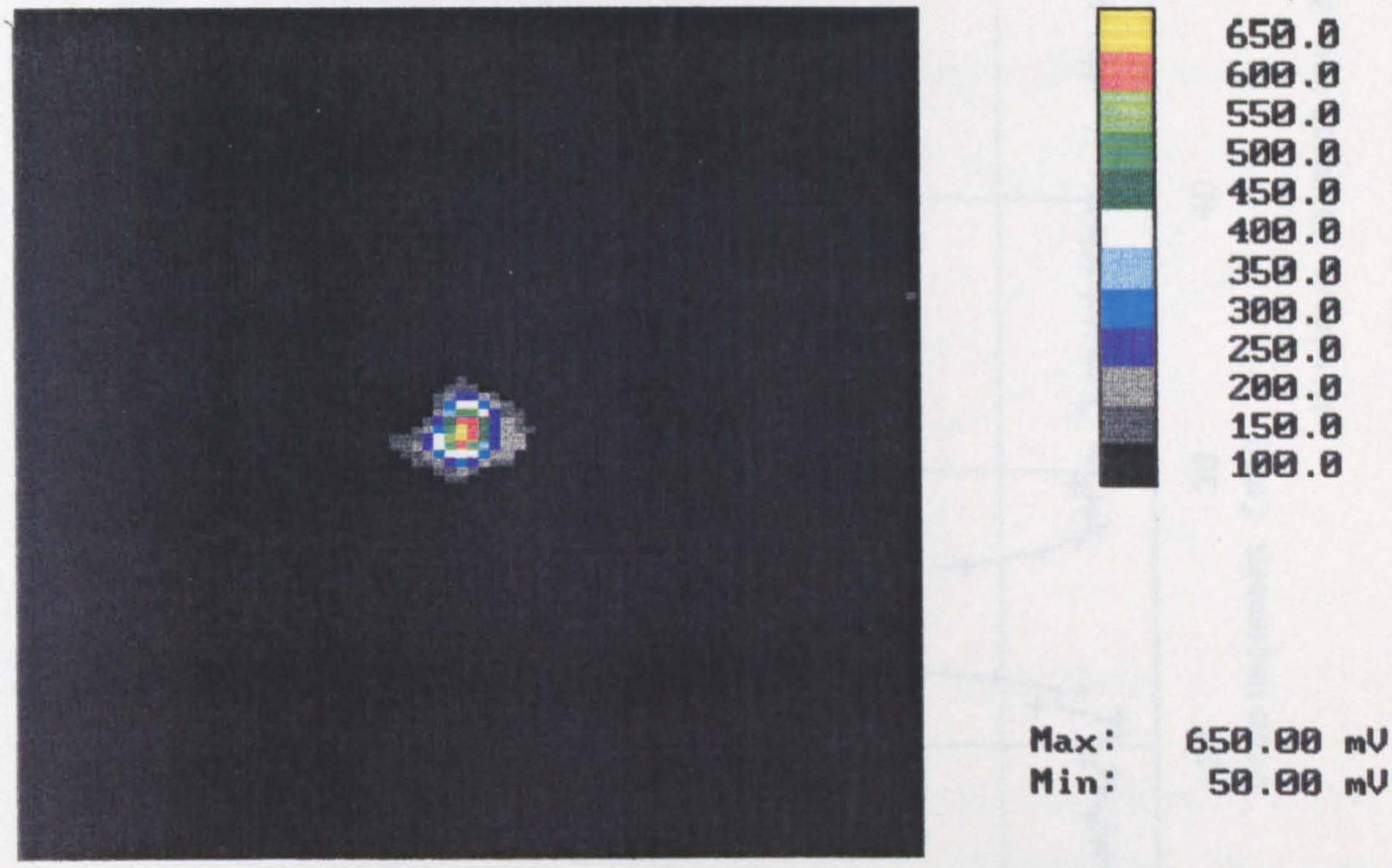

Figure 23: C-Scan Beam Plot of 7x7 PVdF Array Transducer (TX/RX mode).

These results appeared to demonstrate the viability of the Array transducer concept. The transducer can be seen to be responding only to the crossing point of the two active elements, even in the presence of a conducting sample (The steel plate.)

A cross section of this beam plot is given in Figure 24. The beam width at 35mm is seen to be 7 mm. This corresponds to a divergence of 11.5°, which compares very favourably with the theoretical half-angle value of 6° calculated from the worst case model in Chapter 2.

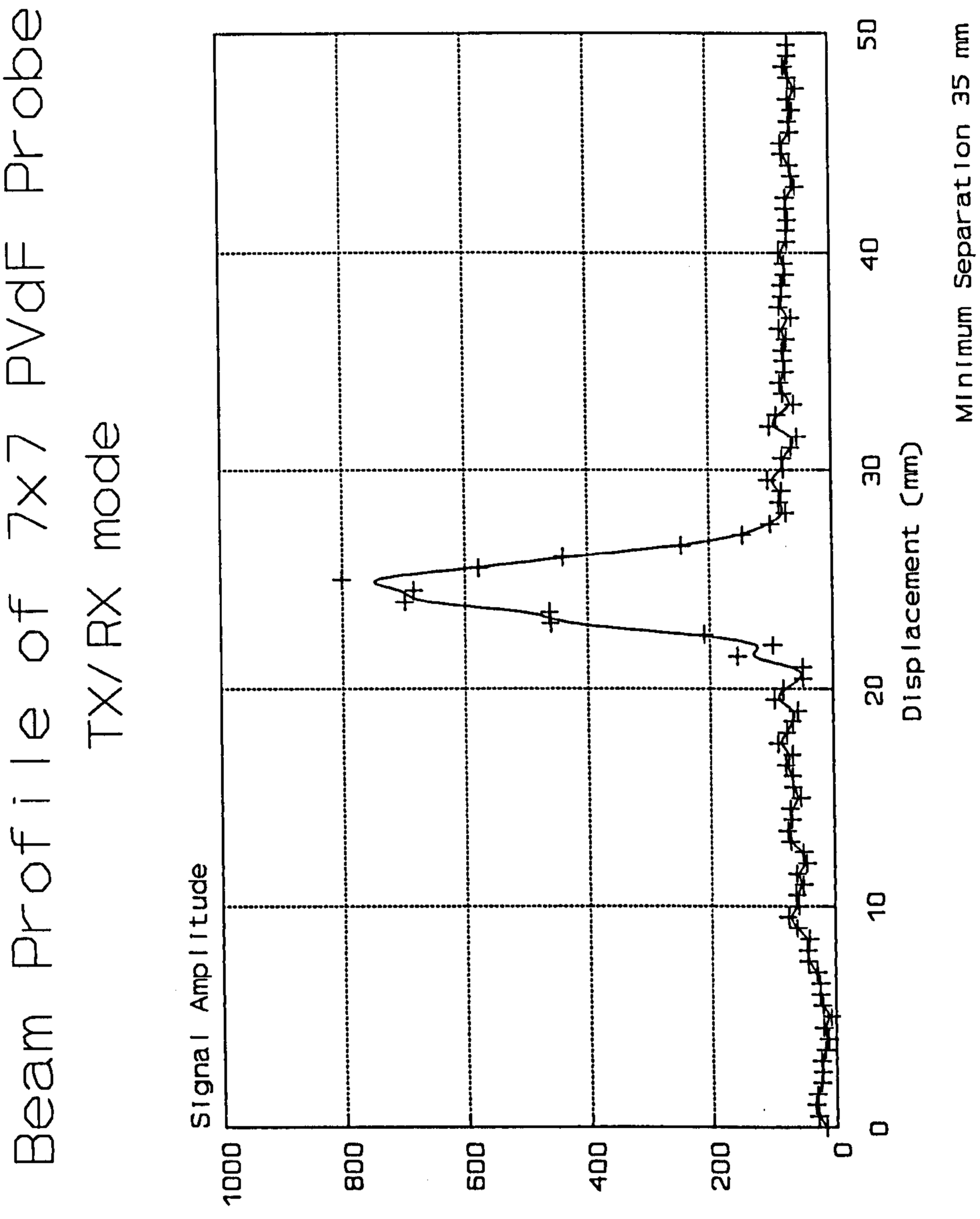

Figure 24: Vertical Cross-Section of Beam Plot in Figure 23.

4.4 Experiments with an Aluminium Test Block.

In order to test the operation of the array transducer in a controlled sample, an aluminium block was machined to the dimensions given in Figure 25.

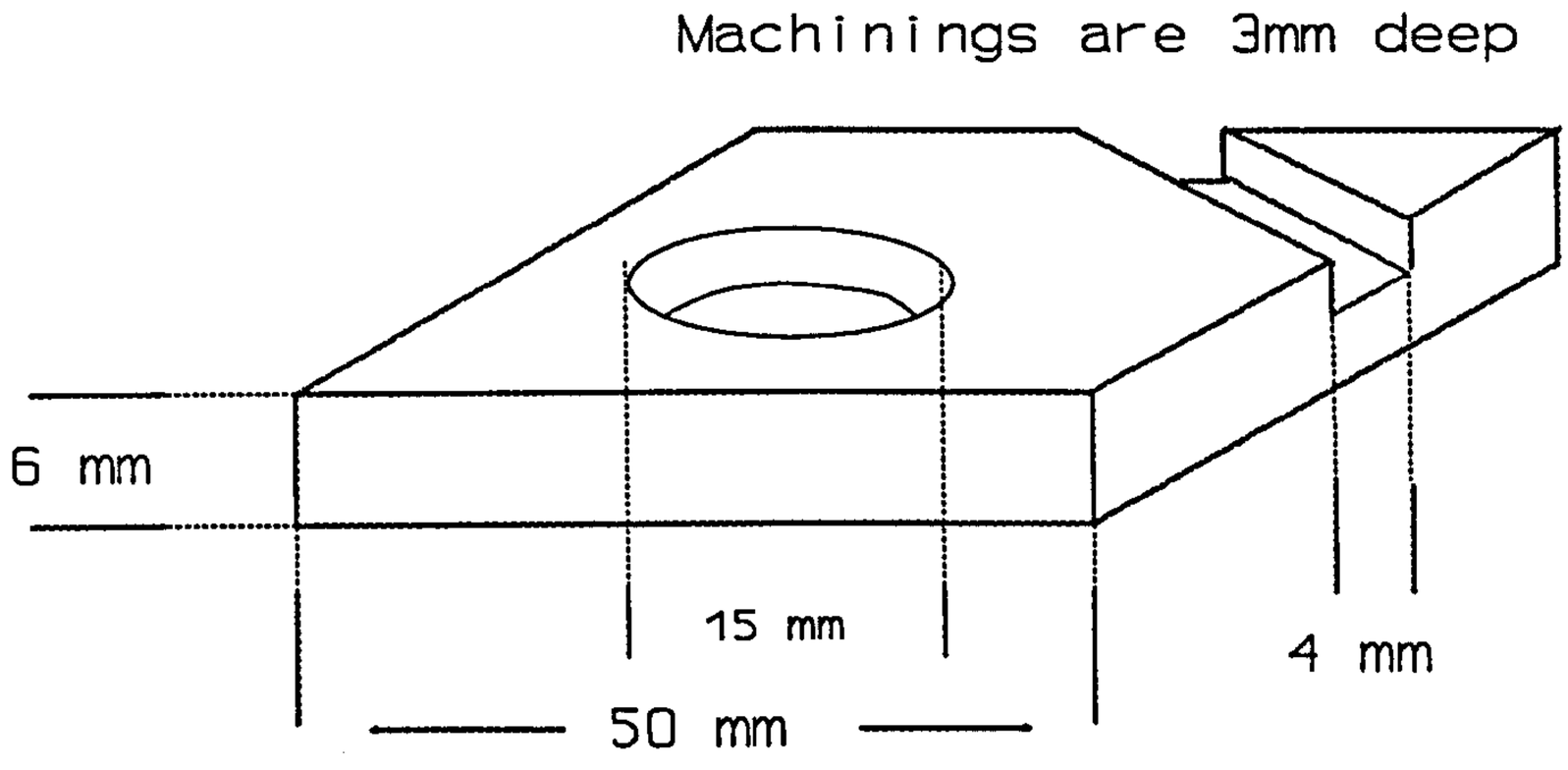

Figure 25: Dimensions of the Aluminium Test Block

The machinings were flat-bottom milled, with parallel sides, to minimise spurious reflections and mode conversions. The mat probe was laid onto the plain face of this test block, using a thin layer of standard coupling gel, and the individual elements connected to the transmit and receive sockets on the test set.

By changing the connections, it should be possible to observe variations in the time of flight of the repetitive echoes which indicate the back face of the test block. It was again found necessary to use about 85dB of gain, with the test set tuned to 5MHz. Photographs of some of the traces obtained appear in Figures 26 to 28.

The first photograph was taken from crossing point away from the machinings, and shows a normal 6mm echo, with the exponential decay on repetitive echoes which is typical of an ultrasonic indication of a back wall or complete disbond.

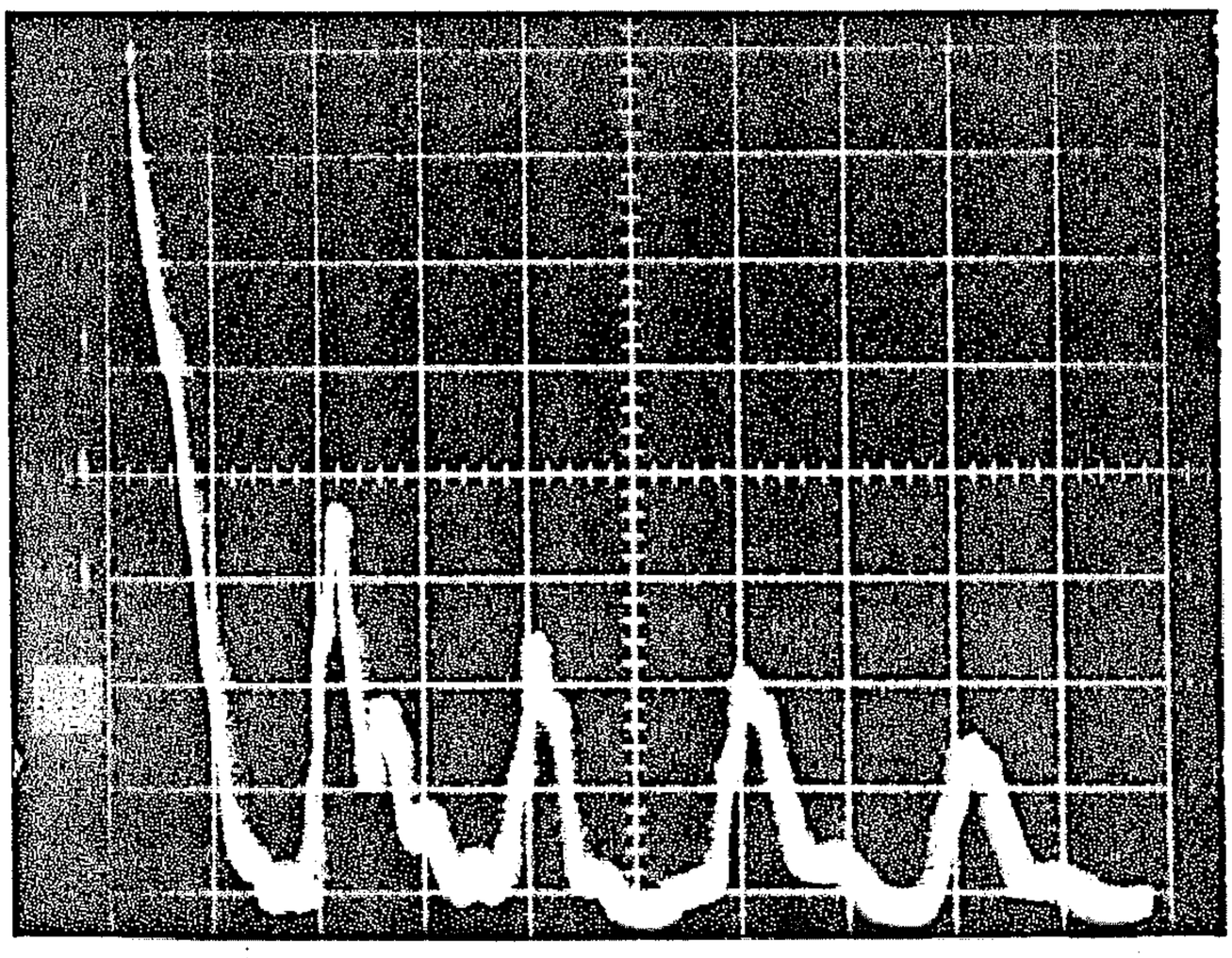

Figure 26: Back-Wall Echoes from the Test Block Using the 7x7 Array Transducer. (Scale 3 mm / horizontal division)

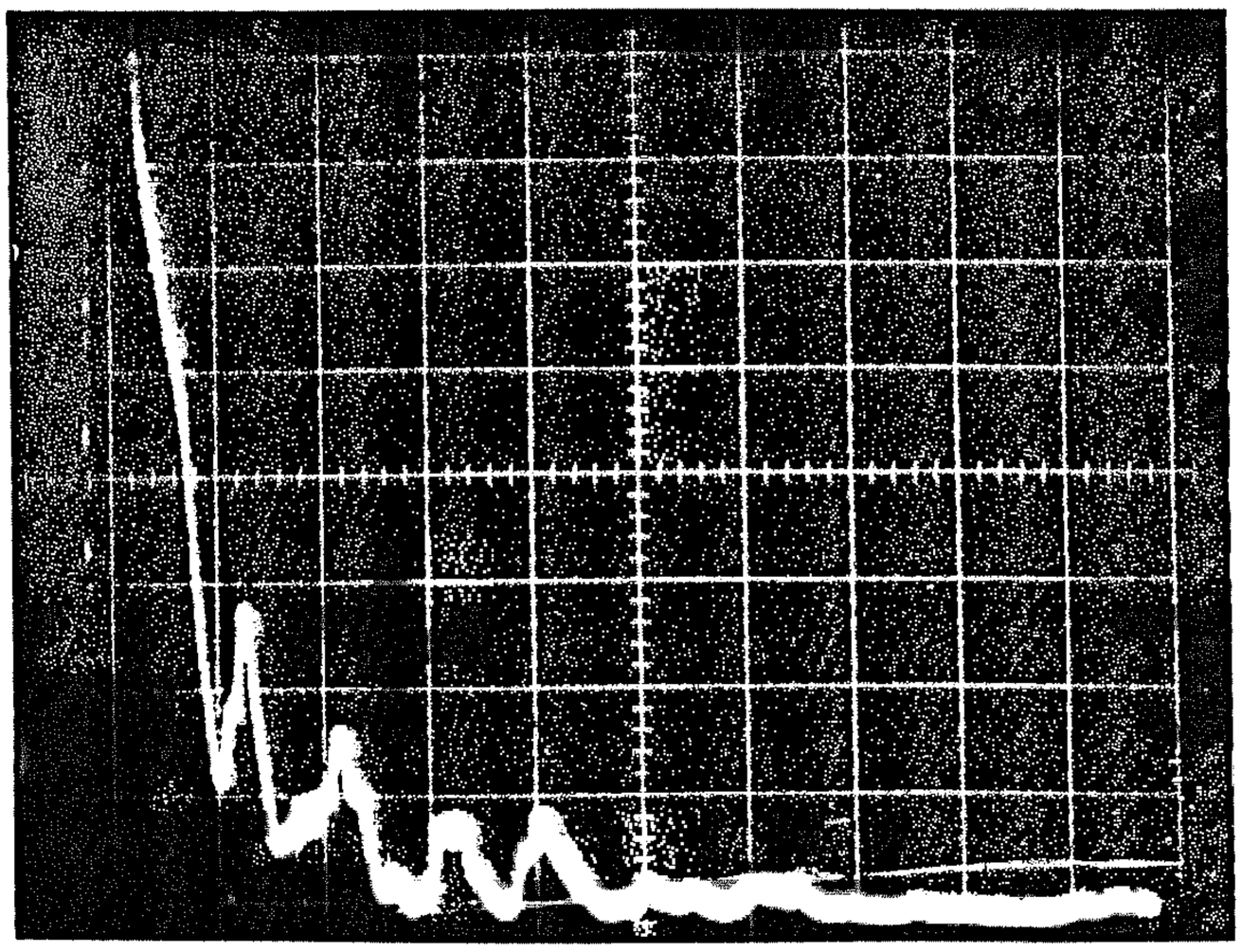

Figure 27: Back-Wall Echoes from the Test Block Machined area, using the 7x7 PVdF Array Transducer.(Scale 3mm / horizontal division).

The second photograph shows the echo derived from a crossing point directly opposite to the circular drilling in the test block. Note that the high gain applied obscures the first 3mm echo, as the pre-amplifier is still in the 'dead zone', (i.e.recovering from the transmit pulse.)

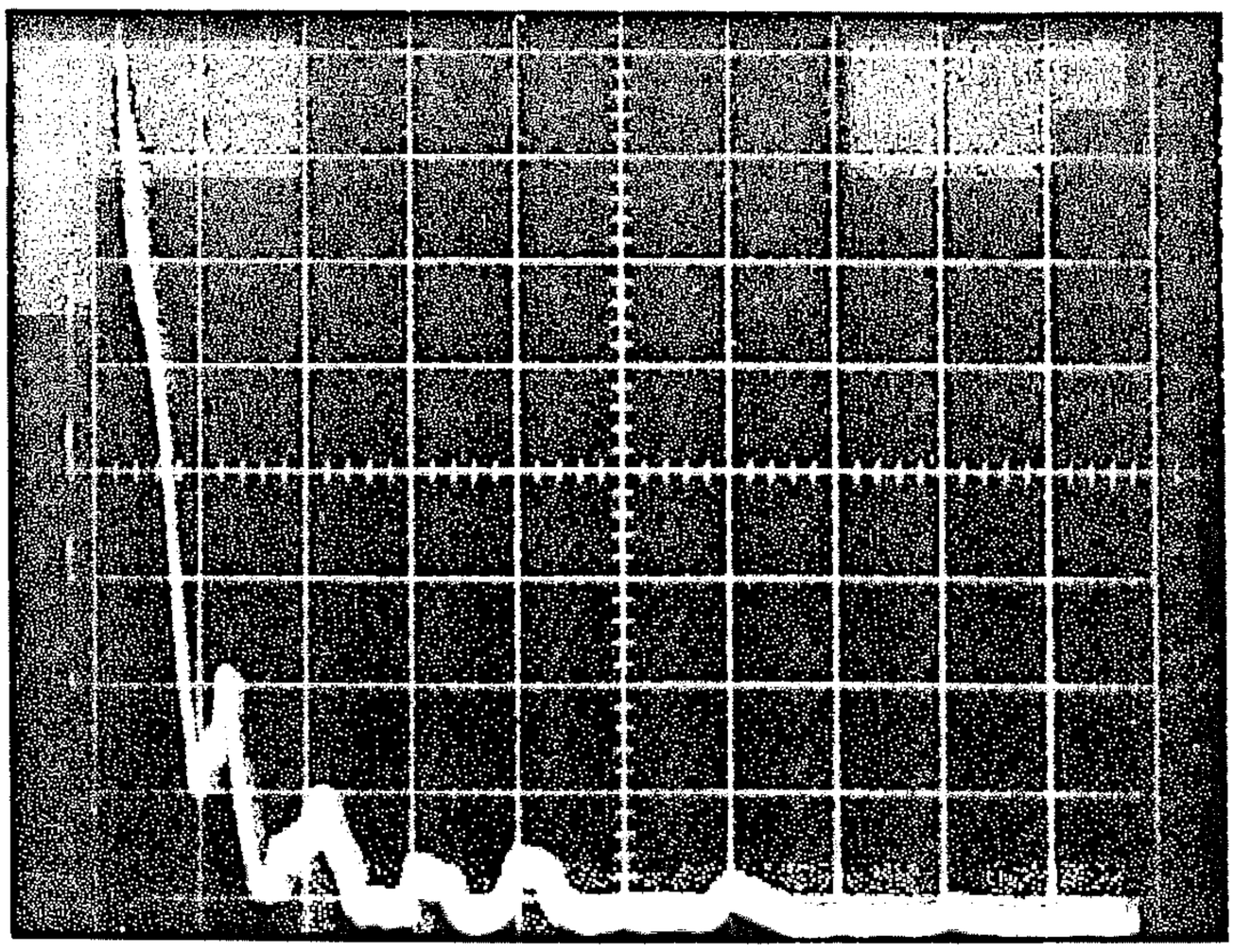

Figure 28: Back-Wall Echoes from the Test Block Machining Edge Using the 7x7 Array Transducer.(Scale 3mm/division).

The third photograph indicates the edge of the diagonal machining, in which both 3mm and, more predominantly 6mm echoes are present. For a human NDT operator, the nature of the defect would be determinable by moving the transducer around and observing the changing shapes of the echo signals. Experience and training would allow correct identification of the defect type even with such conflicting information on the screen. This sort of

interpretation is of course impossible with the proposed array transducer, since the scanning is supposed to be automatic, and the probe should not be relocated during the scan.

The ambiguities of the A-scan information were noted at this point, but until the data could be captured and stored in the computer, no decisions could be taken about the best way to interpret it.

4.5 Summary of Results from the 7x7 Array Transducer.

The series of experiments carried out on the prototype array transducer were largely successful, and indicated three major conclusions.

Firstly, that the bi-laminar configuration proposed after the initial investigations, exhibits the predicted spatial resolution.

Secondly, that the signal level is considerably lower than the preliminary experiments indicated, and rather inconsistent over the area of the array transducer.

Thirdly, that the interpretation of the echoes will require careful software programming in order to obtain consistent indications. This last point is perhaps superfluous in the laboratory, but the degree of confidence required from NDT techniques is very high, and it was considered reasonable to keep this in mind.

The next phase of the study was, of course, to find a way to connect the transducer to the automatic multiplexing, data processing and display units.

CHAPTER 5 - DESIGN OF A DATA CAPTURE SYSTEM

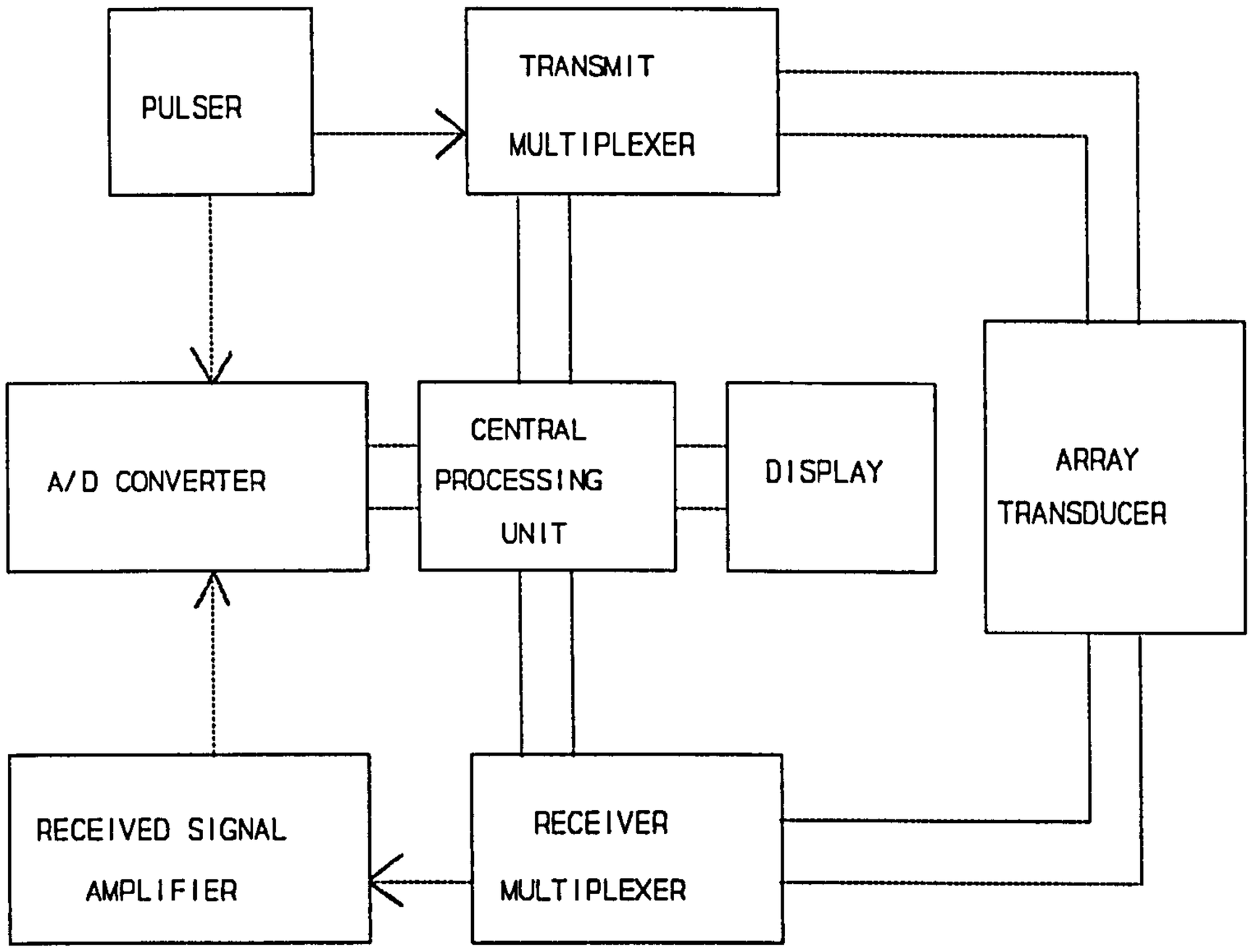

Figure 29: General Outline of the Proposed System.

5.1 Overview.

A generic diagram of the system required to drive an array transducer is given in Figure 29. A pulser/receiver combination generates the required analogue signals. These are multiplexed under processor control, to the individual elements of the array transducer. The received signal is amplified, rectified and filtered, then digitised and fed to the CPU for processing and display.

The display technique is programmable, and either a simple A-Scan, or a false colour map of depth or amplitude can be displayed.

Careful thought had to be given to each of the component parts, and these considerations are outlined below.

5.2 Central Processing Unit and Display

Digital multiplexing of the transducer elements was central to the array transducer concept. This consideration, combined with the requirement to display scan results on some kind of 2-dimensional map, made it obvious that a central processing unit would be required. A number of options were considered for this part of the system, including constructing a purpose built Z-80 system, or utilising a general commercial processing unit such as the Amstrad CPC-464. Eventually, it was decided that the flexibility and ease of use of an IBM compatible PC clone would be the most cost effective development route. An INTEL 8086 based OPUS PC-III was acquired with EGA colour graphics capability, and subsequently utilised throughout the project, both for experimental work, and the necessary PCB design and program development.

Initially, the programming for this system was done in GW-BASIC, which came with the machine. This language was fully capable of driving the ports, the display, and doing any necessary calculations. However, the processing speed was insufficient for the later programs, particularly the implementation of non-linear regression. The later programs were therefore written in 'TURBO C' which was purchased for the project.

These programs are listed in the appendices to this report.

5.3 Digital Interface to the PC.

Within the PC architecture there is an 8-bit I/O BUS, separated from the memory bus by using different timing lines and Op-Codes, and readily available on the built-in expansion ports. IBM recommend that development boards access the addresses 300-3FF (hex). A prototyping board with partial address decoding built in for these addresses was obtained from RS Components, and the first circuits were built onto this board. At this stage, only four 8-bit ports were needed, and it was decided to decode these at the high end 3F8 to 3FF, using a 74LS138 decoder. This chip asserts one of eight CS lines (low) from 3 input address lines, with other pins used as chip enable to select the correct space in the I/O map. The lines from the 138 were originally connected direct to the CS lines of the 74LS244 and 74LS245 IC's which were used to latch the information onto the I/O bus. The address decoding of the 138 was too fast, however, and the latches in the 245's were firing before the data had stabilised on the PC's internal I/O bus. Consequently, the M1 clock line was taken from the PC architecture and fed to the D-type flip-flops. The decoded address line from the prototyping board triggered these, but the output was not asserted until one complete clock cycle later. This gave sufficient time for the data to be presented on the bus before the latches were triggered.

5.4 Analogue to Digital Converter.

As mentioned in Chapter 1, the examination of metal structures usually involves frequencies between 1 and 10 MHz. This would set a lower (Nyquist) limit on the sampling speed of 20 M.Samples/sec. Digitisers are available as expansion cards for the IBM type computers that sample at over 200 M.Samples/sec., but the cost of these prohibited their use in this research. It was quite simple, however, to design a PC-Based digitiser which would sample at up to 10 M.Samples/sec., and consequently it was decided to operate the probe between 2 and 5 MHz, and digitise the rectified and filtered output from the test set.

However, at 10 M.Samples/sec, the access time of memory IC's would have to be 50nS. This is too fast for the typically 120nS DRAM in a PC clone, and a temporary store was needed. Commercial cards build their own memory on board, which is mapped into the memory of the PC, in the same manner as video adaptor memory. This requires address decode logic and control, the insertion of wait states in the PC read cycle and collision detection, so that the same byte is not read and written at the same time from the two different sources. The technique is elegant, fast, but complicated. Because of the limited time, expertise and financial resources available to this project, it was decided to use an asynchronous transient recorder configuration instead.

The A/D was a 6-bit flash converter, rated up to 20 MHz. Its reference voltages were derived from a stabilised zener diode, and were designed to coincide with the test set monitor voltages.

The conversion clock was derived from a 20MHz crystal oscillator. This was fed to a BCD counter, and from there to a digital multiplexer. The output of the digital multiplexer went through a D-type flip-flop configured as a divide-by-two counter. The reason for this was that a BCD counter has an uneven mark/space ratio on its output, and the flip-flop restored the clock to a regular square wave. Overall, the timing arrangement gave programmable clock speeds of 10, 5, 2, 1, 0.5, 0.2 and 0.1 MHz, selected from the control byte.

As a later modification, it was envisaged to use the transient recorder in pre-trigger mode, using the HALF-FULL flag on the FIFO, so the control cycle for the read/write timing was designed to make this possible. In its neutral state, therefore, the A/D ran continuously, writing its data directly to a 512 byte FIFO buffer. The buffer was kept empty by alternating read cycles with the write cycles from the conversion clock. The transient recorder was armed from the control byte of the PC interface, and then waited for the SYNC. pulse from the test set. This pulse disabled the read line to the FIFO, so it filled up with the next 512 clock cycles of A/D data. When it was full, the write line was disabled, and the FIFO then had to be emptied by the PC to restart the cycle. Software reset was also provided in case the system hung at any point.

Furthermore, the PC's READ line cannot be disabled, and if the PC were to read data from the FIFO when it was being written to it would lead to more than 512 reads being required before the system would restart. A second check was therefore implemented for the FIFO status. By connecting the EMPTY flag into the otherwise unused high bit of the data word, it was made possible for the software to determine the state of the FIFO.

The PC's READ line accessed both the FIFO, and the 74LS244 line driver, and it was not necessary in this case to delay the address decoding, since the data was not being latched. Output from this buffer was mapped onto a parallel I/O port in the PC, and transfer to the main memory area occurred when the software placed the required port address into register DX, and issued an INPUT statement. This command places the port bit pattern into register AL, which can then be stored at a memory location (eg. a 1-dimensional array).

Although this technique is not as elegant or as fast as directly mapping the A/D converter output into memory (as used by the commercial cards), it is simpler to implement or modify.

5.5 Multiplexers.

Initially, it was hoped to keep the transmit pulse at either TTL, or CMOS logic levels, so that the PC interface could drive the transmitter directly. The multiplex control circuit shown in Appendix 1 still has this idea implemented. Early experiments had shown that the 74LS374 bus driver IC generated a good, clean U-S pulse from PVdF which was clearly detectable with a PZT receiver. With this arrangement, any given bit pattern could be fired simultaneously, and expansion to a greater number of array elements would be very simple.

The received signal was multiplexed on the prototyping board by TTL compatible reed relays. These were single-pole normally-open, so that any relay with an asserted LOW input connected that line of the array to the pre-amplifier.

5.6 Pre-Amplifier.

As discussed in the earlier chapters, a piezoelectric transducer is capacitive. PVdF has a quoted DC impedance of $>10^7$ Ω, and transducers made from it are therefore highly susceptible to airborne electrical interference, whether at Mains (50Hz) frequency or RF. Unlike strongly resonant PZT transducers, the mechanical impedance of a PVdF transducer cannot be matched to 50 Ω, and therefore the signal/noise ratio of a PVdF transducer connected to a standard ultrasonic test set is going to be less than ideal. There was a need therefore, for a matched front-end pre-amplifier, whose output could be connected to the RX socket of the test set. However, the electrical impedance of a PVdF transducer is dominated by the clamped capacitance, which depends on the size of the transducer element. At this stage in the project, the dimensions of the array transducer had not been finalised, which meant that the impedance could not be matched over a number of different experimental transducers. There were two possible solutions to this problem, using either a very high impedance voltage amplifier, or a very low impedance charge amplifier. The charge amplifier is the better solution, since it eliminates stray capacitance and low-frequency roll-off, but charge amplifiers are unstable and require comprehensive screening. The susceptibility of the transducer to noise would have required an individual amplifier for each element, sited on the edge of the array transducer. A FET impedance converter was therefore envisaged as the most likely solution to the impedance problem.

On the basis of this argument, the first stage of pre-amplification implemented on the prototyping board is a low-gain wide band impedance converter. This circuit had been found to have

a gain limit of x8 to x10 and was limited in this circuit to a voltage gain of 5.

The FET first stage fed a second stage built around a Phillips NE 592 differential amplifier, which had been chosen as the replacement for the µA 733 IC used by Preston in his work on PVdF hydrophones, and for the ease with which the frequency/gain curve could be modified. The impedance of the power rails for this amplifier were found to be critical to the stability and a transistor stage was designed to supply the chip's +ve and -ve rails.

The output from the NE592 is differential, so it was connected to a transistor stage which converts the signal to a single ended voltage output. The overall design gain at 5MHz for this amplifier was adjustable with a single resistor, up to 40dB, and when bench tested, it behaved exactly to specification.
Full circuit diagrams for this prototype data capture system appear in Appendix 1.

5.7 Program 1 - Transient Recorder.

As explained earlier, the A/D converter and multiplexer was initially built on a prototyping expansion card designed to plug in to the PC. Digital I/O ports were available on this card at addresses 300H to 3FFH, and a program was written, first in interpreted GW-BASIC, and later compiled in 'Turbo C' to set up the digitising speed, select 'X' and 'Y' elements from the array transducer, arm the trigger and display the data from the A/D converter as an oscilloscope-type trace.

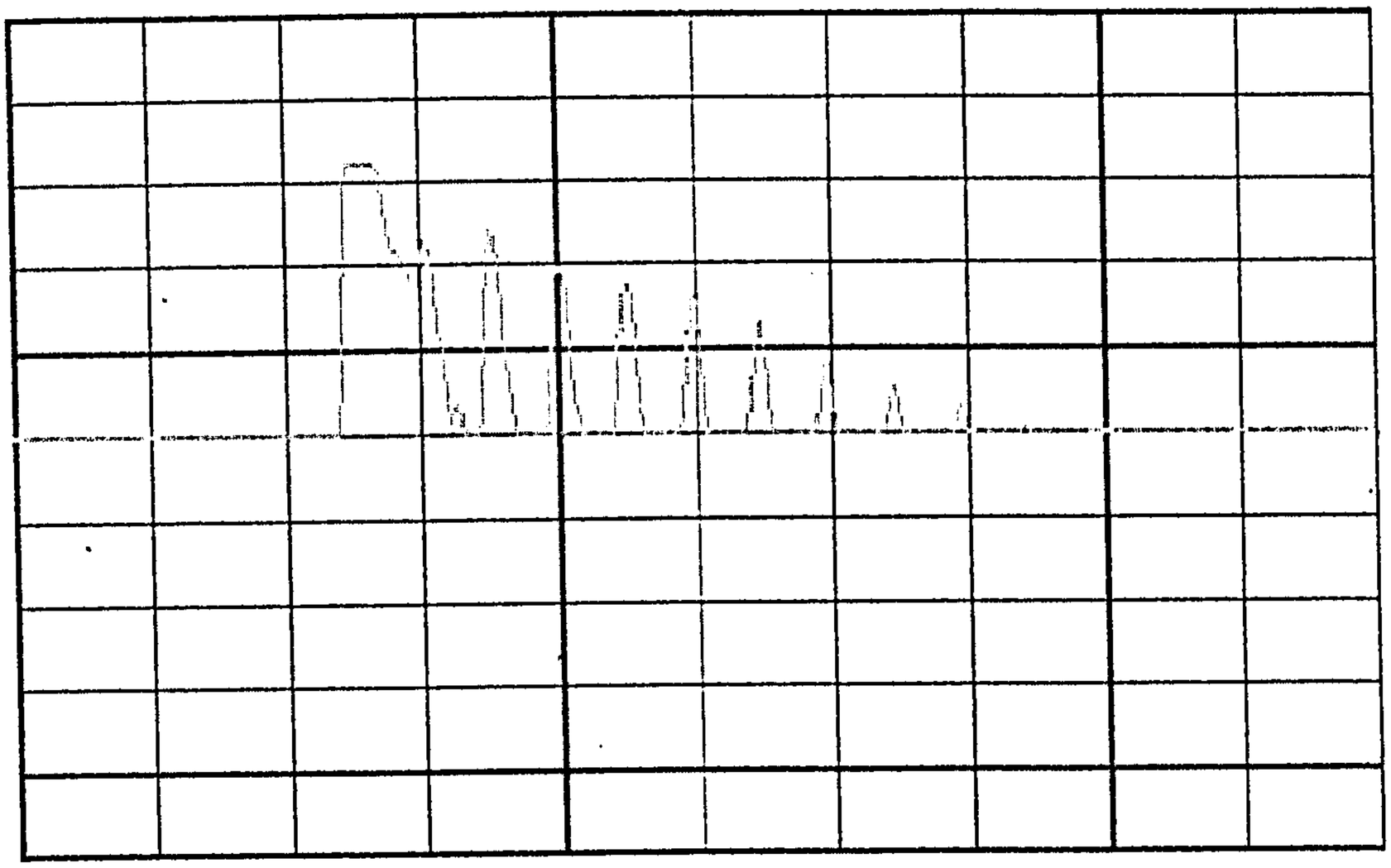

Figure 30: Digitised A-Scan of the Test Block Using a commercial 5MHz PZT Transducer.

This program (Listed in Appendix 2,) was successful, and a typical trace displayed on the PC screen is shown in Figure 30. The trace was obtained from a 5MHz PZT transducer connected to the test set. The echoes are from the back-wall of the aluminium test block described in Chapter 4.

The prototype array transducer was then connected to the test set through the multiplexers and it was expected that similar results could be obtained, even though the signal levels were very much smaller.

However, as Figure 31 shows, the signal to noise ratio of this arrangement was so poor that the ultrasound signal could not be clearly determined.

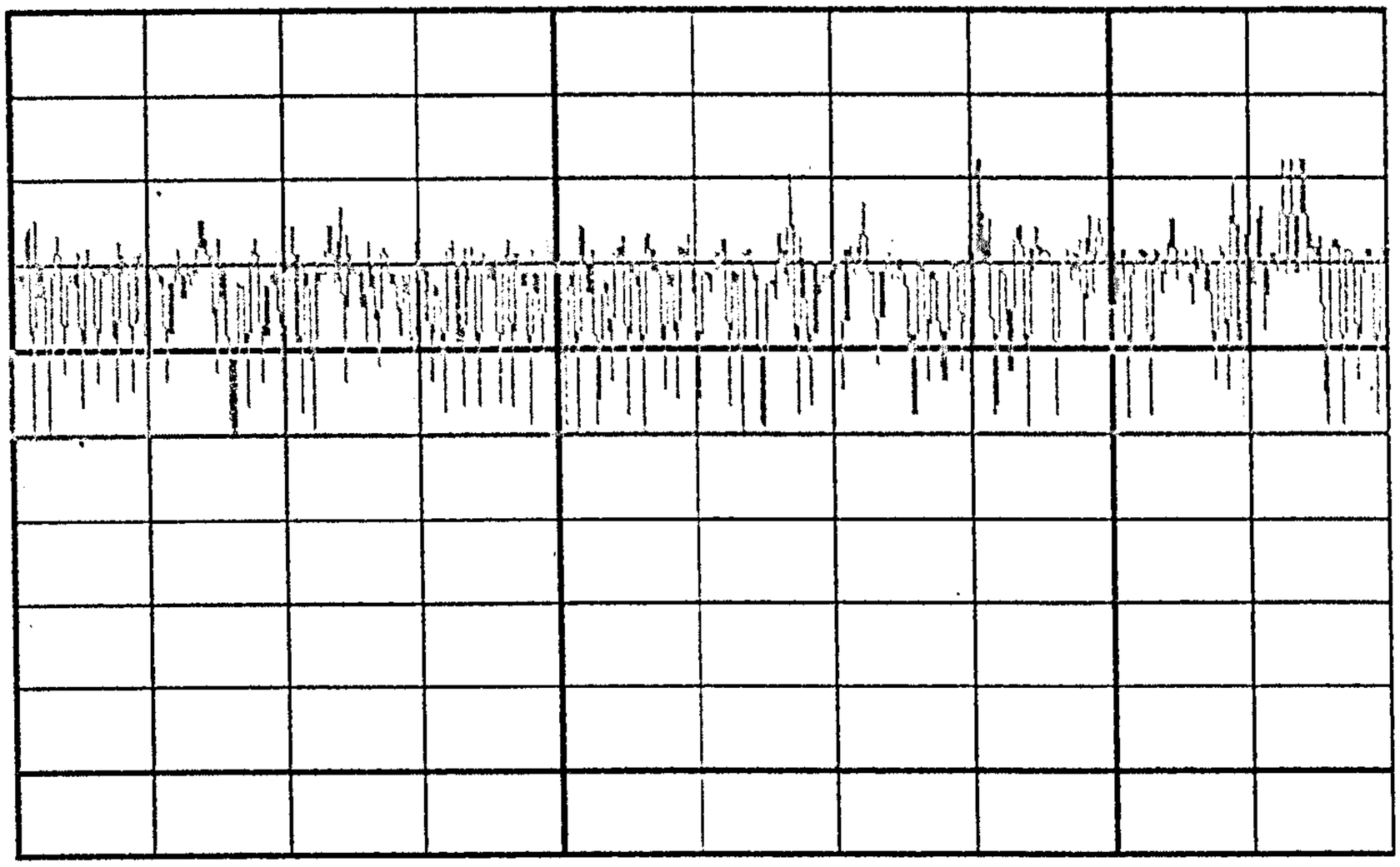

Figure 31: Digitised A-Scan of the Test Block Using the 7x7 PVdF Array Transducer.

At this stage in the research, it had been shown that a bilaminar PVdF array transducer would possibly exhibit the predicted resolution for defect imaging, and a transient recorder for capturing A-scan data had been successfully built.

The signal from the PVdF transducer, which had been clearly visible on the analogue A-Scan, was not available through the digitiser however, although the very much stronger signal from a PZT transducer was clearly indicated on the PC screen. The only remaining problem therefore, was to increase the signal/noise ratio of the system, and there were three possible ways of doing this. Firstly, a more sensitive transducer could be manufactured. Secondly, a pre-amplifier with a better noise figure could be designed, or thirdly, the analogue system could be isolated from the digital noise generated by the PC.

Efforts were made to find a more sensitive material, since improvements in the original PVdF had been reported. Samples of gold-plated PVdF co-polymer (with TrFE) were obtained, and had measured sensitivities around 5 times higher than the homopolymer material. The highly crystalline nature of the co-polymer makes it brittle, however, and the prototypes were liable to snap, or micro-crack under normal handling or operational conditions. A further sample of thick-film 'voided' PVdF was also obtained, being around 200μm thick, with a thick copper coating suitable for solder connections. The main application of this material according to the manufacturers is in SONAR arrays, at much lower frequencies than ultrasonic NDT requirements, and it was found that the ultrasonic attenuation in the voided material was too great for any improvement in signal strength.

The next stage of the research, therefore, had to be to examine ways in which the pre-amplifier could be improved, and to isolate the digital noise from the analogue signal path.

CHAPTER 6 - THE ISOLATED SYSTEM

6.1 Overview.

The data capture system described in the previous chapter had been designed and built for this project as an interface for the PVdF array transducer. Although it functioned well with a commercial test set and single element PZT transducer, the signal/noise ratio when used with the PVdF transducer was too low to determine the ultrasound signal. Several attempts were made to strengthen the signal. Firstly, the TTL pulser was replaced with the -400V pulse from the test set, selecting elements manually. Next the transmit pulse itself was generated by the PZT transducer. But in neither case was it possible to improve on the meaningless data shown in Figure 31. Oscilloscope measurements of the amplifier output showed substantially the same signal as the A/D program, even when the transducer was disconnected, and the hypothesis was formed that the amplifier had become unstable. It was duly taken out of circuit, and the array transducer was connected directly to the test set, as it had been during the previous phase of the research. With this arrangement, it was rapidly discovered that the PC system was generating the noise, since with the PC switched on, it was not possible to observe the same signals as before, whereas with the PC switched off, the A-scan trace again became visible. Further oscilloscope measurements showed the noise to have a peak to peak amplitude of between 150 and 200 mV, and frequency components between 100kHz and 10Mhz. The noise could not therefore be filtered out of the signal path, since it was broad-band across the same frequency range, and an order of magnitude larger than the ultrasound signal itself.

The possibility of this sort of interference had been considered beforehand, and attempts were made to shield the array transducer. It was believed that the interference was airborne, so the leads were screened up to their connections on the PVdF, the test block was grounded to the test-set chassis, the entire array and test block area was placed inside a screened enclosure, and the PC was removed up to 2 metres away from the experimental area. (Remembering that lead capacitance would degrade the signal level still further, it was not considered reasonable to extend the leads any further than this.) These measures should have reduced the effect of airborne interference, but none of them had any observable effect on the signal/noise ratio.

Eventually, a series of differential measurements with an oscilloscope which was allowed to 'float' relative to the Mains Earth, revealed that the noise was appearing between different places in the system ground. Specifically, between the ground plane of the PC and the grounded side of the test set connections to the array transducer. Although this effect was not fully understood, particularly in the light of the screening attempts mentioned earlier, it was suggested that the analogue side of the system would have to be electrically isolated from the PC and contained within a separate, screened enclosure before any reasonable results could be expected at these low signal levels.

To implement the isolation, a backplane eurocard system was obtained, and the various sections of the circuit were transferred to plug-in cards to fit the new enclosure. Digital connection to the PC was through a commercial parallel IO board obtained from Blue Chip, with similar I/O port addresses to the earlier system. This

card connected to an opto-isolator card within the enclosure via 2 metres of ribbon cable, to allow some distance between the PC and the experimental area.

6.2 I/O Port Allocation.

Although the parallel I/O board made similar addresses available to the isolated system, the I/O ports themselves needed to have different functions, since the PC's I/O Read and Write lines were no longer available to the A/D converter. The ports were configured as a Control Byte on 308H, a Multiplexer select port on 309H and a Data Byte at 30AH. The multiplexer select port was divided into two 4-bit nibbles, each controlling up to 16 elements in either the X- or the Y-direction. The allocation of bits in the Control/Status byte is shown in Figure 32.

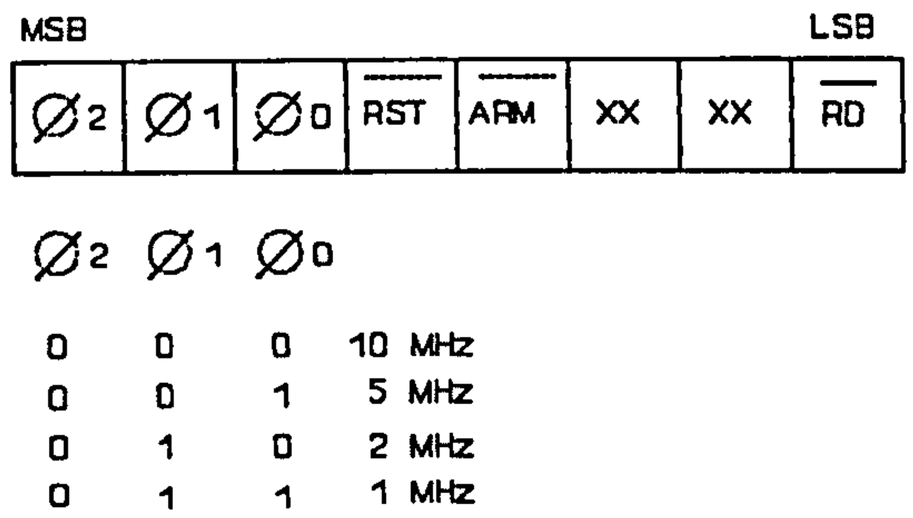

Figure 32: Control/Status Port 308H

Reading data from the A/D converter now entailed toggling the reset bit, then the arm bit, pausing, and then interleaving toggling the read bit in the Control Word with reading the Data Word. This slowed down the data capture process since three I/O operations were now needed to obtain each Data Byte.

6.3 Transmit Pulse Multiplexers.

The transmit pulse multiplexing relays were kept to a separate board to help to isolate the pre-amplifier from the high-voltage pulse. Sixteen single pole reed relays were divided into two groups, each controlled by a 3 to 8 decoder (74LS138), with the fourth bit of the address used as a chip enable line, so that only one of the relays could be energised at a time. It had been hoped to put an HT supply on this board, which could be fired from the PC control word. This, coupled with the integral pre-amplifier on the analogue board, would have enabled the system to operate independently from the test set. However, a considerable time had to be spent on the other aspects of the research, and it was not possible to develop this in the time available.

6.4 The Analogue Board.

Full isolation of the analogue section of the electronics required a pre-amplifier independent from the test set. This was because the test set SYNC. pulse was connected to the digital control section of the transient recorder. The new preamplifier would have to be able to completely replace the analogue pre-amplifier in the test set, and produce full-wave rectified and filtered ultrasound signals with 1-2 volts p-p amplitude, from the PVdF transducer. This required up to 80dB of gain, and a precision rectifier which would work at 10MHz.

The FET follower was found to be highly susceptible to RF interference, and was abandoned, along with the band-pass amplifier around the NE 592, which was unstable at the high gains required.

One configuration which was tried, with some success, was the MAX 455 video amplifier. This IC has an 8-way multiplexer on its inputs, and a working bandwidth of >10MHz. It therefore seemed ideal in this application as a front end pre-amplifier. The first time it was used, however, the multiplexing side of the IC failed. The reason for this was thought to be the energy in the cross-talk from the transmit pulse to the receiving elements. Measurements showed that spikes of up to 30 volts were present on the amplifier's input which were enough to break down the gate insulation in the CMOS multiplexers.

This meant that pulse suppressors needed to be introduced into the receiver lines. This was first attempted with FET switches which grounded the inputs to the multiplexer while the transmit pulse occurred. (Figure 33)

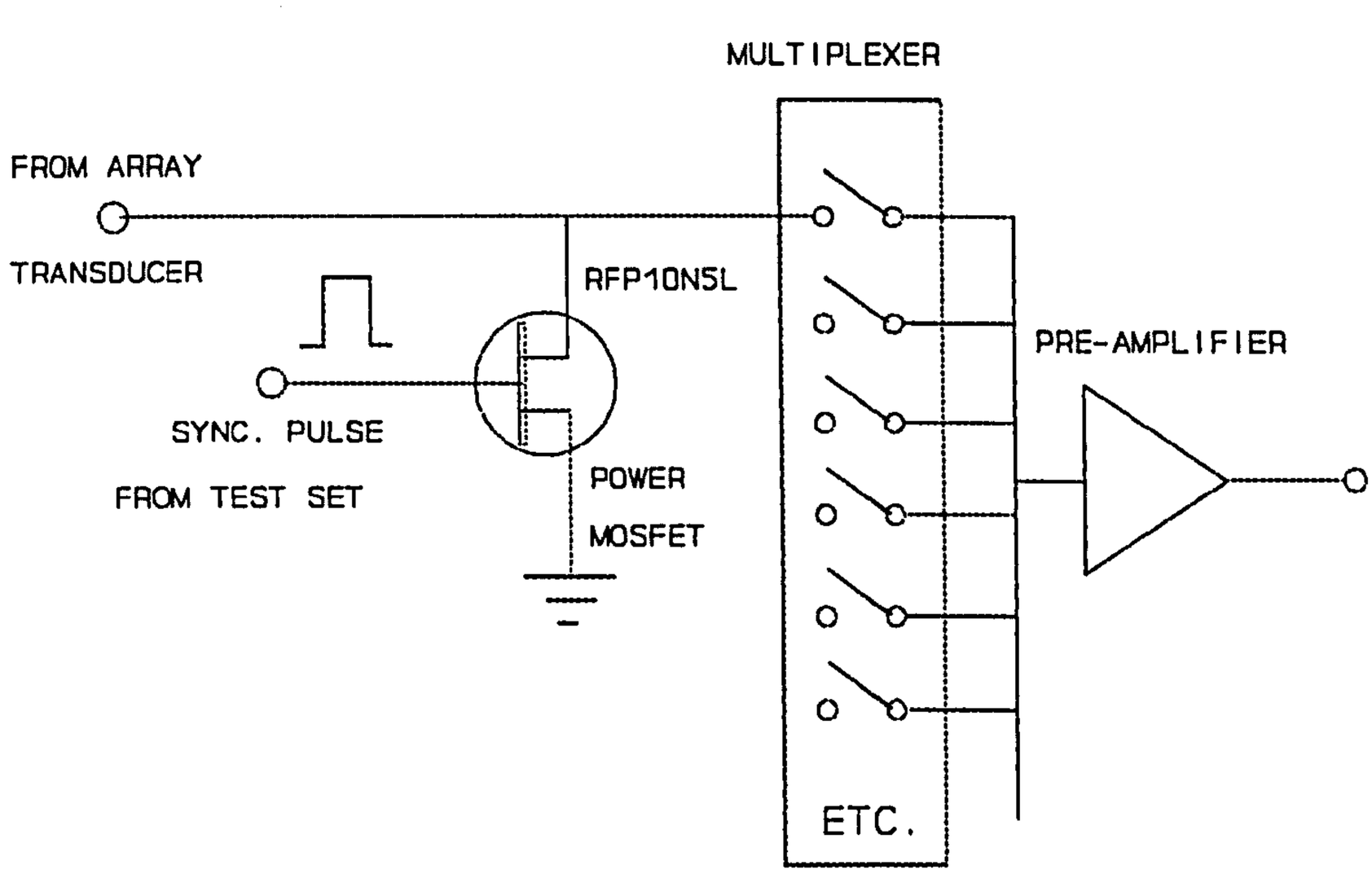

Figure 33: FET Switch Pulse-Suppression Technique.

This should have worked, and reduced the pre-amplifier dead time to well within the near-field of the transducer. However, the

signal on the multiplexer inputs exhibited 'bounce', and with the effective input impedance of the amplifier being of the order of 10^6 Ω, the stray capacitance of the elements and leads gave an extended dead zone of around 10 μS (60mm equivalent in steel!).

A more traditional pulse suppressor technique is to put two diodes of reverse polarity from the signal path to ground. The choice of the diodes is important in obtaining fast recovery time, low 'ON'-resistance, low junction capacitance and high breakdown voltage. A number of different types were tried before the BY206 was chosen.

Again, the dead zone was found to be too long for voltages below the 0.6 volts conduction threshold of the diodes, since there was no signal path to ground at low voltages. This had been thought to be a requirement for a voltage amplifier working with PVdF, because of the capacitive nature of the transducer. Calculations showed however, that the introduction of 2k2 Ω resistors across the input lines would not seriously degrade the signal at high frequencies, but would reduce the dead zone to less than 1μS. This was tried, it functioned as expected, and remained the pulse suppression technique for the rest of the research.

Later measurements of the impedance of one of the rigid array transducers confirmed the calculations and the capacitive nature of the PVdF array elements.

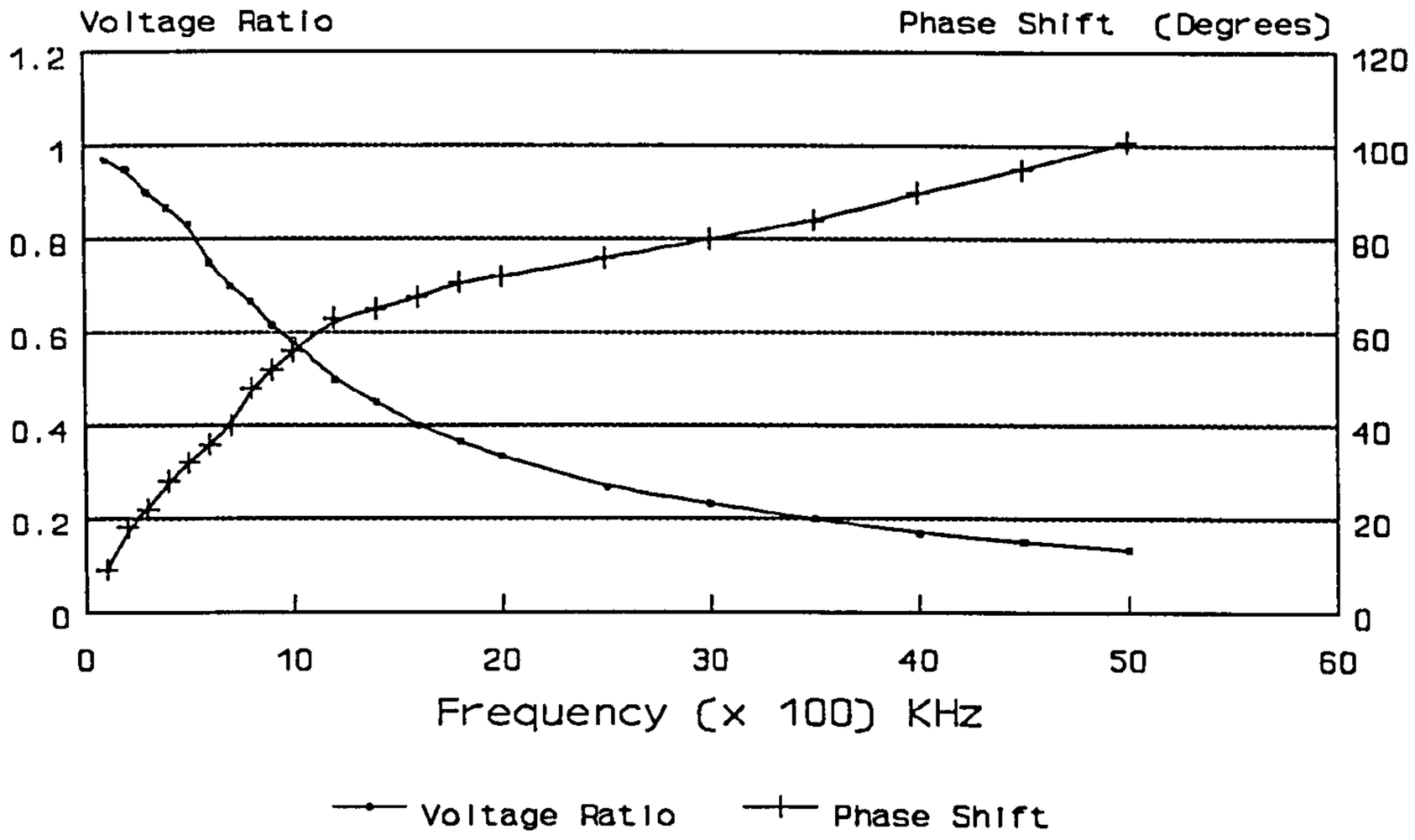

Figure 34: Measured Voltage Drop and Phase Shift across a 1kΩ resistor in series with an Array Element from the first Rigid Transducer.

One added benefit of this pulse suppressor arrangement was that low frequency signals still exhibited a source impedance well above 1 MΩ. The mains pick-up from the transducer and leads was thus reduced from several hundred millivolts, to the microvolt level of the ultrasound signals. With the addition of low frequency roll-off to unity gain in the pre-amplifier therefore, the airborne mains hum ceased to be a problem in the signal path.

6.5 Isolated System Power Supply.

The Analogue circuits were designed to run from ± 8 Volts, as this was the required voltage both for the MAX 455 and for the NE5539 op-amp. These, and the +5 Volts needed for the digital IC's

were originally provided by a linear laboratory PSU. However, the isolation of the ground output from the mains earth at high frequencies was poor, and a switched mode PSU was obtained which slotted into the card frame. The outputs from this PSU were ± 15 Volts, and +5 Volts, so that linear regulators were needed to reduce this to a stable ± 8 Volts for the analogue board.

6.6 Results with the isolated system: Program 2.

The isolated system, with the MAX 455 in place as analogue multiplexer/pre-amplifier, was now tested with a re-write of the transient recorder program from earlier. (Appendix 4). System functionality was checked with a PZT transducer driven from the test set, and the monitor signal digitised.

The rectified A-Scan was clearly indicated, so the system was then connected for the 7 x 7 prototype PVdF array.

The signal from the more sensitive elements was now found to be clearly above the noise, and although the signal/noise ratio was not good, it was thought possible with some signal averaging and smoothing of the data, to get reliable peak detection, (and therefore depth information) from this data.

Unfortunately, the intensity of the ultrasound signal varied by up to 10dB between combinations of elements, and in some combinations the ultrasound signal failed to appear above the noise level at all.

C-Scans of the 7 x 7 transducer were attempted, and showed much the same variation between combinations of elements, until the excessive handling to which the prototype had been subjected, coupled with its prolonged immersion in the water bath led to the delamination of a number of its electrical connections,(including the ground plane). While a number of possible reasons were put forward for the sensitivity variations, which are discussed in Chapter 8, it was decided that the next transducer would be bought ready-laminated from Pennwalt, as a 16 x 16 array.

To cope with the expansion from 7 x 7 to 16 x 16, two new designs had to be incorporated into the Analogue board.

The multiplexer, which had been designed around the 8-way selectable input video amplifier IC (the MAX 455 IC) was now expanded to 16 input lines by using a DG535 CMOS analogue multiplexer IC.

The second new design was the analogue pre-amplifier and rectifier. After some consideration of wide band video amplifier design, it was decided that the op-amp stage of the 455 was probably not the best front-end for the ultrasound signal. This led to the amplifier being designed as three separate stages.

The first gain stage consists of a discrete wide-band differential amplifier based around the CA3046 transistor array, which has a gain limiter circuit incorporated, to decrease the overload recovery time. (Necessary since even with the pulse suppressors in the input lines, transmit pulses of about 1.5 volts were present on the amplifier's input).

The second gain stage was based around the NE5539 ultra high speed op-amp, and allowed adjustable gain through a single variable resistor, to cope with possible variations in transducer sensitivity. The third stage was a fast precision full-wave rectifier, again based around the CA3046 transistor array, which fed a single pole integrator with very fast rise time, and a decay time constant ($1/2\pi RC$) of approximately 1μS.

Bench-tests of this amplifier showed that it was stable up to 70dB of gain, with a roll-off around 6.5 MHz. A PZT transducer was connected direct to the input, and oscilloscope traces of the output were in accordance with the test-set display for the same gain setting. Software development for reliable depth indications was then undertaken whilst the new transducer was under construction.

CHAPTER 7 - NON-LINEAR REGRESSION ALGORITHM

7.1 Overview.

The discussions and results outlined above show clearly that the ultrasonic signal from an array transducer will be small, noisy and erratic in amplitude. For reliable NDT information to be obtained with the PVdF array transducer therefore, it will be necessary to smooth the data array obtained from the A/D converter, and obtain clear indications in the software of where the peak amplitudes occur in the A-Scan trace. These peaks are very hard to quantify in terms of an analogue signal, since there is a decay curve superimposed on the trace, which varies with the material under test, and is related to the relative sizes of repetitive peaks. (For instance a lossy material, with many defects, will show weaker, and fewer repetitive echoes, which will also have multi-path stretching in the time axis, compared to a steel block with flat faces, for example.) This is a situation where a human operator uses 'common sense' and 'experience' to give flaw indications with a degree of confidence. The computer, however, cannot use 'common sense' or 'experience', without the implementation of either a Neural Network or an Expert System embedded in the software. The feasibility of either of these options was considered, as there is a good deal of research into this area at the moment in the field of NDT. However, neural nets need training sets, and the array transducer had not yet proved capable of providing these. Expert systems, too, need a set of rules, and provision and testing of the determining factors for flaw-types was deemed to be outside the scope of this project. In consequence, it was decide that general signal-processing techniques would be used, to screen out unwanted details from the A-Scan data, and provide

indications of the location of peaks in the time axis. Acknowledging the possibility of the software missing the occasional peak, and the problem of the dead zone of the amplifier, which can mask the first indication, the approach in this project was to collect all the indications and look for the most frequently occurring separation between echoes. The use of this "most likely" approach was considered to be a valid approximation to what the human operator is looking for on an A-Scan, but it will only work when the attenuation in the material is low enough to provide detectable repetitive echoes.

7.2 First Trials.

Early attempts to smooth the data were based on signal averaging. To accurately simulate a low-pass filter, the current data point was averaged with the previous data point(s) and the new value replaced the raw data in the array. This operation was repeated along the array, by incrementing the index of the current data point.

The first technique for peak detection was similarly simple, in that the software was testing for data values less than the current data value on either side of the current index. However, the results of this simple combination were sporadic, and highly sensitive to noise giving only about 80% reliability of peak detection. Adjustments were tried, lowering the pass-band of the filter by including more data in each average, but this technique reduced the amplitude of the genuine signal peaks, without sufficiently improving the reliability.

After some discussion, it was suggested that a more rigorous technique for smoothing the input data would be non-linear regression using a least squares approximation to a quadratic function. The curve fitting would operate on a small set of points, and the set could be shifted along the whole input data array, producing a smooth curve between the data points collected by the A/D converter. The pass-band of the smoothing effect of this technique is adjusted by the number of samples in the sub-set of the data array, but because the regression is to a quadratic function, there can only be one pole in the sub-set, giving strong attenuation in the stop band, and virtually no attenuation in the pass band.

7.3 Non-Linear Regression.

Mathematically, the argument is quite simple. We first make the assumption that the small set of points was really meant to fit the first three terms of a power series

$$f(x) = a*x^2 + b*x + c \qquad (7.1)$$

To minimise the errors in this assumption, we make it a condition that the sum of the differences between the measured values and the theoretical ones should be as small as possible. However, it can be shown for any random set of values, that the sum of errors about the mean is zero. It is normal therefore, to take the squares of the differences before summing them, and insist on the condition that

$$\sum_s \left(y(x_s)-(ax_s^2+bx_s+c)\right)^2 \quad \textit{is least} \qquad (7.2)$$

To find the minimum of this function, it is necessary to partially differentiate with respect to the three coefficients a,b and c, and set the resultant functions to zero.

After some manipulation,

$$\frac{\partial}{\partial a} \textit{ gives } \quad \sum_s x_s^2\left(y(x_s)-ax_s^2-bx_s-c \right) = 0 \qquad (7.3)$$

$$\frac{\partial}{\partial b} \textit{ gives } \quad \sum_s x_s \left(y(x_s)-ax_s^2-bx_s-c \right) = 0 \qquad (7.4)$$

$$\frac{\partial}{\partial c} \textit{ gives } \quad \sum_s \left(y(x_s)-ax_s^2-bx_s-c \right) = 0 \qquad (7.5)$$

Since the coefficients are constant multipliers, they can be taken out of the sums, and the three equations 7.3, 7.4 and 7.5 expanded to give

$$\sum_s x_s^2 * y(x_s) - a\sum_s x_s^4 - b\sum_s x^3 - c\sum_s x_s^2 = 0 \qquad (7.6)$$

$$\sum_s x_s * y(x_s) - a\sum_s x_s^3 - b\sum_s x_s^2 - c\sum_s x_s = 0 \qquad (7.7)$$

and

$$\sum_s y(x_s) - a\sum_s x_s^2 - b\sum_s x_s - nc = 0 \qquad (7.8)$$

A further simplification occurs if an odd number of samples (n) is used, where s ranges from -k to +k, since the sums of odd powers of x now equate to zero.

As an example, using n=5, and k=-2 to +2

$$\sum_{x=-2}^{x=2} x^2 = 10 \qquad (7.9)$$

$$\sum_{x=-2}^{x=2} x^4 = 34 \qquad (7.10)$$

and we can find the coefficients in the power series from the simultaneous equations

$$10*a + 5*c = \sum_{x=-2}^{x=2} y(x) \qquad (7.11)$$

$$10*b = \sum_{x=-2}^{x=2} x*y(x) \qquad (7.12)$$

$$34*a + 10*c = \sum_{x=-2}^{x=2} x^2*y(x) \qquad (7.13)$$

7.4 Software Implementation.

One of the advantages of this technique is that it is easily implemented in software with a one dimensional array of values taken at regular intervals. (Such as the array of A/D converter readings in the transient recorder programs in the Appendices.)

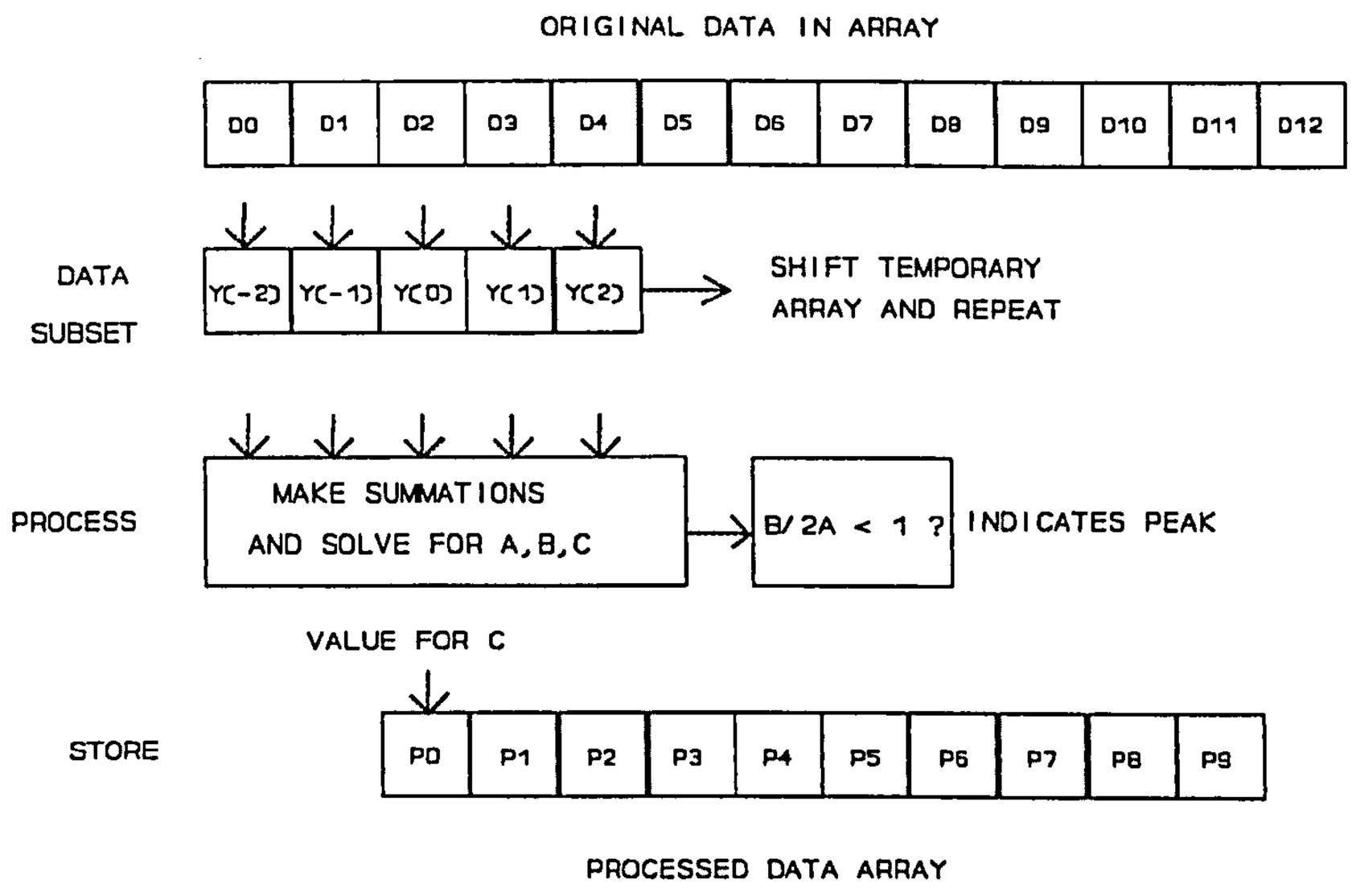

Figure 35: Implementation of "least squares fit" algorithm.

A set of (eg) five data points is taken from the array, indexing from the base of the array plus 2, and the sums calculated, from index - 2 to index + 2. The new theoretical value for the array at this index is given by the coefficient 'c', since at this point 'x' is taken as equal to 0.

The process is then repeated with the array index (which we are taking as x=0) incremented, and so on along the raw data array, calculating the values for a new array, based on the power series approximation.

7.5 Peak Indications in the Algorithm.

An additional advantage of this technique is that it is possible to determine the positions of peaks in the data.

Remembering that the data is assumed to fit the function

$$f(x) = a*x^2 + b*x + c \qquad (7.2)$$

the maximum or minimum occurs where the differential of this is 0, ie.

$$2*a*x = b \qquad (7.14)$$

If we could assume that all the maxima and minima would fall exactly on one of the data samples, then it would only be necessary to indicate data sets for which 'b'= 0. As this is not generally the case, it is more reliable to set the condition that

$$\left|\frac{b}{2*a}\right| < 1 \qquad (7.15)$$

That is, the calculated curve would have a maximum or minimum within +/- one sample of the zero point of the current data set.

It would be expected that this would give two adjacent indications for each turning point in the data, unless the calculated turning point coincided exactly with the integer sample point taken as x=0 for the current sub-set. If this occurred, of course, there would be one indication for that turning point.

7.6 Example Program and Test Data.

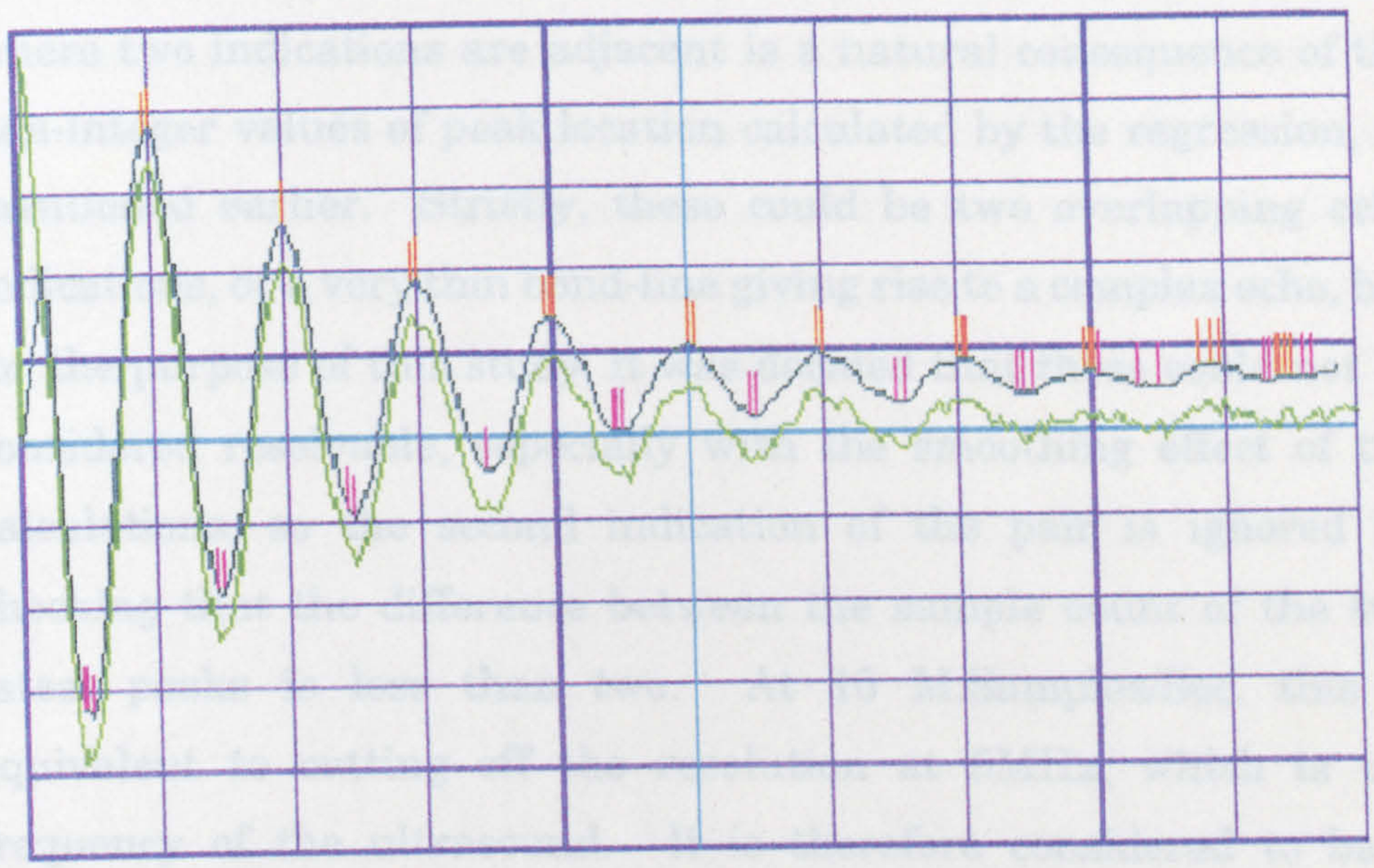

Figure 36: Demonstration of the Signal-Smoothing and Peak-Detection Ability of the Regression Algorithm.

The "least squares" approximation program was written as a sub-module and tested with a trial data set, composed of a decaying sinusoidal curve with small random fluctuations. This trace is shown in Figure 39, where the lower trace is the raw data, and the upper trace is the calculated approximation. There is a y-axis displacement applied to the two sets, to separate them on the screen, and the peaks and troughs can be seen clearly indicated, until the signal/noise ratio drops below 2:1.

The peaks and troughs (maxima and minima), are separable in the maths by the sign of the second differential of the function. In this case, all that is needed is the sign of the coefficient "a", so a line is added to the conditions for indicating a peak, that "a" is less than 0. The indications are also shown to need a threshold, to keep them from appearing in the noise of the baseline, which is covered in the test for "c" greater than 5, and this threshold could be adjusted interactively if required, with very little re-programming. The cases where two indications are adjacent is a natural consequence of the non-integer values of peak location calculated by the regression, as mentioned earlier. Strictly, these could be two overlapping echo indications, or a very thin bond-line giving rise to a complex echo, but for the purpose of this study, it was decided that these could not be considered resolvable, especially with the smoothing effect of the calculations, so the second indication of the pair is ignored by checking that the difference between the sample count of the two latest peaks is less than two. At 10 M.Samples/Sec. this is equivalent to cutting off the resolution at 5MHz, which is the frequency of the ultrasound. It is therefore considered to be a reasonable restriction on the program.

CHAPTER 8 - RESULTS WITH THE ISOLATED SYSTEM

8.1 Peak detection and Depth indication

The regression algorithm was now incorporated into the data capture program, and the parameters adjusted with experimental data, firstly from the PZT transducer, and then from the 7 x 7 array. The filtering proved inadequate with a subset of 5 data points, so this number was increased to 7. The coefficients of the simultaneous equations were altered by this change, but no other modifications were needed. The reliability of peak detection is shown in Figure 37, in which raw data (green trace) is compared with the processed data (red trace), and the A-scan peaks are clearly indicated.

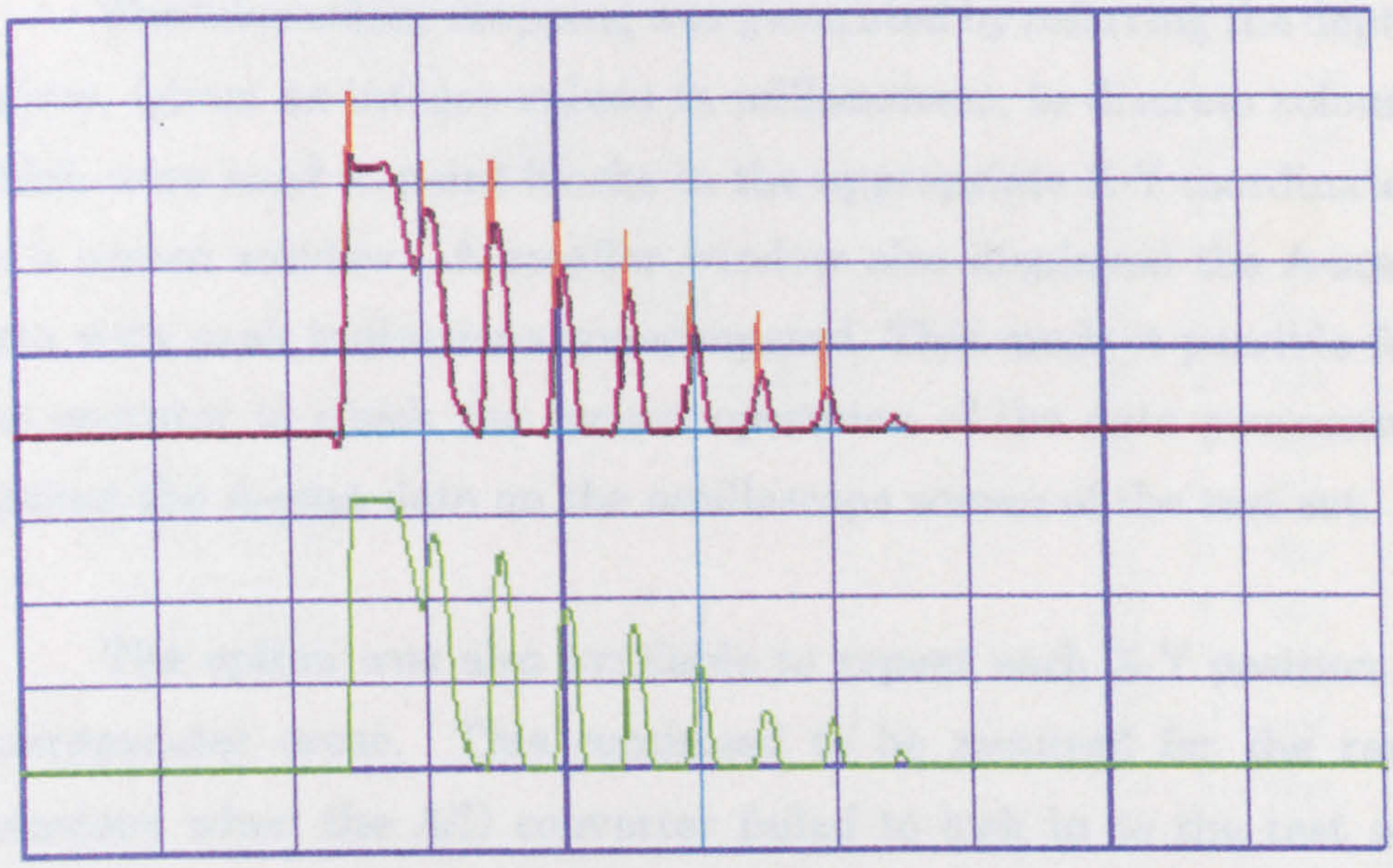

Figure 37: A-Scan Output from the Regression and Peak Detection Algorithm.

The next stage of programming was to find the most frequently occurring separation between the indicated peaks. Each time a peak was indicated, the array index for that subset was stored in an array of sample counts (PEAK[n]). The function that estimated the depth then processed this array by subtracting the sample count of each indication from the count of the previous peak, and storing these separations in a new array (SEP[n]).

This array was investigated to find the separation that occurred most often, to within ± 1 sample count, and the separations with the highest statistical frequency were averaged, before being converted into a round-trip distance by reference to the digitising rate and the speed of sound in the material under test.

The false-colour mapping was generated by referring the depth values, (given as integer values in millimetres), to discrete colours which were used to paint blocks in the appropriate X-Y coordinates on a screen window. A smaller window also displayed the A-scan data with peak indications superimposed. This made it possible for the operator to check the correct operation of the data processing against the A-scan data on the oscilloscope screen of the test set.

The option was also available to repeat each X-Y position if discrepancies arose. This continued to be required for the rare occasions when the A/D converter failed to lock in to the test set SYNC. pulse, or the internal read/write address registers in the FIFO failed to keep in step.

8.2 Array Transducer Imaging Experiments

The individual elements of the system were performing as required, so it was anticipated that some success might be obtained in imaging of the test block. System functionality was tested by placing a 5mm PZT transducer upon the test block in the positions which would correspond with the crossing points of the array transducer elements.

The resultant image, (Figure 38) shows good, reliable depth indications. These are certainly adequate for some classes of NDT, such as disbond indication for product pass/fail.

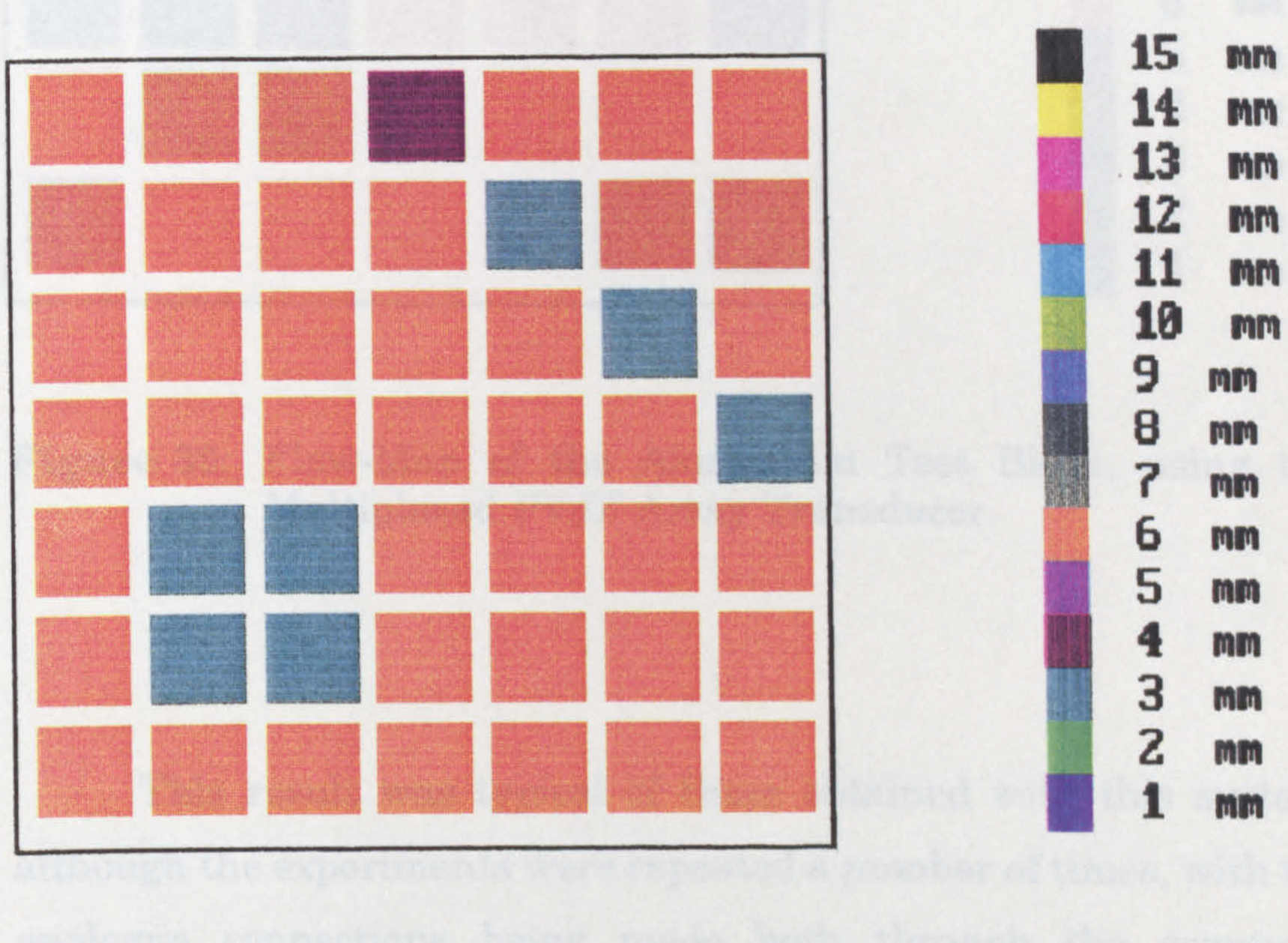

Figure 38: Flaw Map of the Aluminium Test Block Produced by the Data Capture and Display System, using a PZT Transducer for the Generation and Detection of U-S.

When the same system was used with the PVdF array transducer in position however, the quality of image (Figure 39) was much poorer. Reliability of depth indication is less than 40%, which is certainly inadequate for the purpose intended.

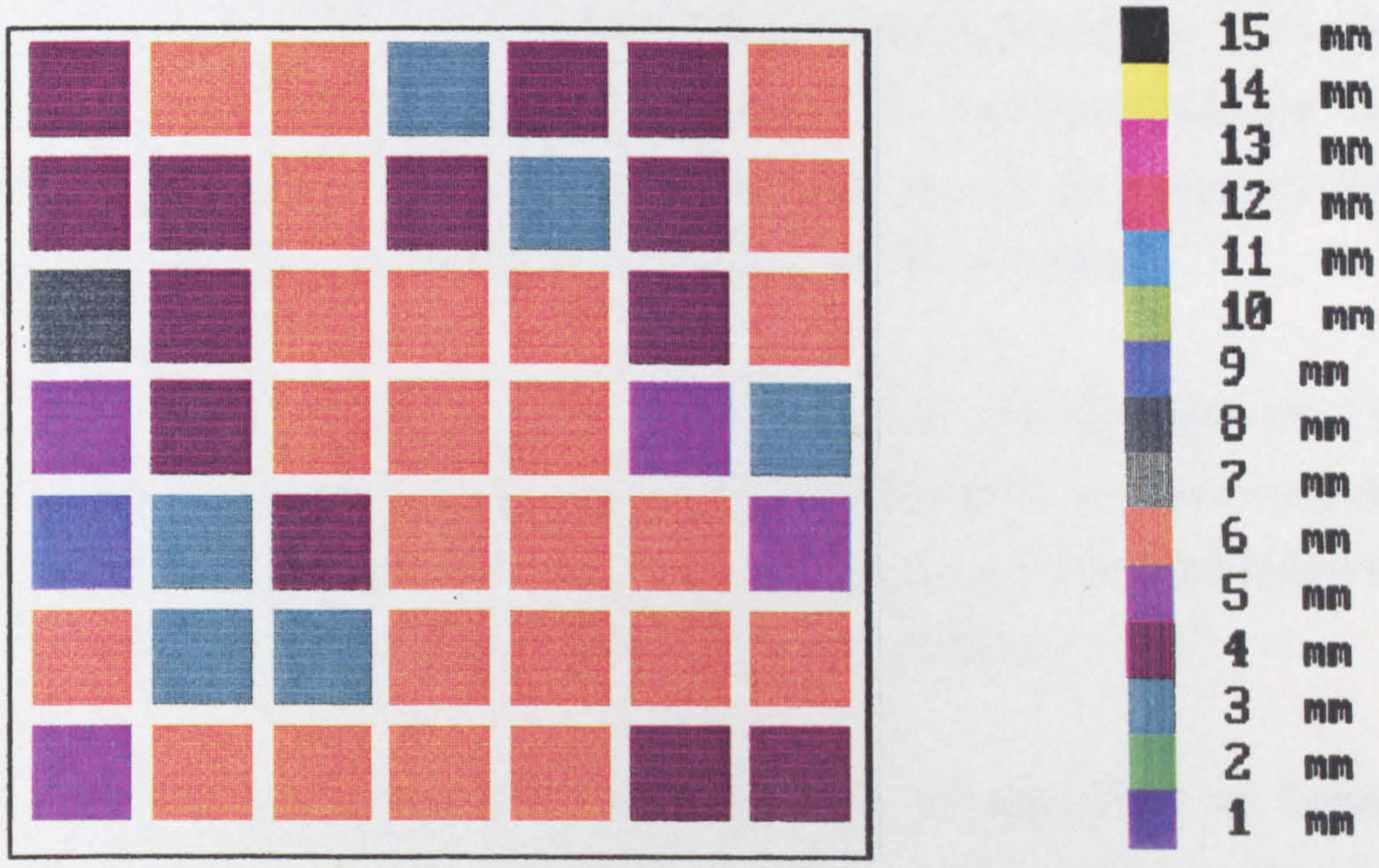

Figure 39: Flaw-Map of the Aluminium Test Block, using the Multiplexed PVdF Array Transducer.

This result was typical of those obtained with this system, although the experiments were repeated a number of times, with the analogue connections being made both through the computer controlled multiplexers, and manually direct to the test set.

8.3 Array Transducer Sensitivity Variations

Closer inspection of the A-scans produced by this transducer showed that the linear elements exhibited poor sensitivity in one location, and good sensitivity in another. This was found to be true for all elements of both axes. The problem is therefore not considered to be due to the electrical properties of the conducting elements. Possible reasons for this phenomenon included local variations in the piezo film, the effectiveness of the couplant layer, and irregularities in the construction of the laminate.

These possibilities are not exclusive, but the idea that the 'poling' applied during manufacture was uneven, giving a variation in piezoelectric coefficients across the surface of the transducer, was considered least likely, and hardest to overcome.

It was believed therefore that irregularities in bonding thickness across the transducer were the most likely cause of the variations in sensitivity. This was confirmed as a possibility through consultation with the film manufacturers (Pennwalt), who expressed the opinion that the construction technique of capacitively coupling the PVdF to the conductors was critically affected by bond line irregularities of sub-micron dimensions.

These transducer variations had been anticipated to some extent, and would not affect the peak detection and depth indication in the software. The importance of this phenomenon lay in the fact that the areas of good sensitivity were marginally above the signal/noise ratio required for imaging, whereas the ultrasound signal from the areas of poor sensitivity was not detectable above the noise leakage from the PC.

As mentioned in Chapter 6, some C-scans of the 7 x 7 transducer were then attempted, as further information was needed about the pattern of sensitivity across the array surface. Unfortunately, the cyanoacrylate bond between one layer of PVdF and the aluminium ground plane delaminated under the prolonged immersion in the C-scan water bath, and the sensitivity map was not completed.

Consistent results had been obtained from the multiplexers, pre-amplifier, digitiser, peak detection and depth indication software. The prototype bi-laminar array transducer had produced results which indicated the viability of the configuration, but had also shown the need for care in construction of the laminate. The next stage of research therefore, was to construct a number of new array transducers by varying techniques, and to tighter tolerances.

CHAPTER 9 - ADDITIONAL ARRAY TRANSDUCERS

9.1 Overview.

The perceived problem with the 7 x 7 prototype array transducer was that the variation in sensitivity of the multiplexed crossing-points of the array elements was too great for reliable materials examination. This variation was thought to be most likely due to inaccurate laminating, and poor electrical coupling from the surface of the transducer to the metallisation.

Enquiries were made to a manufacturer of flexible laminates for the electronics industry, (Flextronics, formerly Dowty Flexible Circuits.) to see if the processes used could be adopted for a flexible array transducer. If this had been possible, it would have yielded a technique able to make a strong, reliable laminate, waterproofed and possibly fitted with an industry standard plug-in edge connector. The manufacturer approached was unwilling to liaise on a small project, however, and also insisted that the cure temperature of their laminating process was 170-200°C. This, of course, is well above the ferroelectric transition temperature of PVdF (c.80°C), and it would therefore be necessary to re-pole the array transducer after manufacture.

Obviously, it is not possible to stretch-pole a laminated transducer after manufacture, and an alternative, corona poling technique would have to be adopted. This would involve a facility with field strengths of around 10^8 V/m (or 10kV for 100μm.) which does not exist within the school.

It would also be necessary to test the success of such a technique by measuring the piezoelectric coefficients obtained, and again the equipment and expertise for this were not available. This line of enquiry was therefore reluctantly abandoned, and other possible ways of manufacturing the array transducer had to be considered.

9.2 16 x 16 Array from Pennwalt.

Discussions with the PVdF manufacturers continued, therefore, and it was agreed that they would attempt to make a one-off laminate for this research. The material chosen was 40 μm thick, and had a coating of vapour deposited copper. Tracks were drawn onto this coating by the manufacturers, using an etch resist plotter pen in a CAD system. The resultant pattern of linear array electrodes was etched out of one side of two identical sheets, aligned along the poling direction. The other side of both sheets was left completely coated. The two sheets were laminated together, with the ground plane faces adjacent and the array elements orthogonal to each other. In this condition, the transducer was delivered, (at a cost of c.£500) as it was necessary to attach leads and investigate the properties of the conducting elements before waterproofing the surfaces. Following the manufacturers instructions, the leads were attached with punch-through crimp connectors supplied, and the electrical contact area enhanced with silver-loaded varnish. After checking the continuity of the connections and elements, the surfaces were coated with a waterproof laminate, and the lead areas potted under adhesive. The adhesive used for potting this transducer was a silicone rubber. This was chosen for greater flexibility than the

epoxy used earlier, since with 16 x 16 elements, with widths of 5mm and 5mm spacing between them, the transducer now had dimensions of 17 x 17 cm. (The element dimensions were chosen as optimum for tracks drawn by the manufacturers CAD system.) Furthermore, the epoxy potting used on the 7 x 7 prototype had become brittle, and was lifting from the surface after the repeated handling to which the transducer had been subjected. It was therefore considered necessary to use a much more flexible potting compound on the new array.

Initial testing of this array uncovered a serious flaw in its manufacture. Individual elements were connected to the test set as receivers, interposing a metal block, and scanning a transmitting PZT transducer over the metal block. These gave good indication of signal sensitivity, but when the transmit pulse was applied to the PVdF element, no signal could be detected. Because of the earlier problems with transducer variation, the test was repeated with several elements. Eventually, it was found that the elements were transmitting for the first few seconds after connection, but that they then stopped transmitting, and would not receive either. The conductivity of the elements was then checked, and the ones which had been used in the test were found to be open-circuit.

It is now believed that this effect was due to the orientation of the elements on the material. PVdF has two piezo coefficients, and will stretch along its 1-direction under an electric field, as well as distorting across its thickness. In consequence, the application of a 400V transmit pulse to an element, at a repetition rate of between 1 and 2 kHz appears to have caused sufficient surface stretching to initiate fatigue cracks in the copper electrodes.

When the experiments were repeated with a 20dB attenuator in the transmit pulse, the elements which had not previously been tested then functioned well, and repeatedly. The loss of signal level is unacceptable however, since the experiments are already on the limits of the signal/noise ratio, and this transducer was therefore abandoned as imaging results could not be obtained from it.

9.3 6 x 6 Array Transducer.

At an early stage in the project, a 16 x 16 transducer had been ordered from Fulmer Yarsley, (the other major manufacturer of PVdF in the UK.) This had been produced as a single sheet, before the requirement for a bi-laminar array had been discovered, and was used in the experiments that led to the bi-laminar array concept. This sheet had been fabricated with gold-sputtered contacts of 3mm width at 2mm spacing, set orthogonally on the faces of a 32μm thick sheet. As the project was now nearing completion, it was felt that this transducer would no longer be required in its single layer form. A 6 x 6 transducer was then made from it, by cutting it into squares, and utilising the gold contacts on the outside surface of the laminate, with a piece of the aluminium foil bonded between the two pieces.

This array transducer was small, being only 4cm square, and contained only six active elements in each direction. Its main purpose was to see if the different poling techniques applied by Fulmer would give a significantly different variation in sensitivity from that of the transducers which had been tested up to this point. If it had been possible to obtain a consistent sensitivity map of this transducer, then it would be feasible that the variations encountered

were due to the poling technique at Pennwalt, rather than the construction of the transducers in the laboratory.
In order to keep the transducer surface flat during the C-scan, the rear face was bonded to a 5mm sheet of perspex.

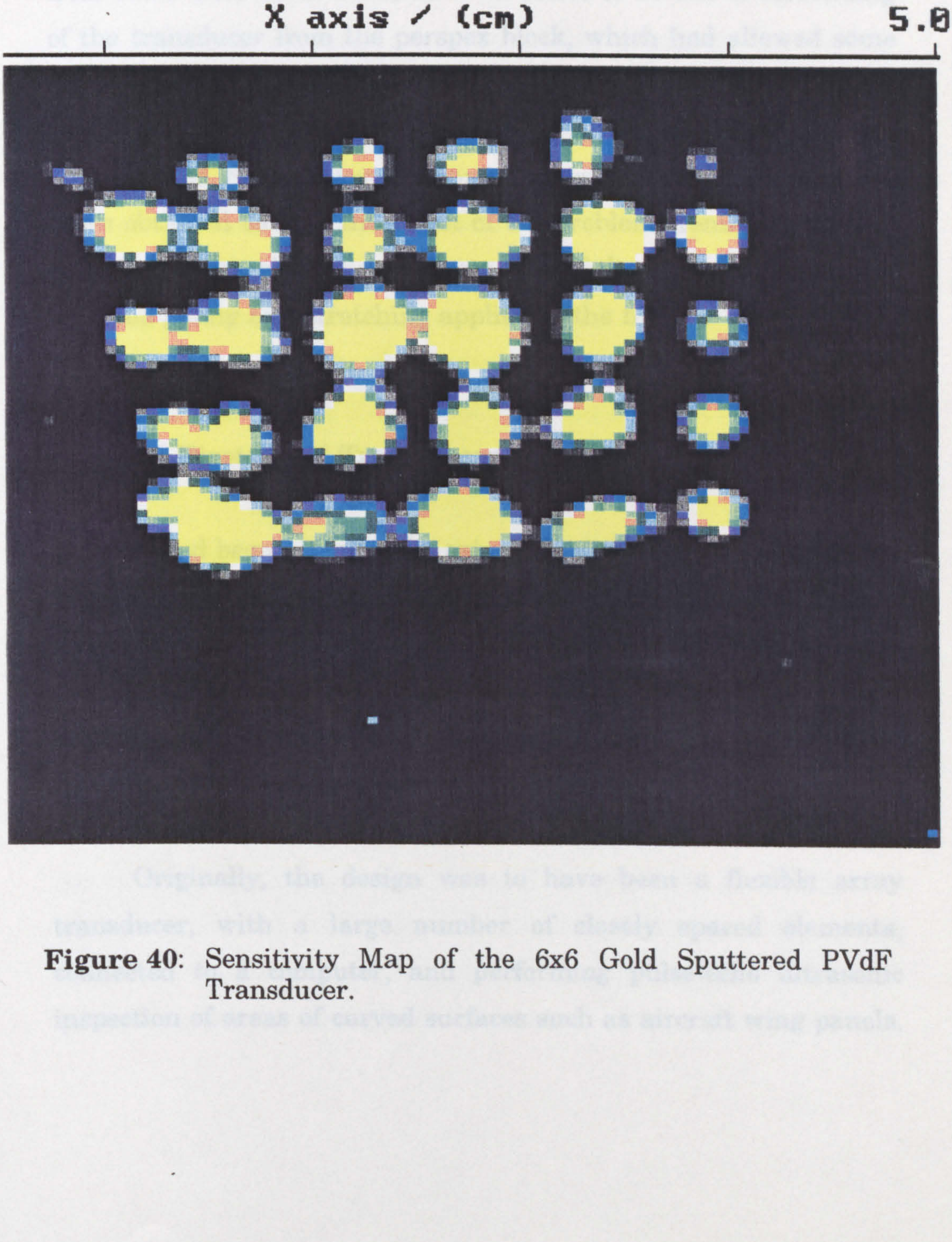

Figure 40: Sensitivity Map of the 6x6 Gold Sputtered PVdF Transducer.

The C-scan of this transducer is shown in Figure 40. The scan exhibits a wider beam width (which was expected with narrower tracks) than the 7 x 7 prototype, and large variations in transducer sensitivity, just as before. There is also an amount of overlapping of active regions in the lower left corner. On removal of the transducer from the C-scan water bath, this was found to be due to disbonding of the transducer from the perspex block, which had allowed some curvature in the structure.

It was clear, however, from the similarity of this result to those obtained earlier, that most of the problems remaining had to do with the actual physical construction of the transducer, and not with the poling and stretching applied to the film.

9.4 First Rigid Transducer.

It had been proved to be extremely difficult to manufacture a reliable array transducer in the laboratory, and neither Pennwalt, nor Fulmer, as major manufacturers of the material had produced information as to how it could best be done. The requirements of the original concept were therefore re-examined, to see if reliable imaging could be obtained in the time remaining for the project.

Originally, the design was to have been a flexible array transducer, with a large number of closely spaced elements, connected to a computer, and performing pulse-echo ultrasonic inspection of areas of curved surfaces such as aircraft wing panels.

It was proposed at this stage that the difficulties of reliable lead attachment could be solved if the requirement of flexibility were removed. A laminate could then be formed to tighter tolerances, with the lower layer of the array transducer bonded directly onto a rigid substrate.

Double sided printed circuit board was chosen as the substrate for a number of reasons. Firstly, that the lower layer of elements could be etched directly in the copper cladding of one side of the board. Secondly, that the opposite side of the board could be used as a grounded screen for the transducers and the co-axial leads, and thirdly, that the glass-fibre composite structure of the PCB would act as a good transducer backing material by dispersing and partially absorbing the ultrasound generated by the array transducer. Unwanted echoes from the rear of the structure would therefore be suppressed.

The leads for the lower layer were fed through holes in the substrate, and soldered to the 5mm tracks (at 2.5mm spacing) before the first layer of PVdF was laid. This layer was overlaid with a layer of aluminium foil, which was then connected by silver paint to an area of copper which had been left surrounding the etched elements. This upper ground plane was connected to the rear face of the PCB by wires soldered through the PCB material at all four corners. This gave ground continuity for the centre of the laminate. Measurements showed this to be less than 1 Ω between points over the entire transducer surface, and from the aluminium foil to the ground connections on the multiplexer boards.

The second layer of PVdF was then placed on top of the ground plane, and an array of aluminium foil elements was bonded to the upper surface. The other set of wires were now connected, using the silver paint and cyano-acrylate technique described earlier, and when these connections had dried and been tested, a waterproofing layer added, as used on the other transducers. RS epoxy resin was used for bonding the various layers, and care was taken to reduce this to a thin layer before adding the relevant part of the laminate. After each piece had been put in place, further manipulation and rolling was used, to reduce the bond thickness, and then the whole laminate was left under pressure for 18-24 hours to cure. The eventual result was a transducer construction that was robust and waterproof. (Figure 41.)

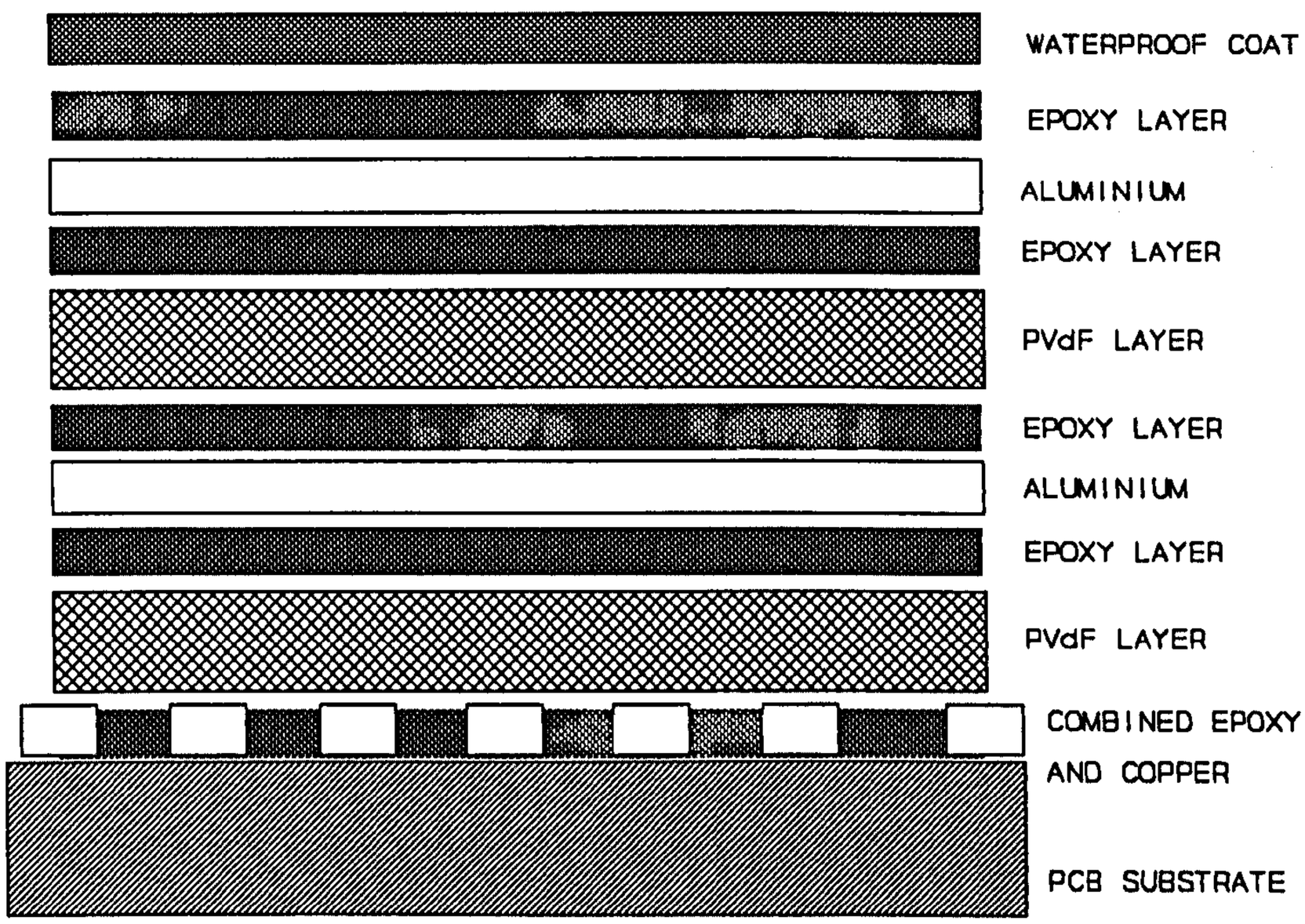

Figure 41: Cross-Section of the Construction of the first rigid Transducer, showing the number of bond-lines required.

The sensitivity of this transducer was found to be 10dB less than the best areas of the earlier prototypes, and the C-scans had to be done in TX or RX mode only. At least 6dB of this reduction was directly attributable to the extension from 7 to 15 elements, and the doubled value of the stray capacitance that results from this. The other 4dB is believed to be at least in part due to the number of epoxy bond lines in the transducer's construction.

A number of C-scans were carried out to check the variation in sensitivity of the array element crossing points. In the event, it was not possible, due to the low signal levels, to use all the receiving elements simultaneously in these C-scans, since the stray capacitance of the receiving elements reduced the signal to an undetectable level. A technique therefore had to be designed to simulate this.

The simulation was effected by connecting each element of the receiver in turn to the test set RX input, and scanning the element individually. The target for these scans was a 5mm diameter steel rod, held in the probe holder, while the elements in the other axis were energised as transmitters. Stray capacitance would not affect the transmit pulse amplitude since the pulse is driven from a 50 Ω voltage source, and the transmit elements could all be fired simultaneously. The area of scan contained the whole sensitive area of the array, so that each scan started from the same physical location on the array, and had the same dimensions. In this way, a series of data files were created, in which the individual pixel levels corresponding to a location, could be added together to obtain an overall picture of the transducer sensitivity.

Figure 42 shows the sensitivity map of the outer set of elements in TX mode (RX was through the 5mm PZT scanning transducer). One element has failed completely and had to be disconnected, due to a short-circuit where the insulated conductor passed through the PCB substrate. The other elements all show wide variations in acoustic sensitivity along their lengths.

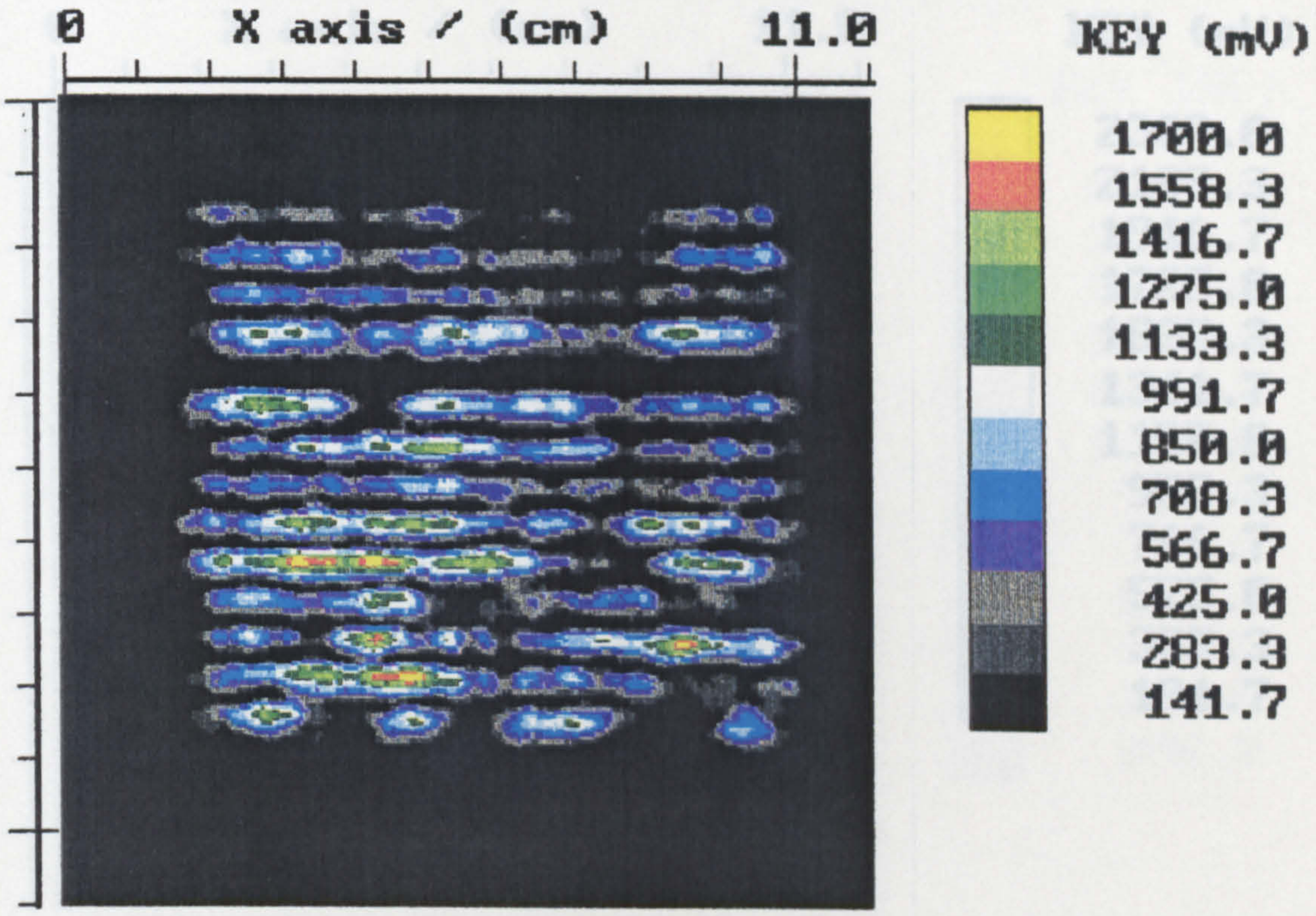

Figure 42: Sensitivity Map of the Lower Layer of the 15x15 Rigid Transducer.

Figure 43 shows a similar sensitivity map of the orthogonal elements of the rigid transducer. In this scan, the PZT transducer was transmitting and the PVdF transducer elements were each connected in turn to the RX input of the test set. 15 linear elements are clearly visible, although the sensitivity of these elements also varies over a substantial range.

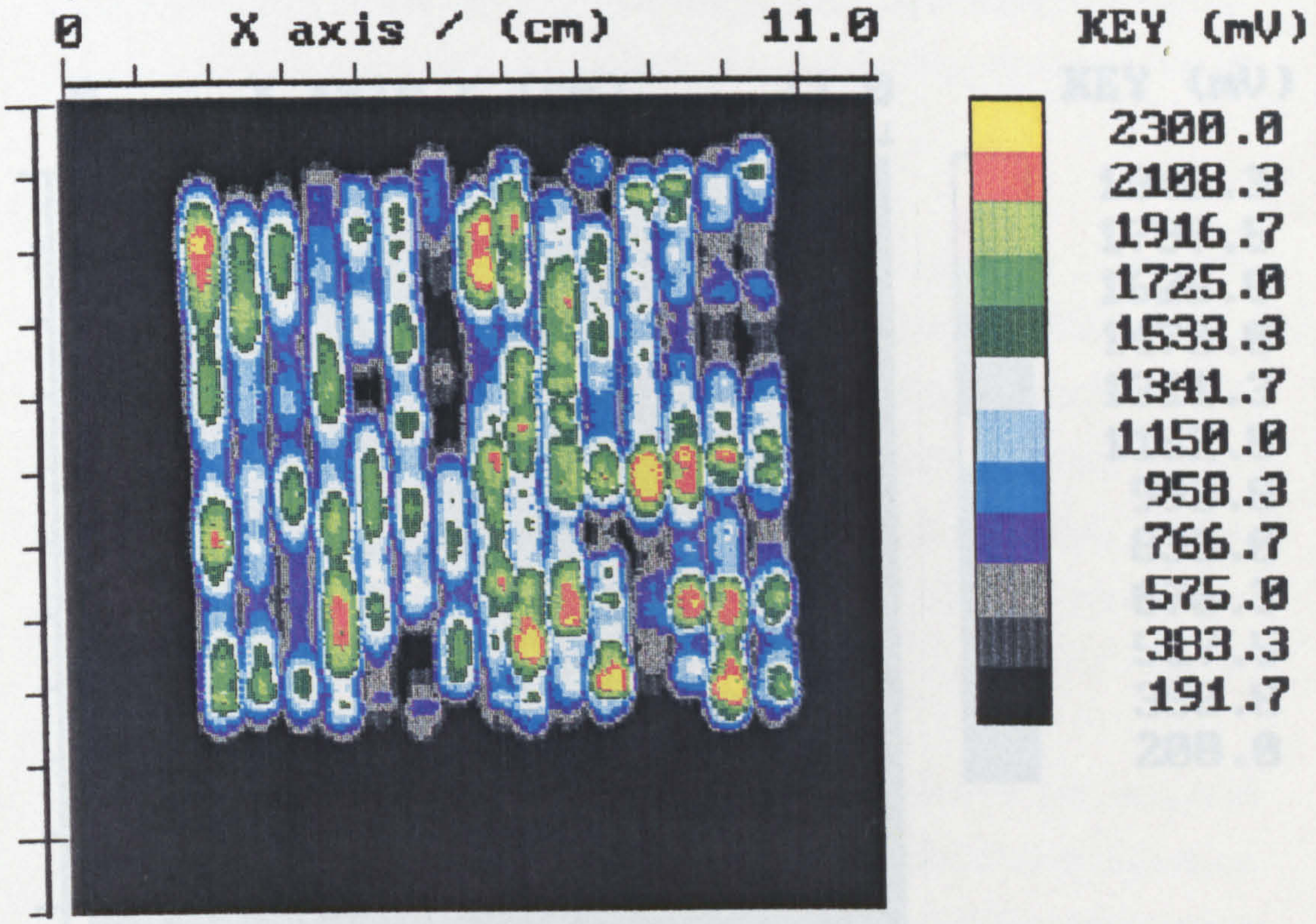

Figure 43: Sensitivity Map of the Upper layer of the 15x15 Rigid Transducer.

Figure 44 shows the effective sensitivity of the first rigid array transducer in TX/RX mode. The ball-bearing used previously did not produce enough signal in this mode to generate a visible pattern, so the scanned target for this image was a 5mm flat faced steel rod.

Some correlation can be observed between the TX/RX scan and the single mode scans, but the variation shows no obvious pattern, and is unlikely to be due to slowly varying parameters.

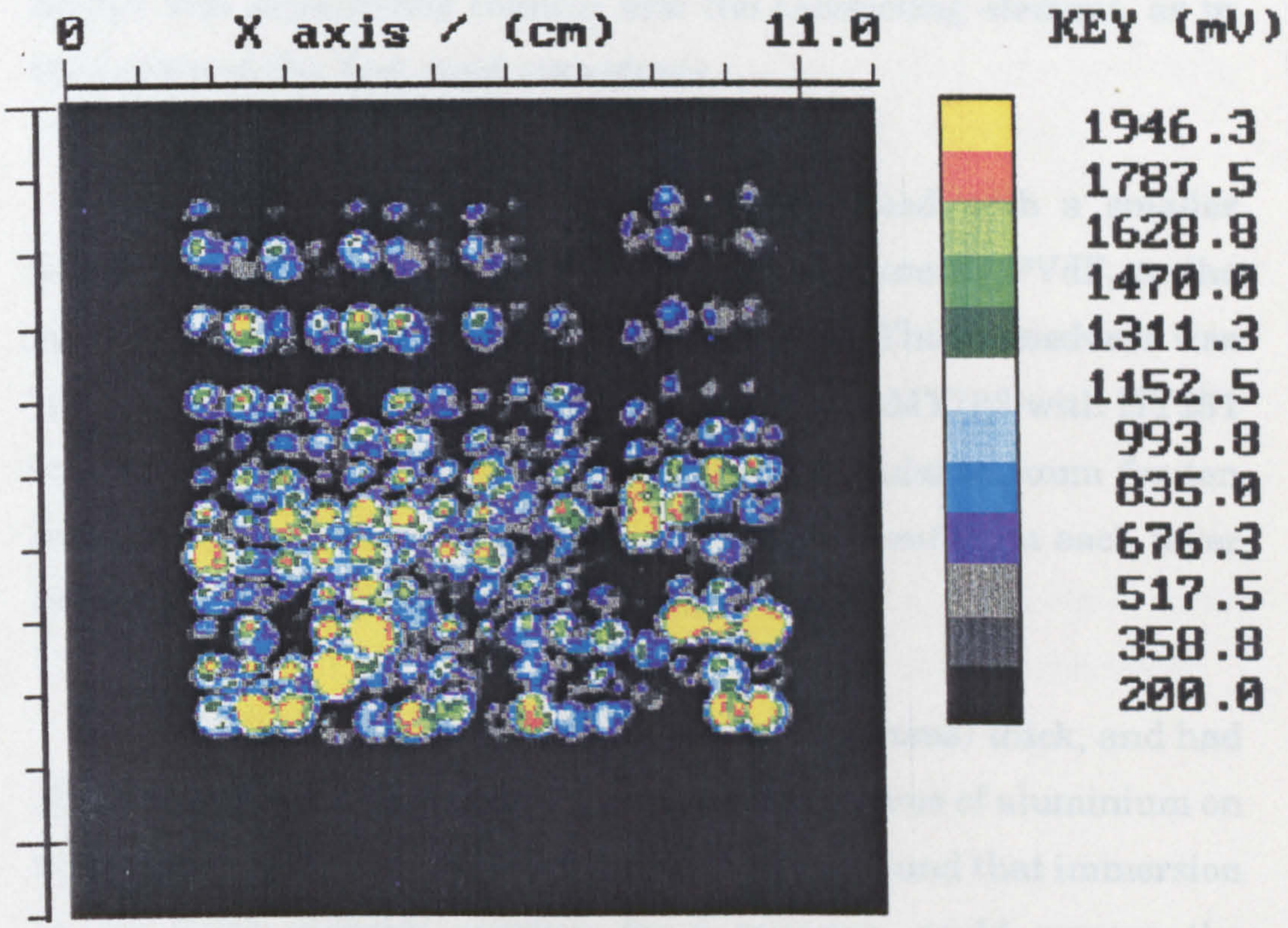

Figure 44: Sensitivity Map of the 15x15 Transducer in Combined Tx/Rx mode.

9.5 Second Rigid Transducer.

Although the sensitivity of the rigid transducer was not good enough for NDT imaging, the use of a rigid substrate had shown significant improvements in reliability of construction over the previous results. In discussion with Pennwalt, again, mention was made of an (unknown) customer of theirs which had recently suffered similar difficulties. It was believed that the signal level varied with sub-micron variations in bond-line thickness, especially where the charge was capacitively coupled into the conducting element, as in the layers of the first rigid transducer.

A final transducer was therefore designed with a smaller number of bond lines, using nickel/aluminium coated PVdF, to the same dimensions as the first rigid transducer. This transducer was laminated using a low viscosity epoxy (Araldite MY733 with HY951 hardener at 12%). The epoxy was degassed under vacuum for ten minutes after mixing, and the glue was rolled out from each layer before being left to cure in a hydrostatic press.

The PVdF chosen was 80μm (8000 Angstroms) thick, and had 50 Angstroms of nickel overlaid with 350 Angstroms of aluminium on both faces. After some experimentation, it was found that immersion in 4% ferric chloride solution for 5 minutes would remove the metallisation at a controllable rate, and the lower layer of the transducer was made from one piece of PVdF which had all the metallisation removed from one face. This was bonded to the elements etched in the PCB substrate, with the metallised face uppermost, to act as a ground plane.

The ground plane of the PVdF was then attached to the ground track on the PCB with silver paint, and the transducer was scanned, acting as a transmitter, to check on the construction technique. (Figure 45)

The scan had to be performed quickly, however, since the metallisation on the ground-plane was visibly deteriorating while the transducer was immersed in the water bath. As a result, only a 1mm resolution scan was taken, but after smoothing, and processing the image (Figure 46), it is clear that the sensitivity variation across the greater part of the active area is tolerable, being less than 20%, rather than the 80% and more of the first rigid transducer.

There is still an area across the middle of the scan, where the sensitivity is markedly lower (less than 50%) than the average, but it was not possible to repeat the scan to investigate whether this was an experimental error or a genuine problem, because of the deterioration of the ground plane.

The results at this stage appeared to indicate that reproducible imaging might be possible from this transducer on its completion.

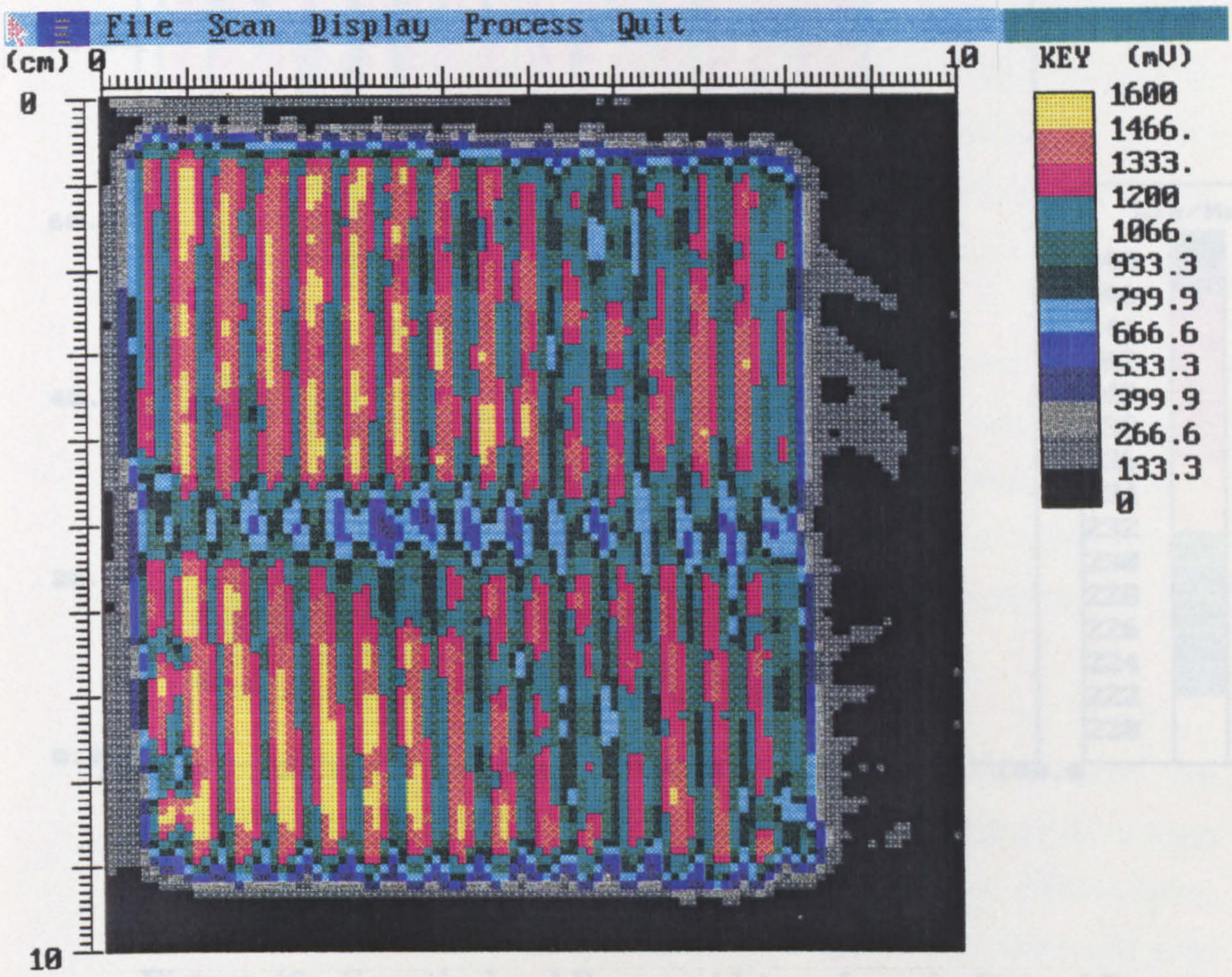

Figure 45: Bottom Layer Sensitivity Map of Final Rigid Transducer, During Construction.

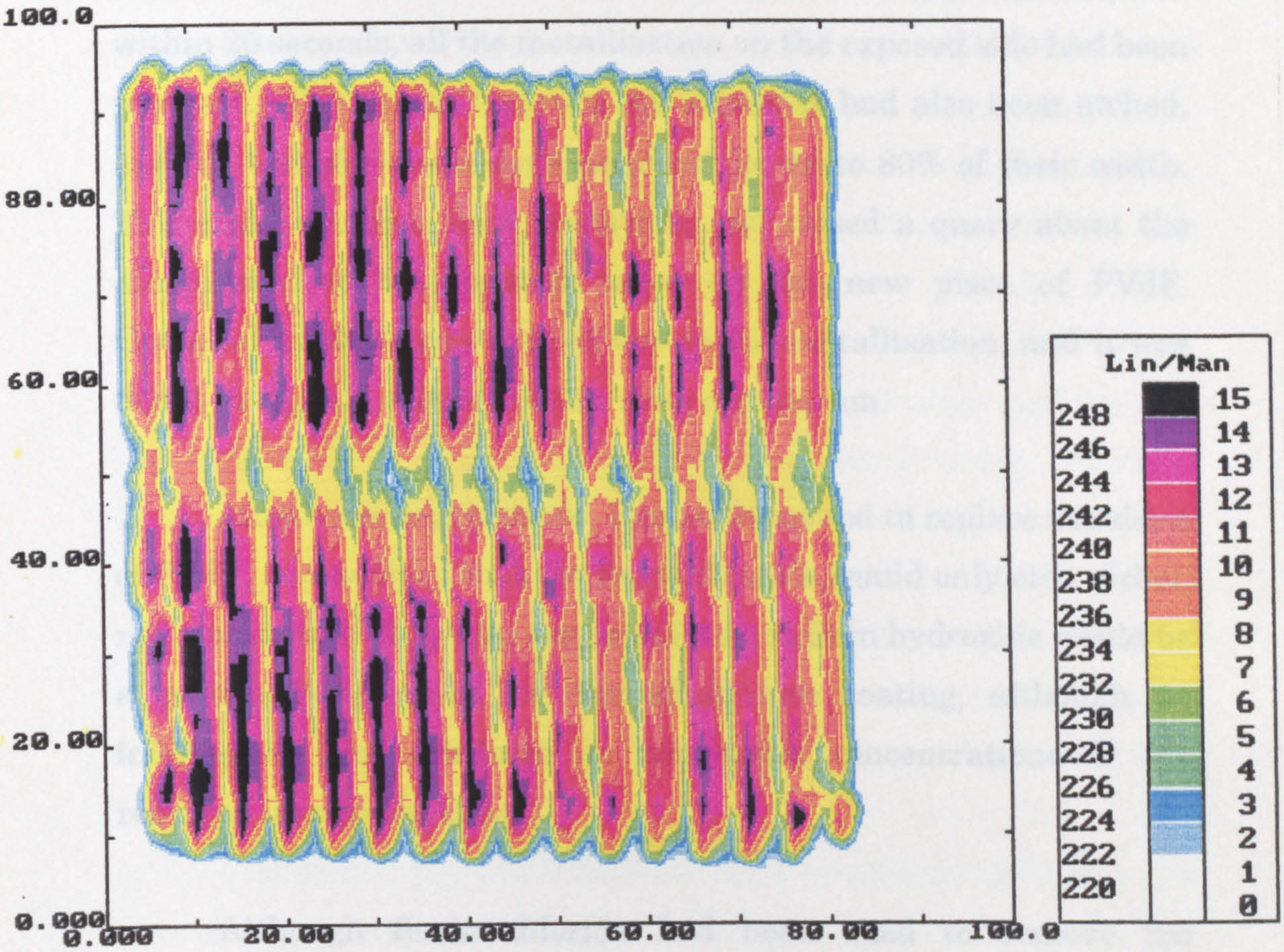

Figure 46: Smoothed and Processed Image from the Data of Fig. 45

The design of the second layer of PVdF required the metallisation to be completely removed from the lower face, and the element pattern etched into the metallisation on the top face. Another piece of PVdF was procured from Pennwalt, and the element pattern was applied with the same etch-resist transfers that were used to make the PCB layer.

Since testing had been carried out for the first layer, the masked sheet was then immersed in the 4% ferric chloride, but within 20 seconds, all the metallisation on the exposed side had been removed. The spaces between the elements had also been etched, and the transfer areas were undercut by up to 80% of their width. This could not have been predicted, and raised a query about the composition of the metallic layer on the new piece of PVdF. Chemical analysis was carried out on the metallisation, and it was found to contain copper, rather than aluminium.

After some negotiations, Pennwalt agreed to replace the sheet of PVdF, and advised that the ferric chloride would only etch nickel, not aluminium. They also suggested that sodium hydroxide would be a good etching agent for the aluminium coating, although no information was available on reasonable concentrations or the required immersion time.

Although ferric chloride had been used to remove the metallisation on the first layer, experiments showed that it was not possible to get clean edges to the array pattern with this etchant. The two mechanisms thought to be involved in the ferric chloride etching of the aluminium were the natural acidity of ferric chloride solution, (which had a measured pH of 0.7) and the possible undercutting of the aluminium layer, resulting in its breaking away from the PVdF, without going into solution.

The two stage etch process suggested by Pennwalt was then investigated. Various concentrations of sodium hydroxide and ferric chloride were used, in experiments on small (1cm x 2cm) pieces of the latest supplied PVdF, and it was found that 20 seconds of immersion

in 2M sodium hydroxide solution, followed by 15 seconds of immersion in 30% w/v ferric chloride solution would produce a well defined etch pattern.

Because of the earlier experience with the micro-cracking of elements laid along the 1-direction, it was decided to lay the transfers across the 1-direction in this transducer. The direction of stretch was quite easy to determine in these samples of PVdF, since the stretching process had produced small, but visible striations in the surface finish. The transfers were laid across these, and then firmed down by rubbing under a sheet of clear acetate, to make sure that the edges of the elements would remain sharp. The two-stage etching process appeared completely successful this time, producing a well defined pattern of 5mm wide tracks on the surface of the PVdF.

The etched piece of PVdF was then bonded straight onto the ground plane surface of the lower layer of the transducer. The transfers were not removed prior to this bonding process, as they provided raised areas to assist the press in making the bond layer between the active areas and the ground plane as thin as possible. When this epoxy layer had cured, the transfers were removed by washing with acetone, and leads were attached to each of the elements. At this point in the construction, the continuity of the connections was checked, and although the lead/element connections were all good, the elements were found to be open circuit along their length.

Further investigation indicated that the resistance over small (5mm) distances was too high for the aluminium layer to still be intact (approx. 0.5 kΩ/cm). It was also found that there were two or three complete breaks in each track. These occurred at varying intervals along the elements, and were not discernable under a reflected light microscope at a magnification of x30, although the continuity checks indicated the location to within a millimetre.

By reproducing the entire etch process on a test piece, it was found that the resistance of an element increased from 8 Ω to around 1.2 kΩ after the sodium hydroxide process, and went open circuit in similar manner after the application of ferric chloride. This phenomenon could only be explained by assuming that the etchant solution was leaching under the etch-resist transfers, along surface flaws caused by the stretch poling of the PVdF during manufacture.

Pennwalt then confirmed that they were aware of this as a possible problem, and that they had recently installed a multi-stage stretching machine to reduce the occurrence of these surface flaws.

The flawed sheet of PVdF was already laminated onto the transducer, and it was considered unlikely that it could be removed without also removing the lower layer, which had proved so successful. A number of attempts were therefore made, to find a way to restore continuity to the upper array elements. The optimum solution would have been to re-deposit electrodes, but even had the facilities been available, the temperature control required to keep the PVdF below 70°C during vapour deposition requires specialist commercial equipment to which we had no access.

Electro-plating, graphite coating and lead-loading were all attempted, without success, so eventually, a mask of adhesive acetate sheet was cut, and RS silver paint, thinned with 80% extra acetone was applied to the surface. It was acknowledged however, that this would not produce results comparable with those from the lower layer.

To finish the construction ready for scanning, a waterproof coating of acetate film was then bonded to the exposed surface. The epoxy rolled out from this layer also served to seal the lead attachment area.

The scan which had been made when the transducer was half-finished was now repeated (Figure 47), and a similar sensitivity pattern achieved, although at a lower amplitude. (Note, the transducer is aligned at right-angles to the previous scan.)

A similar scan of the top layer (Figure 48) shows 60% sensitivity variations which are better than expected, but not as good as the earlier result implied.

A set of C-Scans were then completed, using a 5mm steel ball bearing as the target, with all the elements of one layer simultaneously energised as transmitters, and an individual element from the other layer connected to the test set as a receiver. These scans were then added together, as before, to give a sensitivity map of the final transducer in TX/RX mode. (Figure 49.)

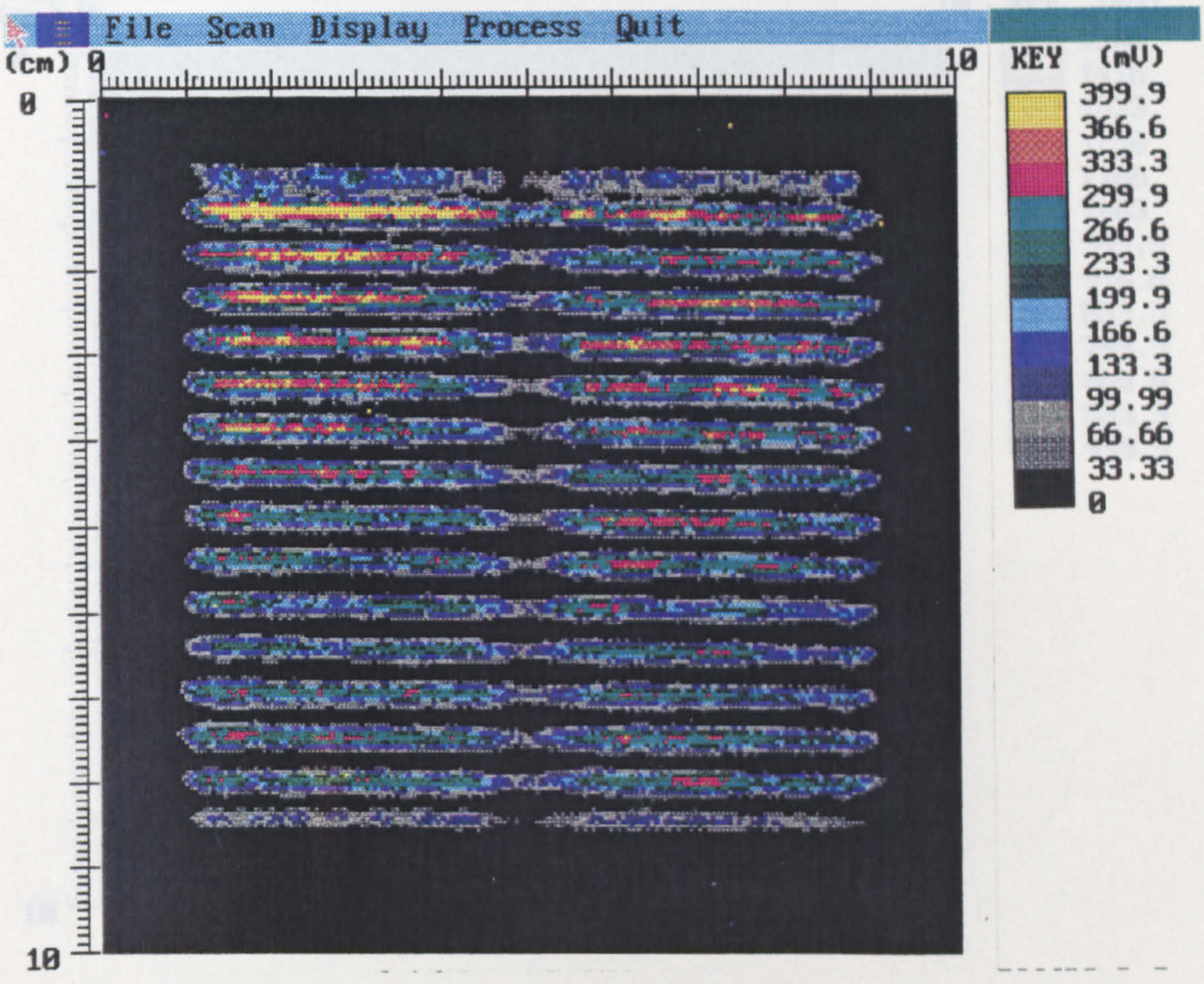

Figure 47: Bottom Layer Sensitivity Map of Final Rigid Transducer.

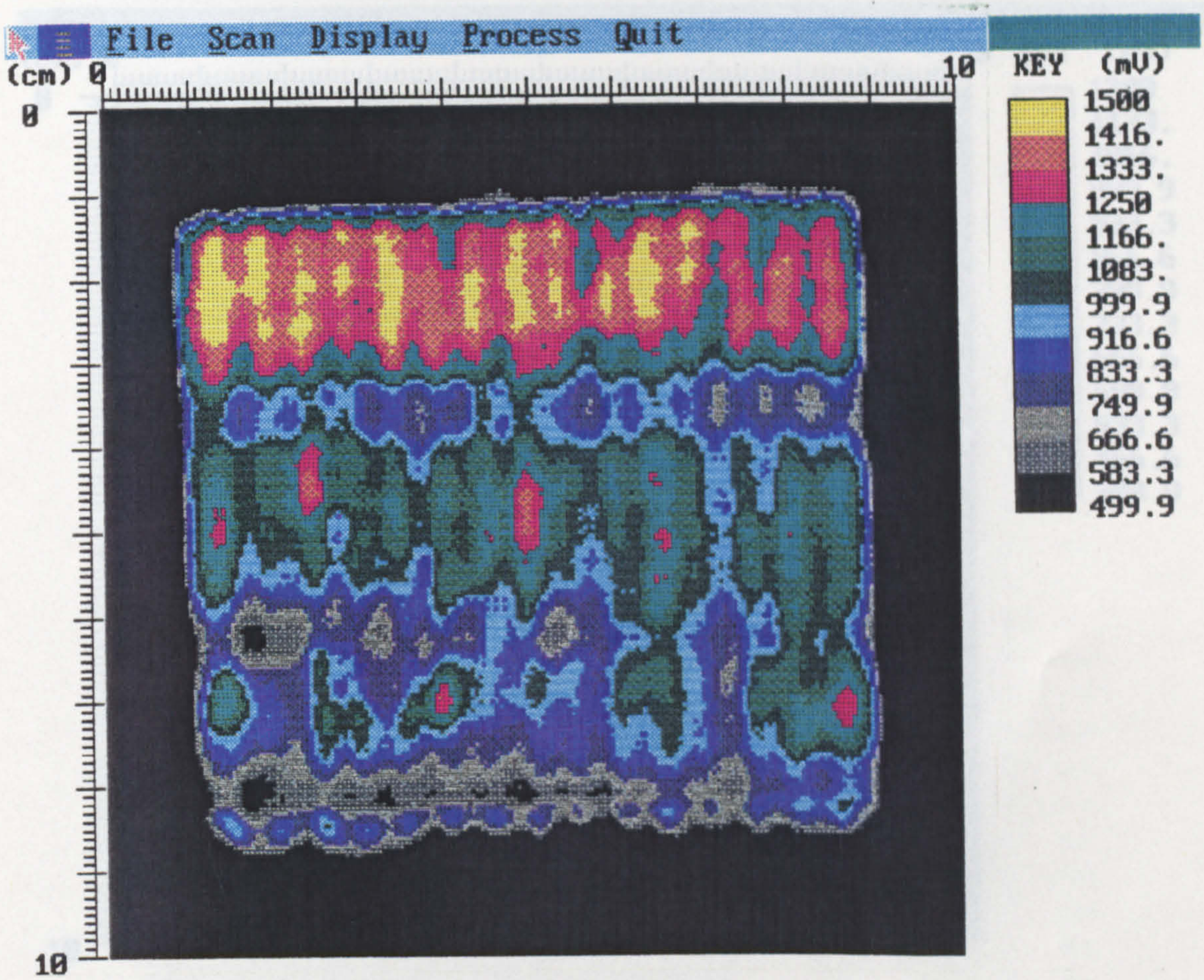

Figure 48: Second Layer Sensitivity Map of Final Rigid Transducer.

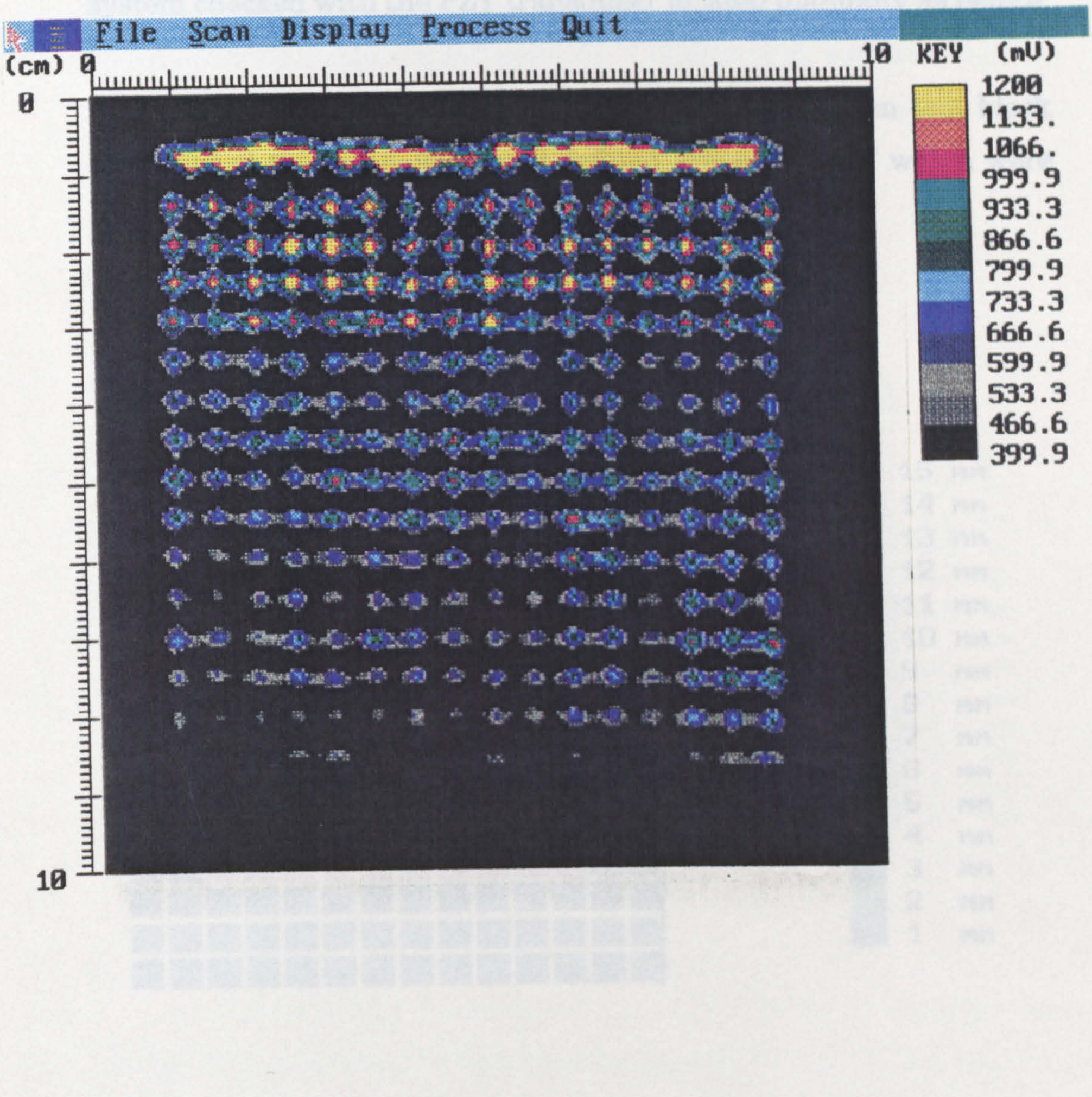

Figure 49: Sensitivity Map of the Second Rigid Transducer in Combined Tx/Rx mode.

These scans indicated that consistent NDT flaw detection may be possible from the rigid array transducer. The system was set up for 16 x 16 elements at the new dimensions, and the reliability of the system checked with the PZT transducer located manually as before.

Figure 50 shows the flaw map of the aluminium test block produced at this time, with well defined areas of "flaw" which were consistently indicated.

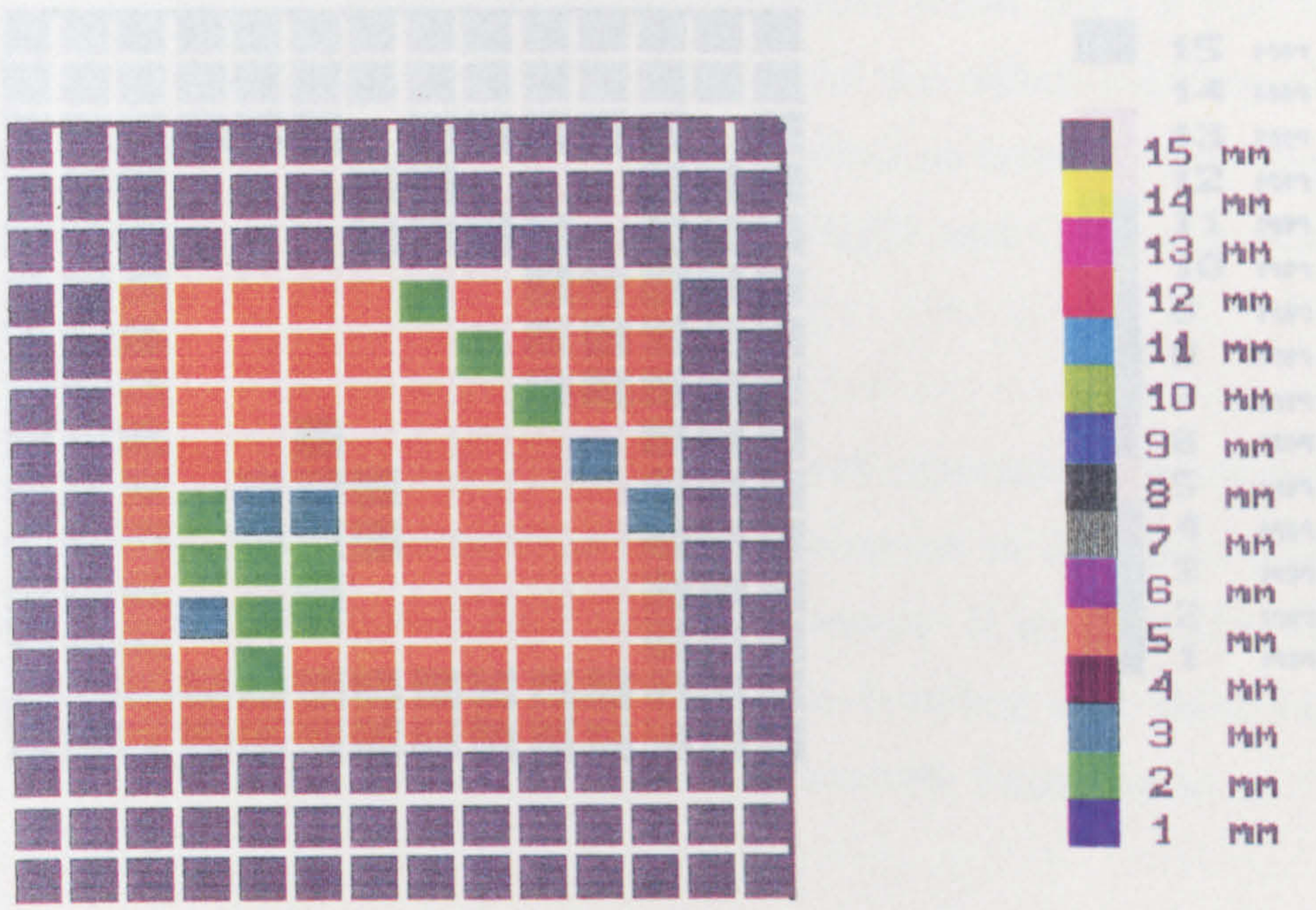

Figure 50: Flaw map of the Aluminium Test Block Produced by the 16 x 16 system using a PZT Transducer.

When the array transducer was attached to the ultrasonic test set, clear echoes were observed from crossing points over the full thickness of the test block, but the amplitude of the echoes from the machined area were somewhat smaller. The flaw map produced by this transducer is shown in Figure 51. Considerably better reliability was now obtained than the prototype transducers had produced, but this has been at the expense of flexibility.

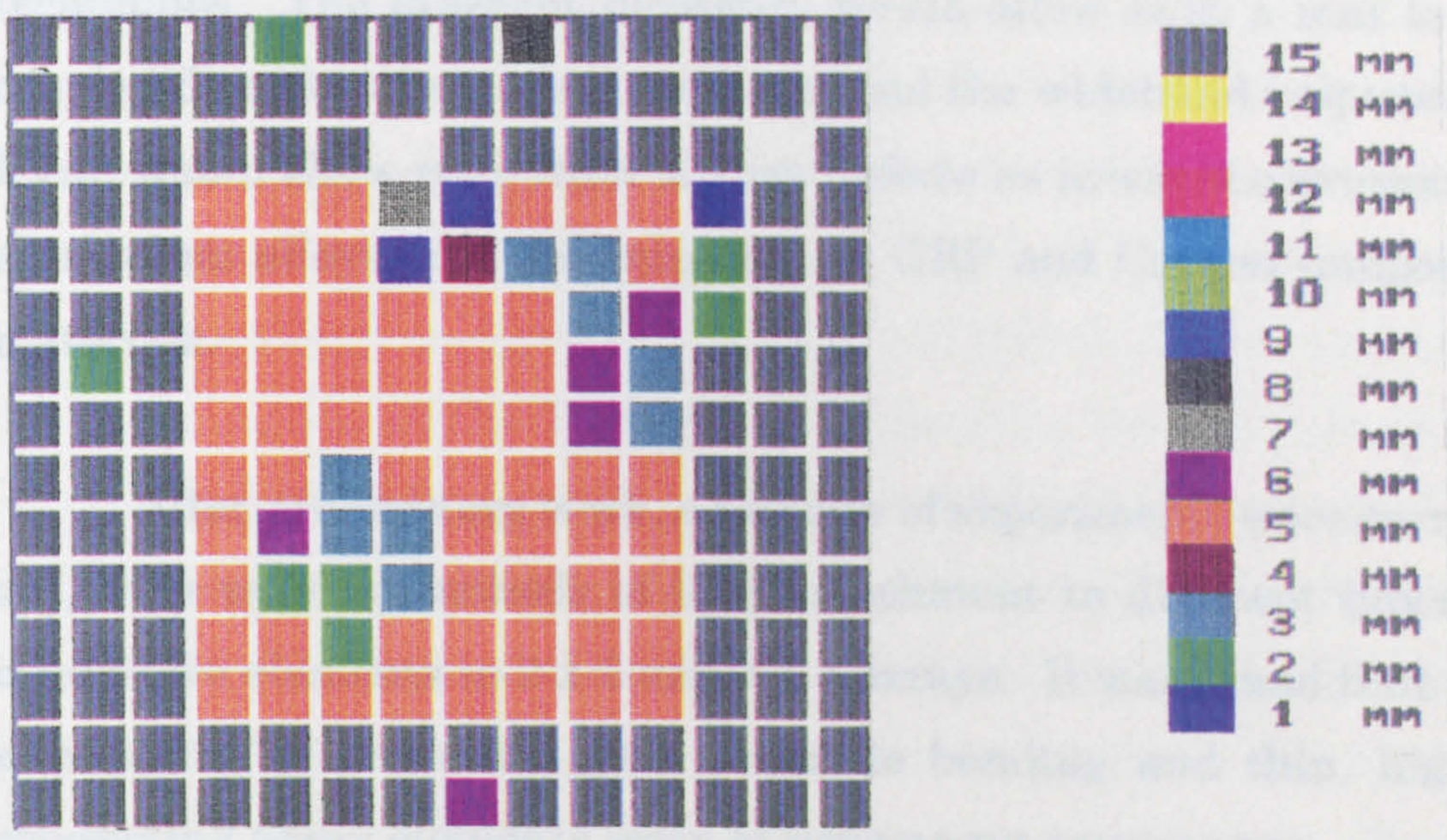

Figure 51: Flaw Map of the Aluminium Test Block Produced by the Final Rigid Transducer

CHAPTER 10: CONCLUSIONS

10.1 Validity of the Array Transducer Concept.

This project was proposed, to investigate the possibility of using a sheet of the piezoelectric polymer PVdF as a flexible pulse echo ultrasound array transducer. It was hoped that by appropriate metallisation of active areas on either side of the sheet, and some computer-controlled multiplexing, an indication of sub-surface defect location and size could be obtained, without the need to use C-Scan techniques. The inherent flexibility would allow such a mat to be coupled directly onto curved surfaces, and the wideband response of PVdF would allow resolution of such defects as internal corrosion in aluminium alloys, and delamination in GRP and Carbon composite materials.

After preliminary work, a number of experiments were carried out, with various methods of lead attachment to different types of conductive elements in 2 x 2 and 4 x 4 arrays. It was found that the elimination of crosstalk, good electrode bonding and thin, highly conducting array elements were of paramount importance.

On the basis of these results, an 8 x 8 array was constructed, using gold sputtered contacts on 32 μm PVdF film. The elements were connected to a wideband differential amplifier, to reject the common-mode crosstalk. The 8 x 8 array was tested in this configuration by being coupled onto the face of the steel test block, and scanning a small diameter ceramic probe transmitter over the array area.

The most important result of this investigation was unexpected in that the upper surface of the array showed good sensitivity along the entire length of the switched element, while the lower surface of the array gave no signal at all. That is, that the transducer surface adjacent to the steel sample was not able to generate any electric field relative to the upper surface.

This result was substantiated by a number of tests, and led to the conclusion that the steel sample was acting as an effective electrical ground, whether it was connected to the circuit or not.

This result presented a major problem for the feasibility of the simple array transducer as it had first been conceived.

After some thought, it was concluded that the original proposal for a single sheet of PVdF would not be feasible, but that a laminate composed of a metal ground-plane sandwiched by two sheets of PVdF, might exhibit the required properties. The linear active elements would be located on the outer faces of the laminate, at right angles to each other. One set of elements would be used as transmitting transducers, and the other set as receivers, thereby obtaining X-Y positioning of the pulse-echo signal.

A prototype array transducer was constructed with 7 elements on each side, made by spraying conductive paint through a mask, and a ground plane made from thin aluminium foil.

The initial results with this transducer were encouraging. When laid on an aluminium test-block with flat-bottomed holes milled into it, it was possible to observe different echo characteristics

from some of the elements over the holes, compared with those over the full thickness of the block. There appeared to be a number of spurious results, of elements only working occasionally, and of a wide variation in crosstalk and sensitivity, but these were considered to be the fault of the hand-built prototype, rather than any inherent flaw in the system as such.

The bi-laminar arrangement has now been tested with a number of different arrays, of varying construction. The transducer elements have been shown to exhibit the anticipated spatial resolution in x and y directions and despite the limitations of PVdF as a transducer material, imaging experiments have been conducted which demonstrate the potential of this type of array transducer.

10.2 Theoretical Limitations

The extent of the differences in electrical and mechanical properties between PVdF as a piezoelectric material, and the commercial ceramic transducers, indicated that it would be unwise to attempt close theoretical modelling of the configuration in the early stages, although a simple comparative calculation (Chapter 2) indicated that a single element PVdF transducer would be approximately 60dB less sensitive than an equivalent PZT transducer, for examining metal samples.

Preliminary investigations were therefore carried out with a single element PVdF transducer to determine the signal levels from a simple air-backed configuration. The pulse shape and comparative sensitivity generated and received by simple PVdF probes was

determined for compression wave transduction into a standard 25 mm steel test block, and compared with the figures achieved by equivalent PZT probes.

The oscilloscope traces obtained using the PVdF transducer were in close agreement with the general characteristics of a wide bandwidth transducer.

The sensitivity was measured, and found to be -30dB for received signals, -40dB for transmitted signals and -70dB overall, referred to an average figure derived from three nominally identical commercial PZT probes. This was considered to be in reasonable agreement with the predictions of the simple model, and more accurate modelling was therefore considered unnecessary.

It was clear at this stage, however, that the low signal level would be one of the major factors affecting the success of the array transducer concept.

One of the factors influencing the sensitivity was the stray capacitance of the areas of active element not directly influenced by the ultrasound pressure wave. In effect, the voltage output of the element was found to be inversely proportional to the length. One possible way out of this difficulty might have been to use charge, rather than voltage amplifiers. However, the susceptibility to noise and leakage of this type of amplifier would have required siting an individual amplifier for each receive element on the PVdF transducer material. This was deemed impractical, and there existed therefore a limitation on how long the receive element could be made, which limits the number of elements in the matrix. The signal from a

single transducer required the application of around 70dB of test-set gain to restore the peak-to-peak amplitude , so the array transducers were first limited to 7 x 7, and required 85dB.

Later transducers were made with 16 x 16 elements, and were mainly investigated in a water bath. The better acoustic impedance match between PVdF and water allowed clear ultrasonic signals to be obtained at around 70dB, instead of the predicted 90dB. (These figures are all approximate because of the large variations in sensitivity experienced with the array transducers.)

The lateral resolution of the proposed array was also studied using the Fraunhofer (Far-Field) diffraction equations for a one-dimensional model. This gives a figure for the ultrasonic beam divergence angle at distances much greater than the transducer diameter. The optimum element width and separation is therefore dependant on the depth of specimen. For a round-trip distance of 50mm in steel, the optimum width is around 5mm for 5MHz, and the Rayleigh criterion requires element separation of 2.5mm. Consequently the array transducers in this research were all made with dimensions of this order.

The element widths of a transducer designed for the imaging of defects in thin plates could, however be much smaller than this, since it would be operating in the Fresnel, or Near-Field diffraction zone. This research did not investigate the possibility of a near-field transducer, however, for three reasons. Firstly, the array transducer concept had not been investigated before, in relation to pulse echo NDT, and the feasibility of imaging was much easier to ascertain using a large-dimension transducer. Secondly, the amplifier 'dead-

zone' on the available test-sets effectively swamps the near-field for small transducer dimensions. This would have required the design and testing of a special pulser/receiver, before any experiments could be performed. Although several pre-amplifiers were designed with this in mind, it has proved to be difficult to improve upon the performance of the test-sets at the high-gains required for a PVdF array transducer. Thirdly, the difficulties of accurately and reliably connecting transducer elements to wires occupied considerable time and effort, even with element widths of 5mm, and would have been considerably harder for elements smaller than this.

10.3 Data Capture and Display Routines.

Work was then undertaken to drive the transducer through multiplexers and digitise the A-Scan, in order to display the Ultrasound information on the computer screen. A 6-bit, 10 M.Samples/sec. flash converter was built into a PC compatible prototyping board, and configured as a transient recorder, armed from the PC and triggered by the Sync. pulse from the test set.

This configuration worked well with commercial PZT transducers, but it was discovered that the low signal level from PVdF was completely swamped by the intrinsic electrical "noise" generated by the PC.

Several attempts were made to "screen" the transducer, but the noise proved to be present on the ground lines of the analogue system, rather than the expected airborne RFI.

After some consideration the A/D converter was removed from the PC prototyping card, and built into a screening enclosure with a separate power supply and a specially designed pre-amplifier . The digital I-O from the PC was coupled into these analogue circuit through opto-isolators, and the multiplexers were expanded from 8-way to 16-way.

Many different configurations of pre-amplifier were attempted, based on easily available video amplifier IC's such as the MAX 455 8 input video amplifier and multiplexer, and the Phillips NE 592 tunable differential video amplifier. A configuration of pulse suppressing diodes, DG435 CMOS multiplexer and a wide-band discrete amplifier based around the CA 3046 transistor array was found to exhibit the best phase-gain margin and stability. It could not, however compete with the stable 89 dB gain of the NORTEC NDT-150 ultrasonic test set and so the test set had to be retained as a basis for the analogue signals. Various difficulties continued to plague this arrangement, consisting of spurious triggering, earth loops, and the occasional unrequested re-booting of the PC, but despite this, it was still possible in the end to display the ultrasound information from the PVdF mat probe on the screen of the PC.

The next stage of the project was to determine the depth of the echo from the Ultrasound trace. Because of the widely varying signal levels, and poor signal/noise ratio it was decided to use non-linear regression to smooth the data and look for peaks. An algorithm was designed which acted as a steep cut-off low-pass filter,(with a cut-off frequency at about 2 MHz,) and also detected echo peaks. The depth of any detected peaks was then passed to a routine which looked for the most frequently occurring separation, and converted that into a

depth. The depth was colour coded, and an indication for that location in the array transducer was put on the screen as a coloured square.

The program functioned well with the commercial PZT transducer being scanned over the surface of the aluminium test block, but imaging results with the PVdF array transducer were rendered meaningless by its inconsistency and unreliability.

10.4 Critical Factors in Array Transducer Construction.

A facility became available, during the last phase of the research to perform high quality C-Scans in the laboratory. By connecting elements of the array transducer to this apparatus, and using a ball-bearing as the target in the scanning arm, it was now possible to investigate the angular resolution of the array transducer, and confirm the theoretical expectations. The uniformity of sensitivity of the array transducer was also studied. This turned out to be highly variable, as was by now suspected. Furthermore, prolonged immersion of the transducer caused the cyanoacrylate to weaken, and the transducer delaminated.

The possible reasons proposed for these sensitivity variations were variations in piezoelectric coefficients in the film, (which would be caused during the poling process in the film's manufacture,) and variations in the bond line thickness between the layers of the laminate. These are not exclusive, and a combination of these effects was thought to be responsible for the poor quality of array transducers that it was possible to manufacture in the laboratory.

During the last phase of the project, therefore, several more transducers were constructed to the same basic design, but with varying details as to element number and width, type of glue and materials used in the elements and electro-mechanical connections. The most promising of these should have been the laminate obtained from Pennwalt, who supplied most of the PVdF used in this study. However, the 16 x 16 matrix of 5 mm elements at 10 mm spacing which they supplied had elements made of very thin copper, which had been vapour deposited on the surface. These elements were aligned along the 1-axis (the direction of stretch,) and when the probe was energised with the transmit pulse, the resultant surface stretching caused micro-cracking of the conducting layer within seconds. It took a number of experiments to find this out, by which time the transducer had been rendered useless.

Two further transducers were constructed in which the need for flexibility was abandoned. The basic design was retained, but the first layer of PVdF was laid on a piece of printed circuit board material, which had the element pattern etched onto it. The adhesive used in the first of these rigid transducers was a viscous epoxy resin, which was rolled out from each layer as it was constructed, and the ground plane and top conductors were made from 2 micron aluminium foil. C-scans of this array immediately indicated that the variation in sensitivity across the surface were too great to obtain any images, and this was borne out by experimentation.

The whole transducer was then re-constructed using nickel/aluminium coated PVdF with a thickness of 80μm. A low viscosity Araldite product replaced the general purpose epoxy resin, and this was degassed and cured under a hydrostatic press. After a number of setbacks, this transducer was completed, although not as well as had been hoped, and it produced encouragingly reliable, and consistent results which give cause to believe that a properly made bi-laminar transducer could indeed be used in pulse-echo ultrasonic NDT, and a number of other applications requiring ultrasonic imaging.

10.5 Suggestions for Further Work.

A working configuration for an X-Y array transducer has been designed, and limited resolution ultrasonic imaging has been obtained from laboratory-made prototypes. However, there are two major factors which need to be overcome for this technique to become widely applicable.

Firstly, the sensitivity of an array transducer made from PVdF is at the limit of conventional electronics. It would be valuable, therefore to pursue a significantly improved pre-amplifier design for this kind of transducer. This would probably be a high-frequency charge amplifier, which would enable arrays with larger numbers of elements to be constructed.

Secondly, the construction techniques available in this research could not produce laminates with tight enough tolerances, or reliable electrical connections. Some further liaison with industry is

recommended, therefore, so that array transducers can be constructed for research into possible applications. The techniques of flexible printed circuit manufacturers seem eminently suitable for this, but facilities would need to be available for re-poling of the PVdF. In addition, facilities for the measurement of piezoelectric coefficients would be necessary to eliminate any effects which may be due to inhomogeneity in the transducer material.

Possible applications which have occurred during this research include small-dimension high-frequency arrays for thin films and small component inspection, conformal arrays for underwater imaging for the offshore industry, and large arrays for the examination of wing-panel delamination in GRP aircraft. The success of any of these possibilities is dependent on the above factors, but it is the opinion of the author that the problems are not insurmountable, and that the two-dimensional bi-laminar array transducer investigated in this research is a useful addition to the imaging and measurement techniques available to the scientific community.

REFERENCES

1. J.Curie and P.Curie, *C.R.Acad.Sci.Paris,* vol. 91, p. 294, 1880

2. H.Kawai,*Jap.J.Appl.Phys.*, vol. 8, pp. 975-976, 1969.

3. K.C.Shotton, D.R.Bacon and R.M.Quilliam, *Ultrasonics*, vol.18, pp.123-126, 1980.

4. A.S.DeReggi, S.C.Roth, J.M.Kenney, S.Edelman and G.R.Harris, *J.Acoust.Soc.Amer.*, vol. 69, pp.853-859, 1981.

5. P.A.Lewin, *Ultrasonics,* vol. 19, pp. 213-216, 1981

6. H.R.Gallantree, 1983 *Ultra.Symp.Proc.IEEE.*,0090-5607/83/0000-0757, pp. 757-759.

7. T.A.Henriquez and R.Y.Ting, *Jap.J.Appl.Phys.*, vol. 24, p. 876, 1985.

8. M.Tamura, T.Yamaguchi, T.Oyaba and T.Yoshimi, *J.Audio Eng.Soc.* vol 23. p.21, 1975.

9. D.W.MacKiernan, *CORADCOM Report* AD-A076952.

10. G.M.Garner, *Systems Technology*, vol. 27, p.22, 1977.

11. J.W.Hunt, M.Arditi, and F.S.Foster, *IEEE Trans.Biomed.Eng.*, vol. 30, pp.453-481, 1983.

12. A.Ambrosy and K,Holdik, *Journal of Physics E-Scientific Instruments*, vol. 17, pp. 856-859, 1984.

13. L.Bui, H.J.Shaw and L.T.Zitelli, *Electronics Letters,* vol. 12, p. 393, 1976.

14. K.F.Bainton, M.J.Hillier and M.G.Silk, *Journal of Physics E-Scientific Instruments,* vol. 14 p. 1313 1981.

15. J.Buchler, M.Platte and H.Schmidt, *Ultrasonics,* vol. 25, p. 112 1987.

16. W.P.Mason in *Electromechanical Transducers and Wave Filters* (Princeton, NJ; van Nostrand) (1948)

17. R.Krimholtz, D.Leedom and G.Matthei, *Electronics Letters,* vol. 6, p. 398 1970.

BIBLIOGRAPHY

1. Alonso M. and Finn E.J. — Fundamental University Physics II. Fields and Waves. Addison-Wesley. (1978).

2. Bleaney B.I. and Bleaney B. — Electricity and Magnetism. Oxford University Press. (1978).

3. Ensminger D. — Ultrasonics. Fundamentals, Technology, Applications (Second Edition). Marcel Dekker,Inc. New York. (1988).

4. Gooberman G.L. — Ultrasonics. Theory and Application. The English Universities Press Ltd. (1968).

5. Halmshaw R. — Non-Destructive Testing. (Second Edition). Edward Arnold. (1991).

6. Horowitz P. and Hill W. — The Art of Electronics. Cambridge University Press. (1980).

7. Jeffrey A. — Basic Mathematics for Engineers and Technologists. The Whitefriars Press London. (1974).

8. Kernighan B.W. and Ritchie D.M. — The C Programming Language (Second Edition). Prentice-Hall International (1988).

9. Silk M.G. — Ultrasonic Transducers for Nondestructive Testing. Adam Hilger Bristol. (1984)

10. Topping J. — Errors of Observation and Their Treatment. (Third Edition). Chapman and Hall Ltd. London. (1966).

11. Wang T.T., Glass A.M. and Herbert J.M. — The Applications of Ferroelectric Polymers. Blackie and Son Ltd. Glasgow. (1988).

12. — The TURBO C Reference Guide. Borland International. (1988)

13. — The TURBO C User's Guide. Borland International. (1988)

14. — CMOS Logic Databook. National Semiconductor Corporation. (1988).

APPENDIX 1: CIRCUIT DIAGRAMS OF TRANSIENT RECORDER

Data Library

IBM compatible prototyping board

Stock number 435-686

Introduction

The IBM personal computer provides five edge connector sockets on the mother board to cater for expansion of the system. These expansion capabilities provide for memory addition, printer interfaces, graphics options, data acquisition, communication modules and so on.

The RS IBM compatible PC prototyping board is designed to fit into one of the expansion sockets on the motherboard, providing on board track layout for signal buffering and decoding, together with a grid matrix area designed to facilitate the development and construction of electronic circuits. In addition, ground and power distribution buses are available throughout the board area and a position is available for fitting an additional I/O connector of 'D' type with up to 37 ways.

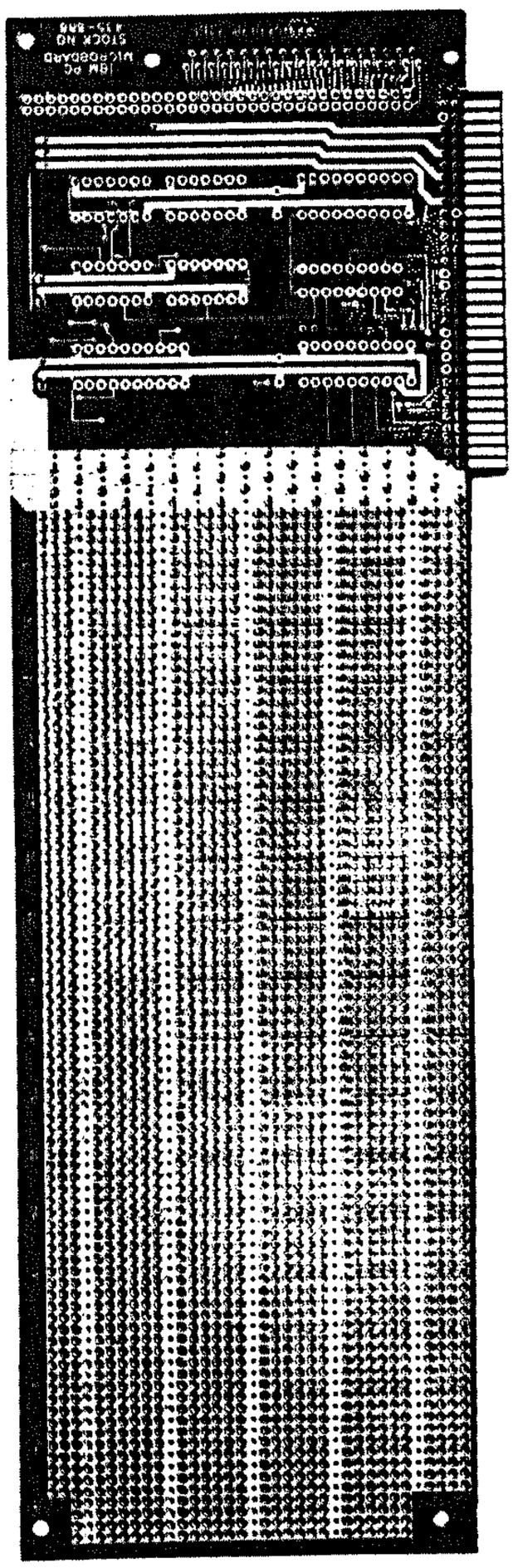

Component side

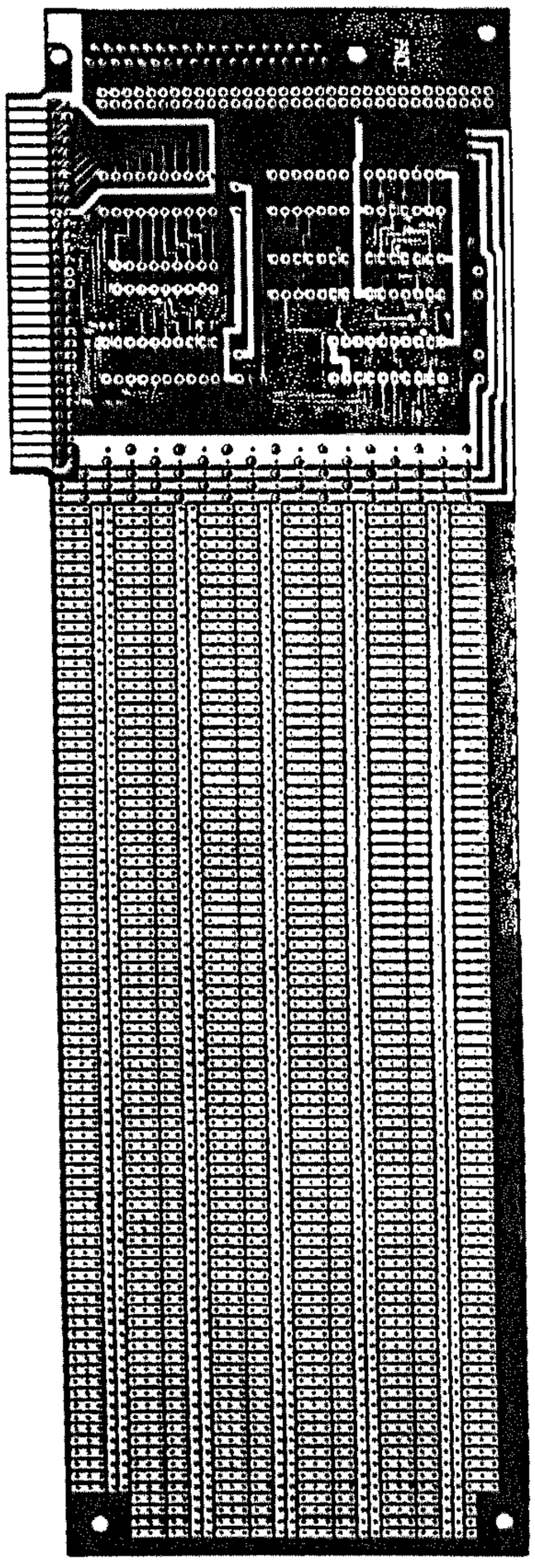

Wiring side

IBM® is a registered trade mark of International Business Machines Corporation.

Important

The board provides a convenient means of interfacing external circuitry with the IBM computer. Its proper use requires further information on the IBM system which is available from relevant IBM publications.

Description

The board measures 99mm high by 333mm long with 2 x 31 way 2.54mm pitch double sided, gold plated edge connector. It is designed to plug into one of the expansion slots in the mother board of the connector.

Signals and power lines are made available on the edge connector as shown in Figure 1.

Note that data and address lines are primarily on the Component (A) side of the edge connector. For more information on the signal lines please refer to the relevant IBM manual.

To simplify the interfacing of the prototype board circuitry to the computer system, on board circuitry is provided to buffer and decode relevant signals. The following buffered and decoded signals are available on the prototyping boards.

8 data bus lines labelled E1,3,4,6-10
1 address decode line labelled E11
5 address lines labelled E2,E5,E12-14
1 memory read line labelled E15
1 memory write line labelled E17

The six low address lines are used together with the address decode line to address on board devices in range &300 to &31F.

(Note: an additional buffer is available if required, input on E18 and output on E16.)

Power rails of +12V, +5V, 0V −5V and −12V are available as indicated on the board.

(Power distribution strips labelled A to E may be tied to power rails as required.)

Interfacing and addressing

The on board circuit layout is designed to buffer the input/output lines and provide an address map as recommended by IBM.

IBM has allocated addresses in the range &300 to &31F to prototyping board devices and the prototyping board decodes the high address lines to give the $\overline{EN}$ signal on E11 leaving the low A0-A4lines available for additional decoding in the range &300 to &31F.

Other addresses could be decoded by suitably gating the address lines.

Similarly, the on board circuit layout makes available those signal lines which would be commonly required. Other signal lines may be accessed if required from the edge connector. In particular, solder pads have been provided to access other signal lines as shown in Figure 2.

Using the prototype board

If the on board buffering/decoding facility is to be used the following parts are required.

U1 74LS245	(308-348)
U2 74LS244	(308-332)
U3 74LS08	(307-519)
U4 74LS04	(307-503)
U5 74LS244	(308-332)
U6 74LS02	(307-496)
U7 74LS21	(305-210)
C10μF tantalum	(101-816)
C2,3,4, 0.047μF ceramic	(124-126)

These items should be inserted into the relevant labelled positions on the component side of the board.

The board has a grid matrix of component mounting positions where a circuit may be constructed. Dedicated ground rails labelled 0V are provided together with uncommitted distribution strips A to E which may be connected to voltage rails or other lines as required. In addition, decoded and buffered signals are available from pins E1-E18 as previously described with additional signal lines accessible if required.

The microboard is designed such that most circuits can be constructed without cutting tracks. Should tracks need to be cut remember this is a board with plated through holes and tracks will need to be cut on both sides.

If required mounting holes are provided for an additional 'D' type connector with up to 37 ways, although not all the output terminals need be used.

Fitting the prototype board

Before fitting the board in the computer it should be checked out for obvious faults, in particular power connections should be checked for short circuits etc. RS Components Ltd can in no circumstances accept responsibility for any damage which may result in installing a faulty assembly into the computer. At no stage use undue force.

Switch off power to the computer.
Remove all rear panel connectors and cable.
Remove the two cover mounting screws at the bottom left and right of the rear panel.
Slide the cover away from the rear. When it will slide no further tilt the cover up from the front and remove from the base.
The five expansion slots are situated at the left rear of the computer.

Note that IBM recommends the use of slot no. 3 if it is not already in use.

If an additional input/output 'D' type connector is fitted to the expansion board then remove the appropriate expansion slot cover by removing its top retaining screw and sliding out the cover.

Fit the expansion board into the appropriate edge connector.

Replace the unit cover by reversing the removal procedure.

Reconnect rear cables and connectors to complete the installation process and fit screws.

If the fitting procedure seems to be difficult, then check your installation.

More details are given in the relevant manufacturer's manual.

Figure 1 **Signal and power line connections**

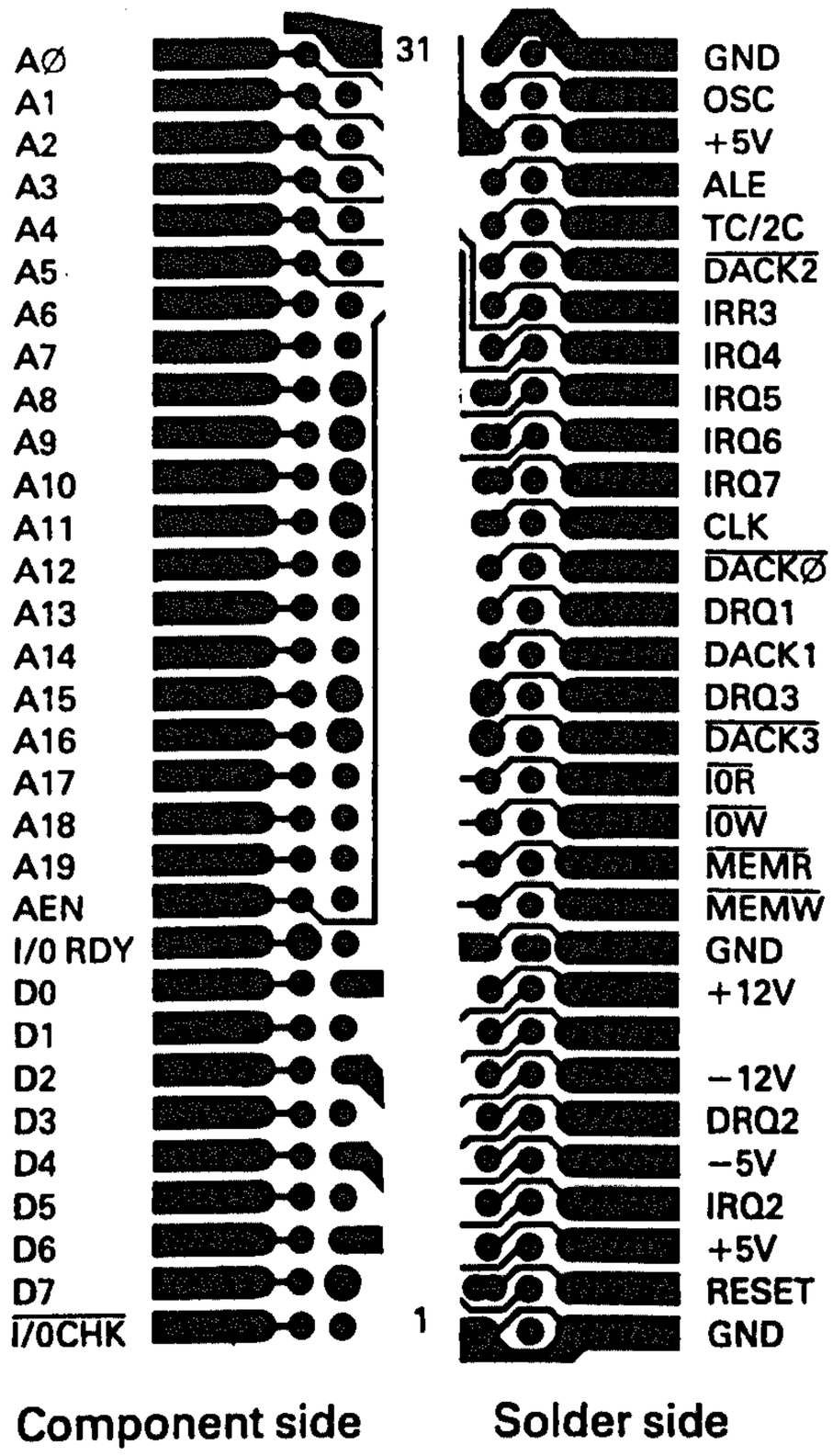

Figure 2 **Solder pad connections**

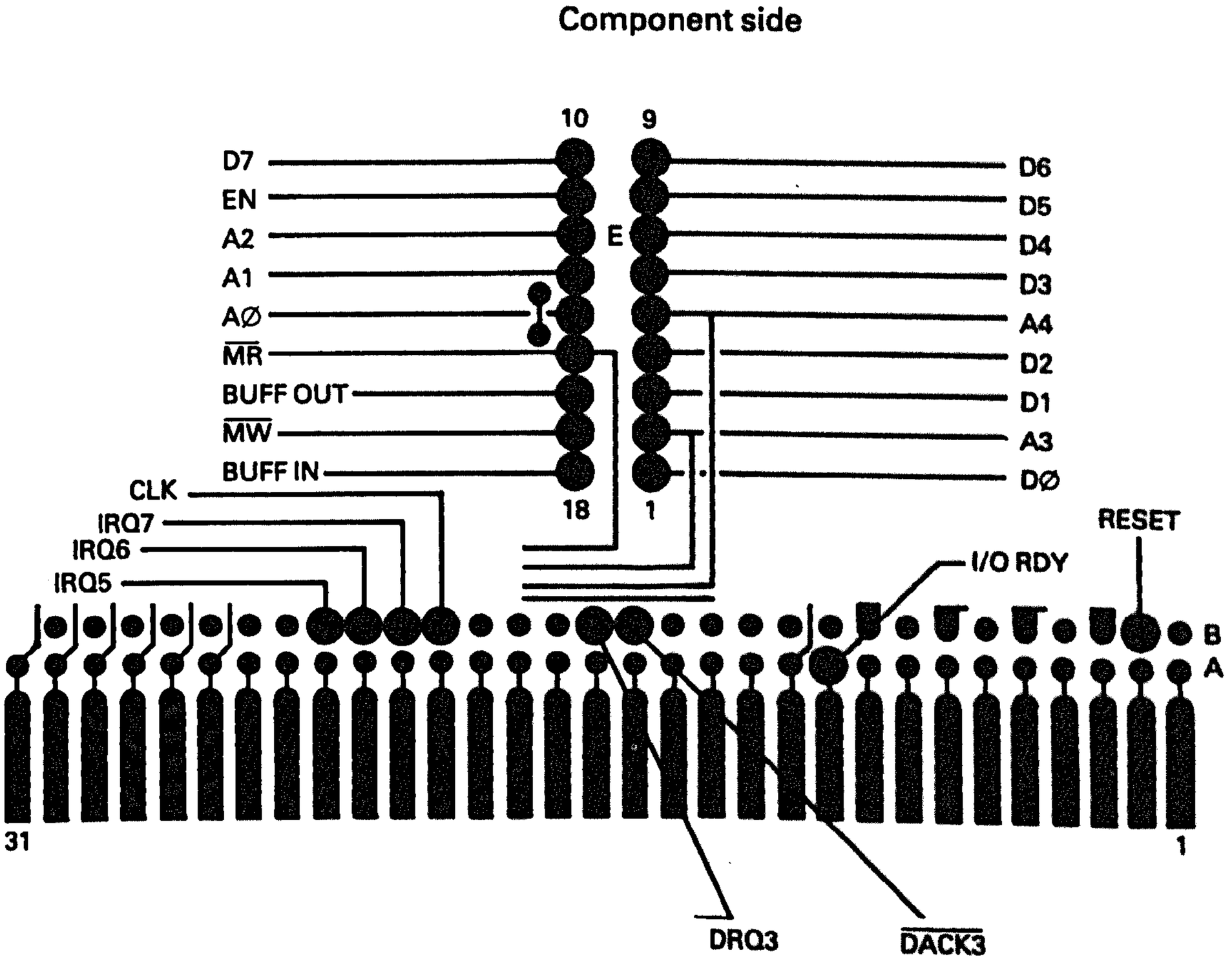

RS Data Library

Figure 3 **Block diagram**

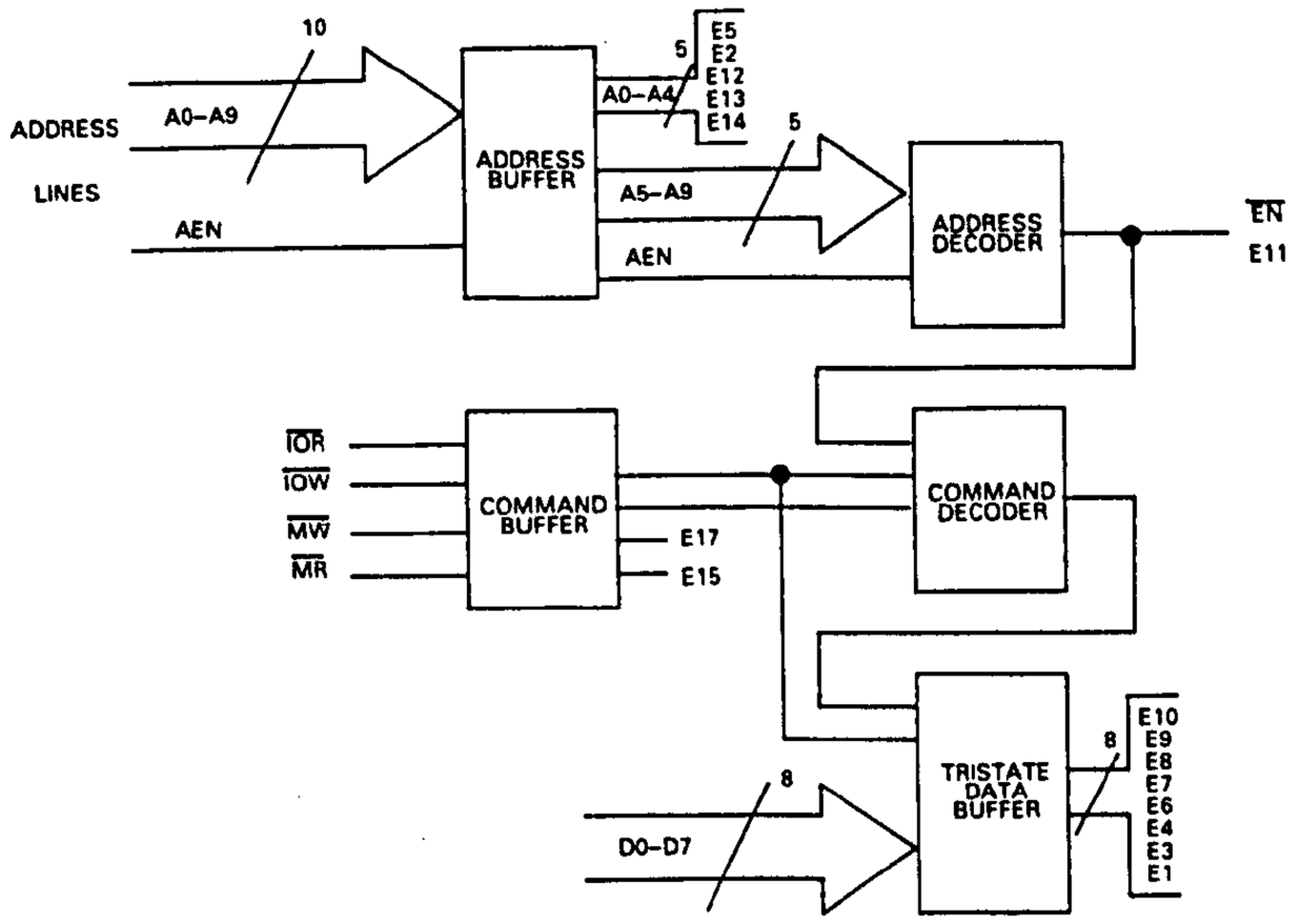

Figure 4 **Circuit diagram**

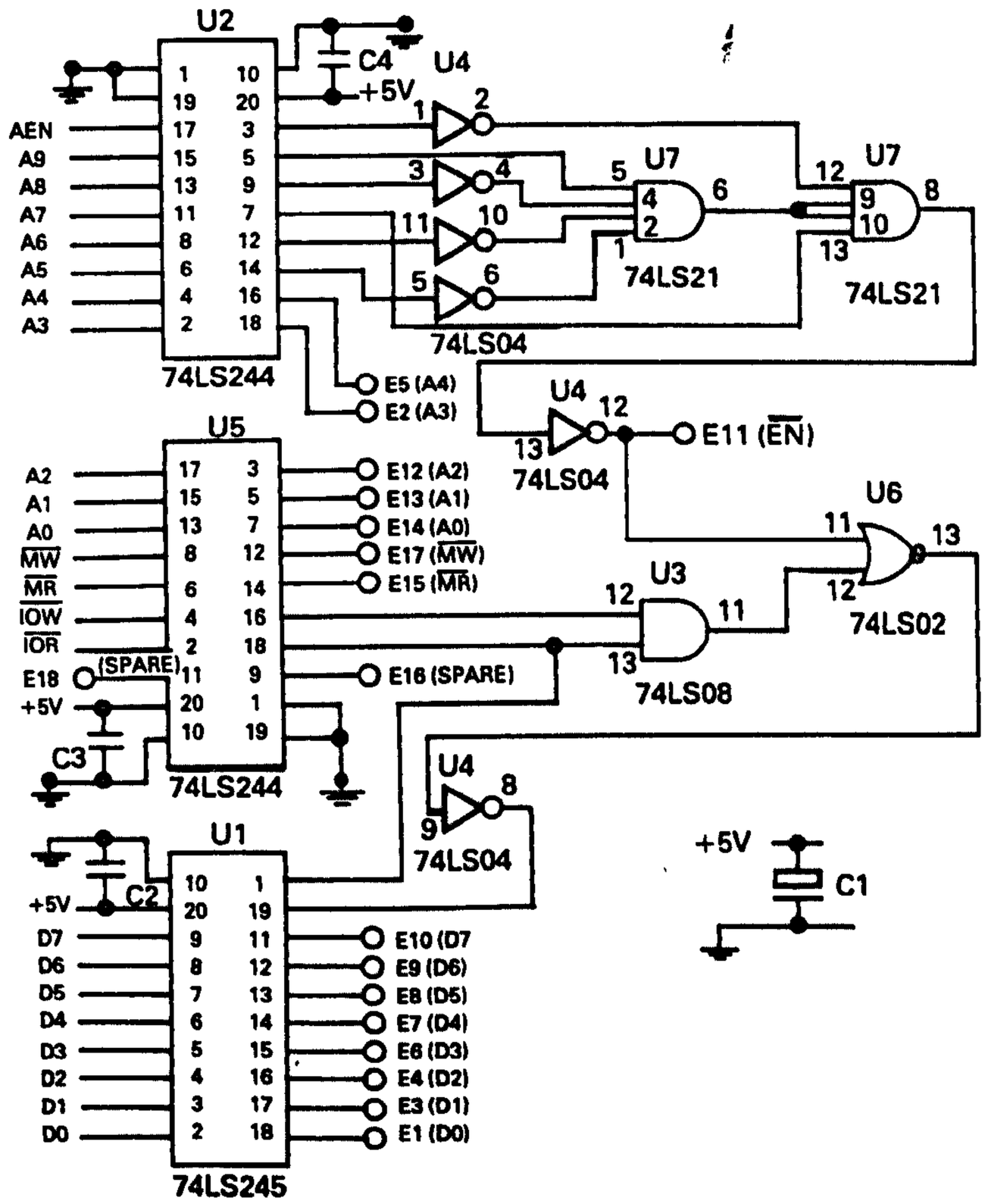

©RS Components Ltd. 1984

PART OF

DO NOT SCALE

SHEET OF

DRG. No.

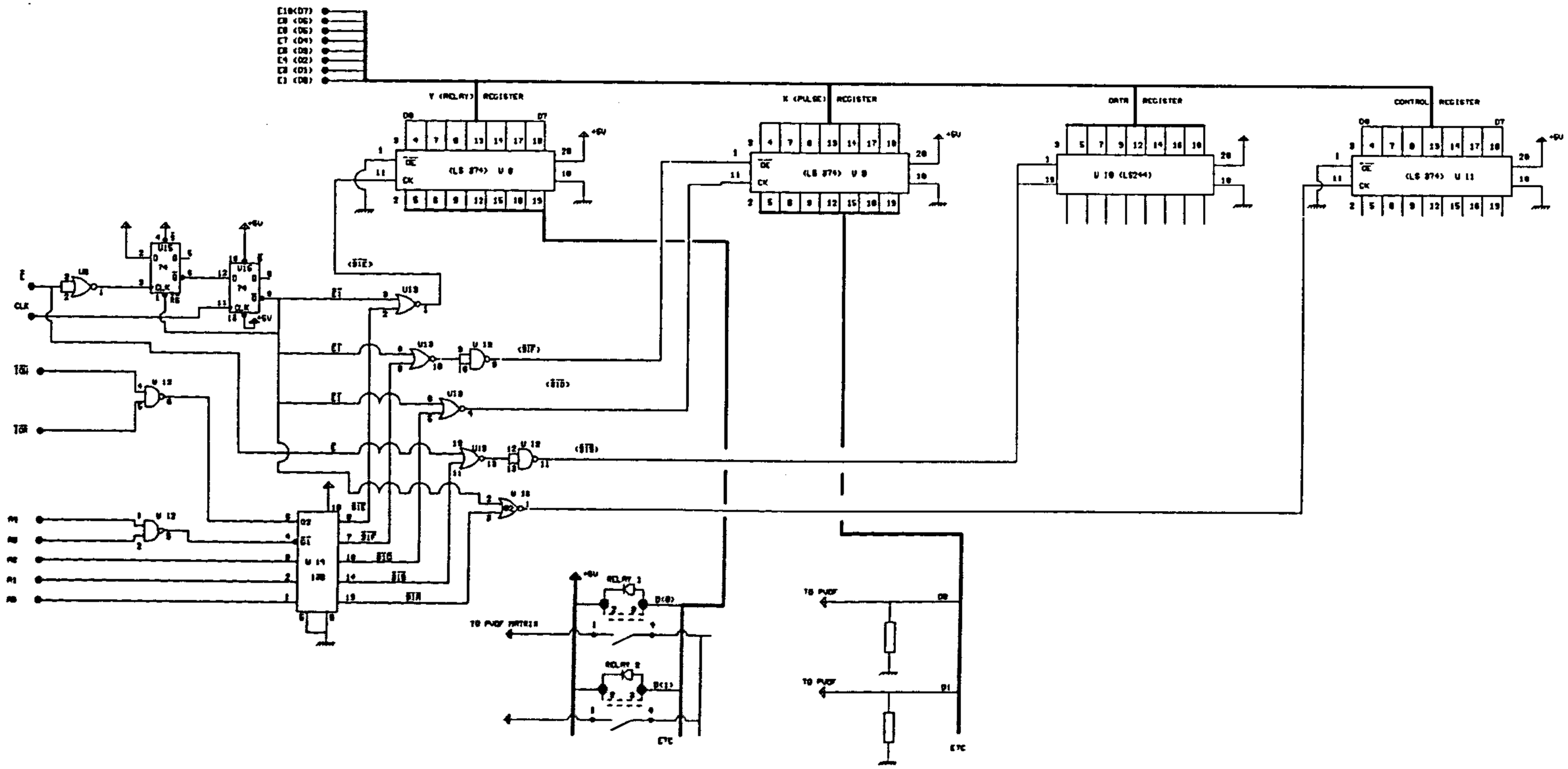

ISSUE	DESCRIPTION	APPD	DATE

TITLE

DRAWN	TRACED	CHECKED	APPROVED	DATE

DRAWING No.

RS 561-375

210 x 297mm A4

PART OF

DO NOT SCALE

SHEET OF

DRG. No.

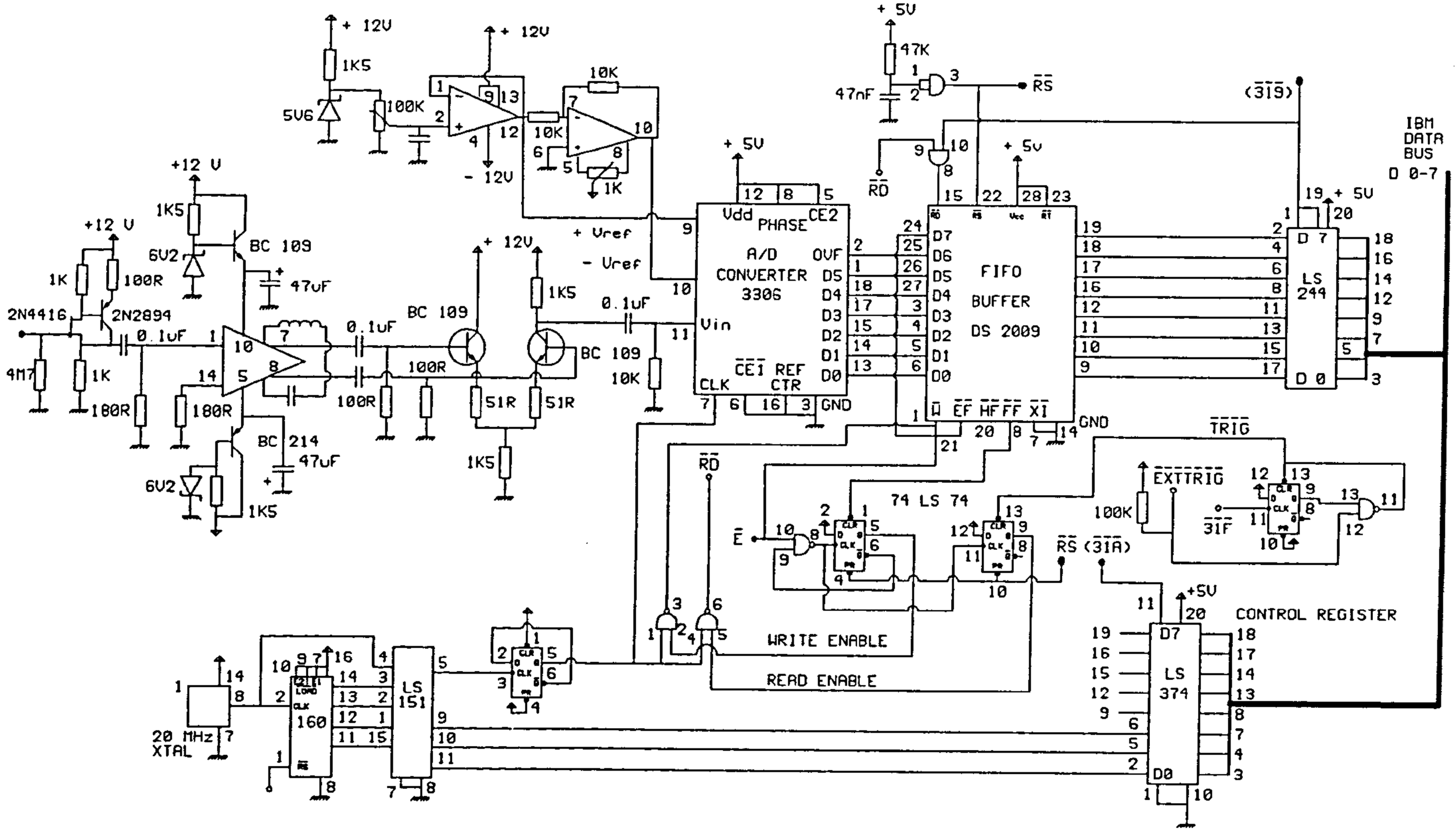

ISSUE	DESCRIPTION	APPD.	DATE

TITLE

DRAWN	TRACED	CHECKED	APPROVED	DATE

DRAWING No.

PART OF

DO NOT SCALE

SHEET OF

DRG. No.

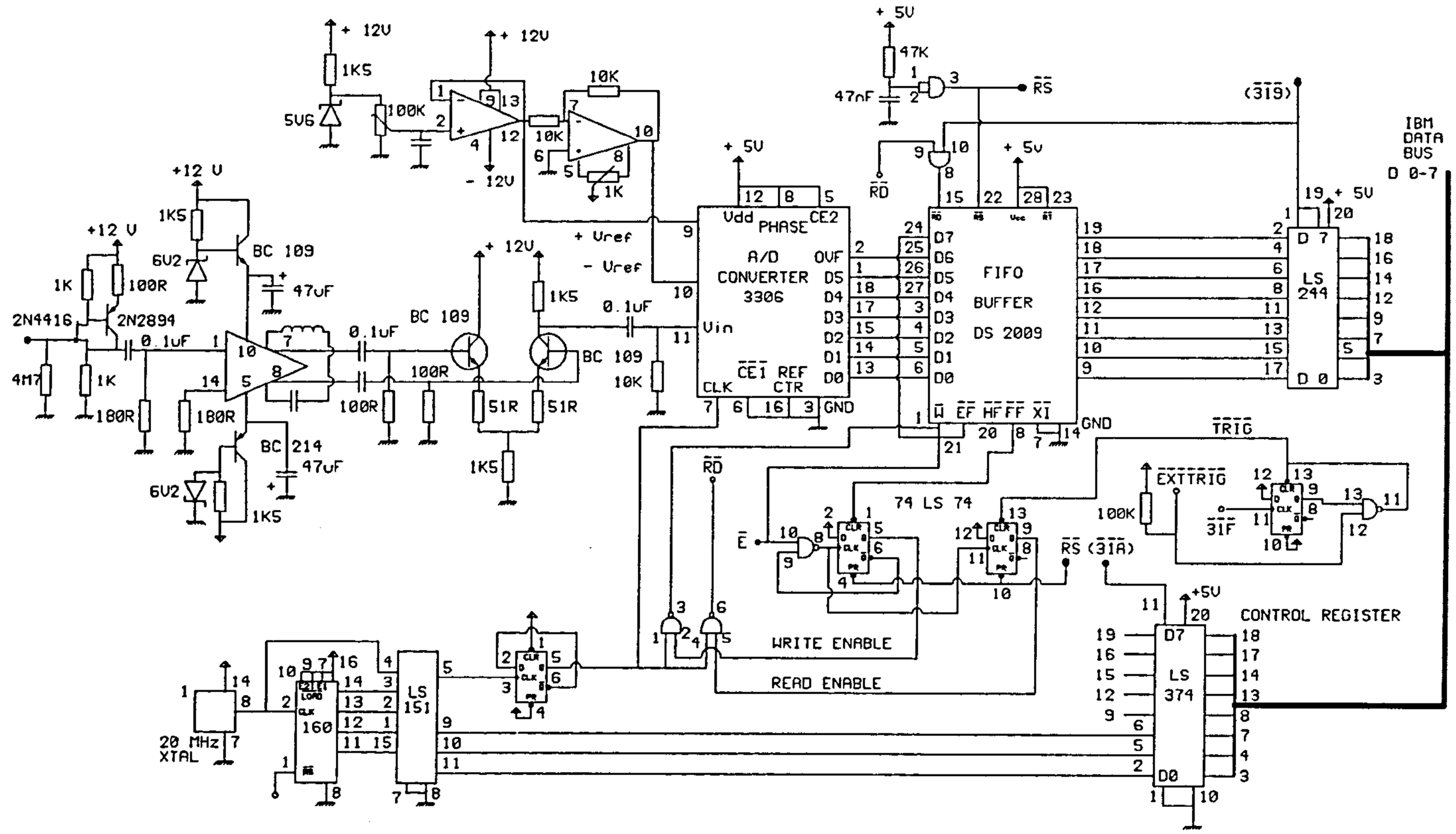

ISSUE	DESCRIPTION	APPD	DATE

TITLE

DRAWN	TRACED	CHECKED	APPROVED	DATE

DRAWING No.

210 x 297mm A4

APPENDIX 2: TRANSIENT RECORDER PROGRAM

```
/***                Scope View of A/D Converter Data      ***/
/***                Version 2: October 27th 1990          ***/

#include <dos.h>
#include <graphics.h>

#define data_port  0x318
#define cs_port    0x31a
#define trig_port  0x31f


int xsize,ysize;

float yplot,twopi;

int fifo_data[513];

main()
        {
set_graphics(); /*** Go to graphics screen mode ***/

do
    {
    outportb (cs_port,'\x1'); /*** Sets 5 MHz clock ***/
    clearviewport();
    grid(400,200);
    outport (trig_port,0); /*** Arms FIFO to receive data***/
    delay(10);      /*** Wait 10mS for trigger event    ***/
    get_array();
    draw_trace(fifo_data);
    outtextxy(1,340,"Press q to quit or any other key to
              repeat");
    }
        while (getch() !='q');
closegraph();   /*** Back to text screen mode ***/
}


/*** That is the main program. These are the called routines ***/
```

```
set_graphics()
            {
            int g_driver, g_mode, g_error;
            detectgraph(&g_driver, &g_mode);
            initgraph(&g_driver, &g_mode, "C:\\TC");
            }
/*************************************************************************/

grid(xsize,ysize)
            {
            int xpos = 0;
            int ypos = 0;
            for(;xpos<=xsize;xpos+=xsize/10)
                {
                if (xpos==xsize/2) setcolor(11);/*** light blue for middle
line***/
                else setcolor (9);
                line (xpos,0,xpos,ysize);
                }

            for ( ;ypos<=ysize; ypos+=ysize/10)
                {
                if (ypos==ysize/2) setcolor (11);/*** light blue for
middle line***/
                else setcolor (9);
                line (0, ypos, xsize, ypos);
                }

            moveto (0,ysize/2);
            }
/*************************************************************************/
get_array()
            {
            int sample=0 ;
            for ( ;sample<=511; sample++)
                {
                fifo_data[sample] = inportb (data_port);
                }
            }

/*************************************************************************/
```

```
draw_trace(int fifo_data[])
        {
        int sample = 0;
                    setcolor (10);
        for (sample=1 ;sample<=400; sample++)
            {
            fifo_data[sample]+=(fifo_data[sample+1]/2
                    +fifo_data[sample-1]/2);
            fifo_data[sample] /= 2;  /*** This produces a weighted
                    average over three samples***/
            yplot = 100 - (fifo_data[sample]-32)*3;
            lineto (sample,yplot);
            }
}
```

APPENDIX 3:CIRCUIT DIAGRAMS OF ISOLATED SYSTEM

U-S MAT PROJECT

BACKPLANE PIN ASSIGNMENT

	1	2	GND	
	3	4	+5 V	
	5	6	X 0	MULTIPLEX CONTROL PORT ADDRESS 304H
	7	8	X 1	
	9	10	X 2	
	11	12	X 3	
	13	14	Y 0	
	15	16	Y 1	
	17	18	Y 2	
	19	20	Y 3	
	21	22	CS 0	CONTROL/STATUS PORT ADDRESS 305H
	23	24	CS 1	
	25	26	CS 2	
	27	28	CS 3	
	29	30	CS 4	
	31	32	CS 5	
	33	34	CS 6	
	35	36	CS 7	
	37	38		
	39	40	D 0	DATA BUS PORT ADDRESS 306H
	41	42	D 1	
	43	44	D 2	
	45	46	D 3	
	47	48	D 4	
	49	50	D 5	
	51	52	D 6	
	53	54	D 7	
+V ref	55	56	+V Analogue	
-V ref	57	58	-V Analogue	
	59	60		
	61	62	+5 V	
	63	64	GND	

DRG. No.

SHEET OF

DO NOT SCALE

PART OF

DATE | APPROVED | CHECKED | TRACED | DRAWN | DRAWING No. | TITLE

DATE | APPD | DESCRIPTION | ISSUE

210 x 297mm A4

PART OF

DO NOT SCALE

SHEET OF

DRG. No.

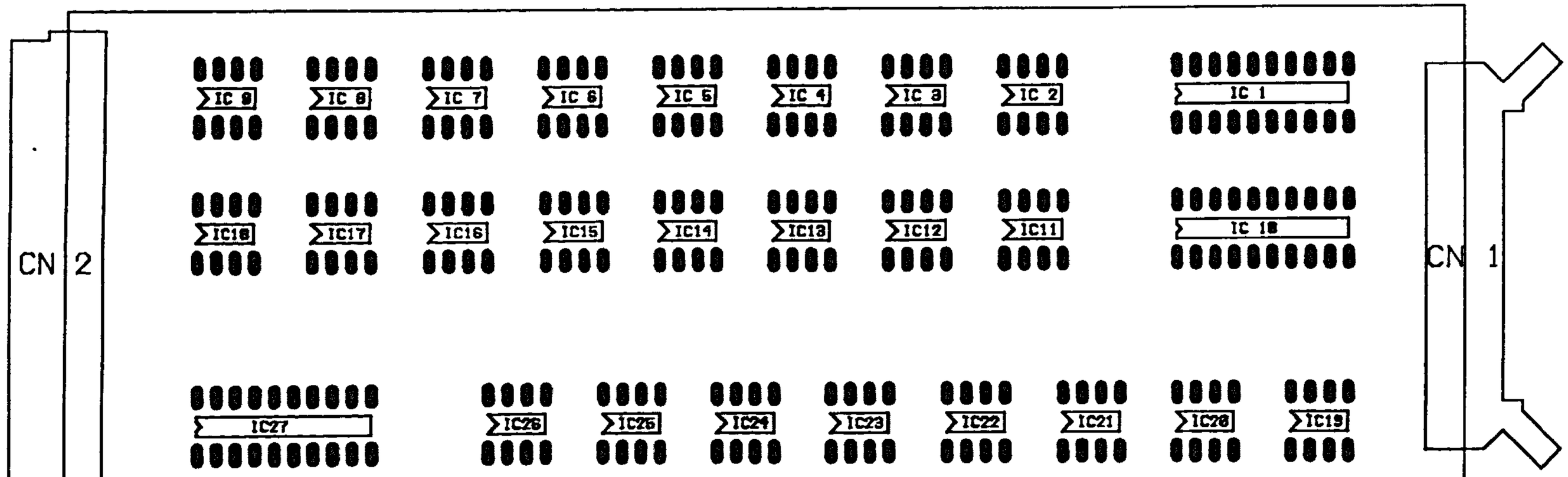

PVdF PROJECT

OPTO ISOLATOR BOARD

1-12-90

ISSUE	DESCRIPTION	APPD	DATE

TITLE

DRAWN	TRACED	CHECKED	APPROVED	DATE

DRAWING No.

RS 561-375

210 x 297mm A4

PART OF

DO NOT SCALE

SHEET OF

DRG. No.

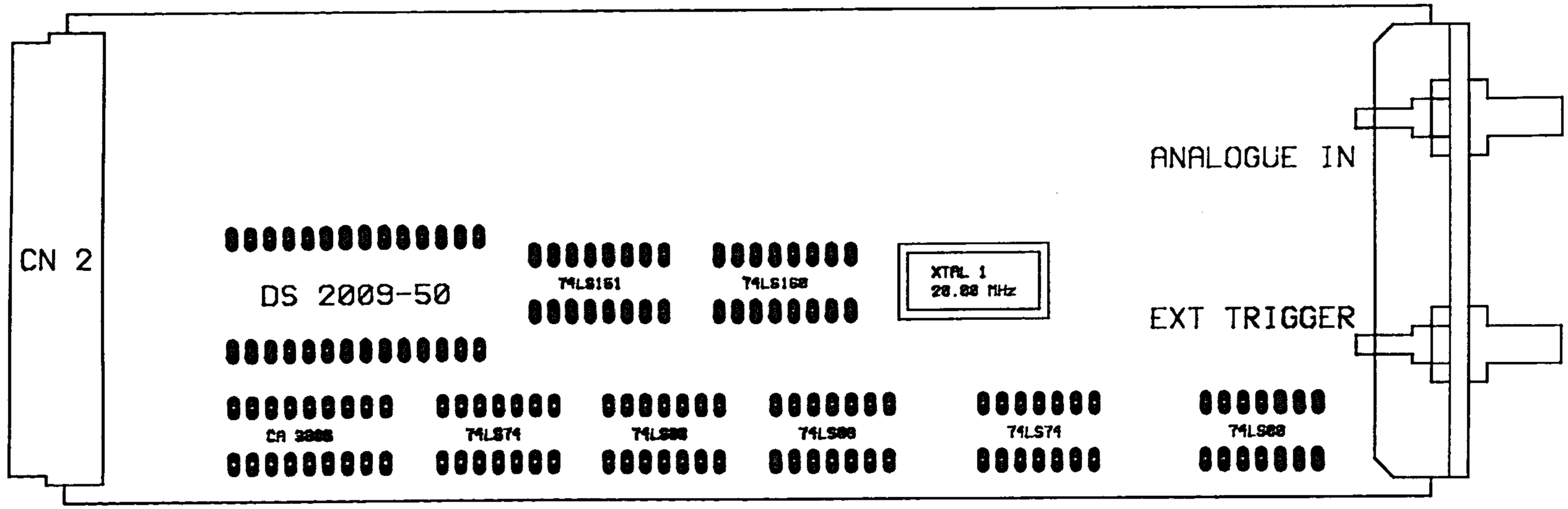

PVdF PROJECT

A/D CONVERTER BOARD

1-12-90

ISSUE	DESCRIPTION	APPD	DATE

TITLE

DRAWN	TRACED	CHECKED	APPROVED	DATE

DRAWING No.

210 x 297mm A4

BS 561 375

PART OF

DO NOT SCALE

SHEET OF

DRG. No.

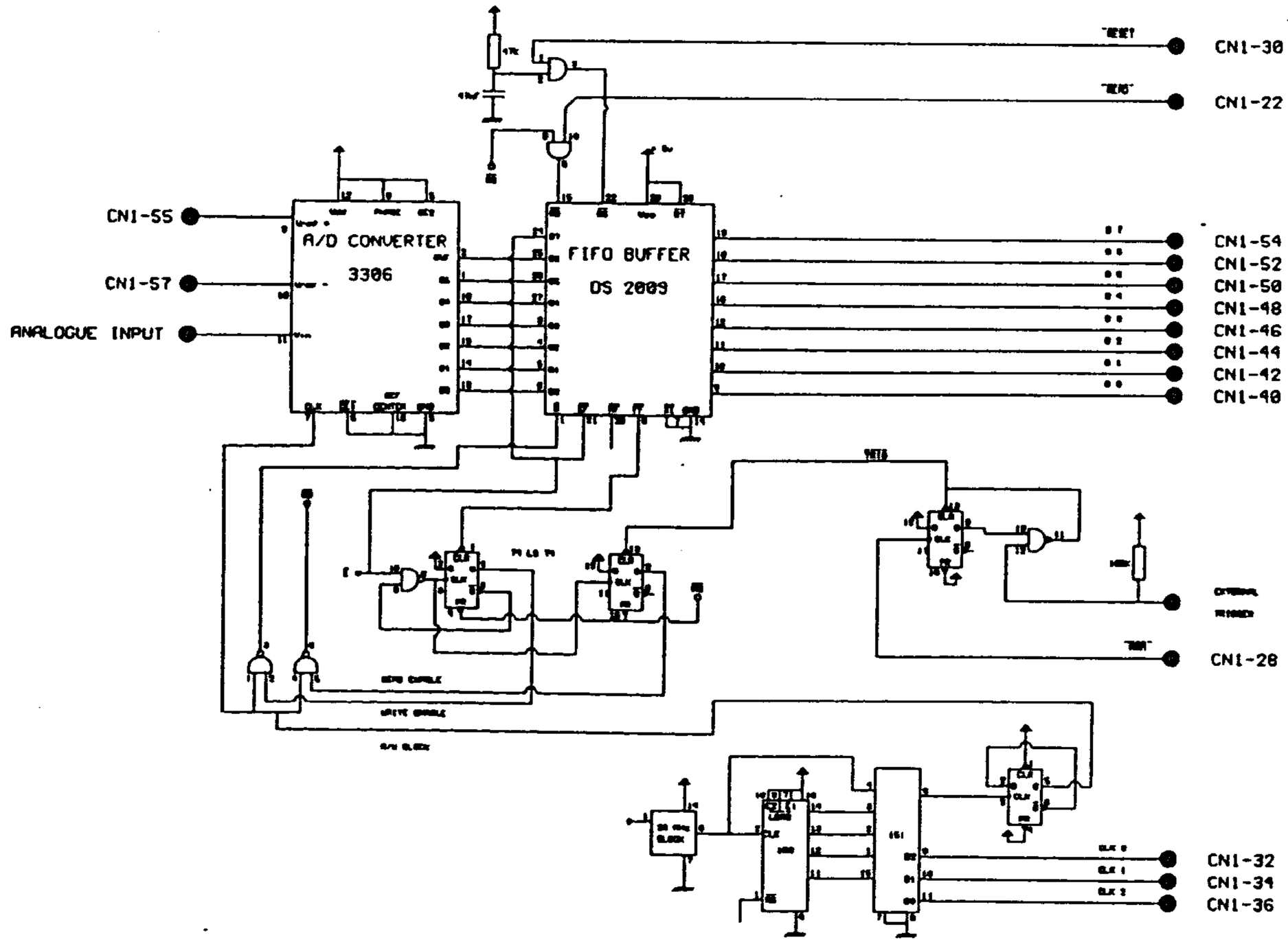

ISSUE	DESCRIPTION	APPD	DATE

TITLE

DRAWN	TRACED	CHECKED	APPROVED	DATE

DRAWING No.

861-875

210 x 297mm A4

PART OF

DO NOT SCALE

SHEET OF

DRG.No.

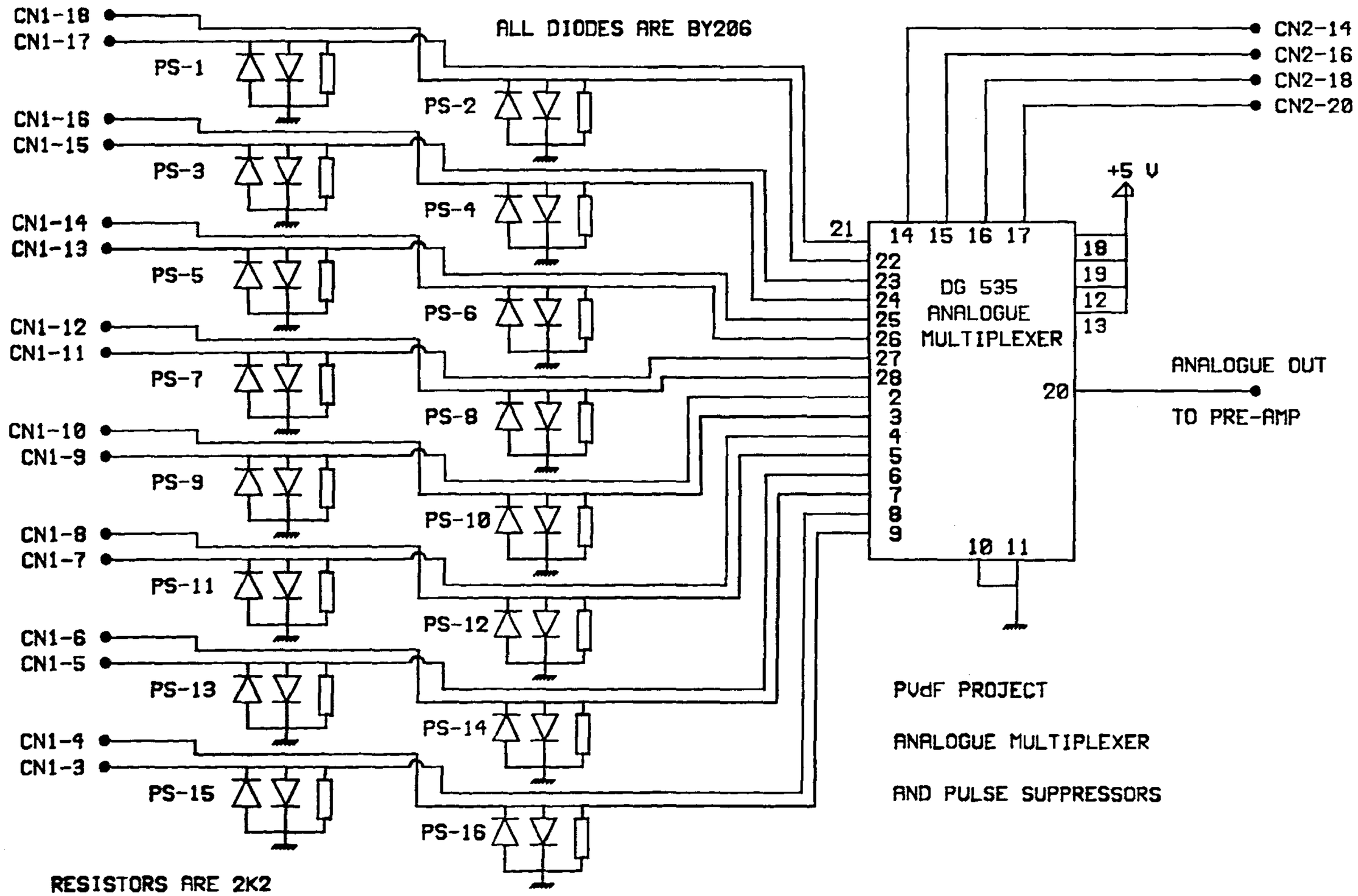

RESISTORS ARE 2K2

PVdF PROJECT

ANALOGUE MULTIPLEXER

AND PULSE SUPPRESSORS

ISSUE	DESCRIPTION	APPD.	DATE

TITLE

DRAWN	TRACED	CHECKED	APPROVED	DATE

DRAWING No.

PART OF

DO NOT SCALE

SHEET OF

DRG.No.

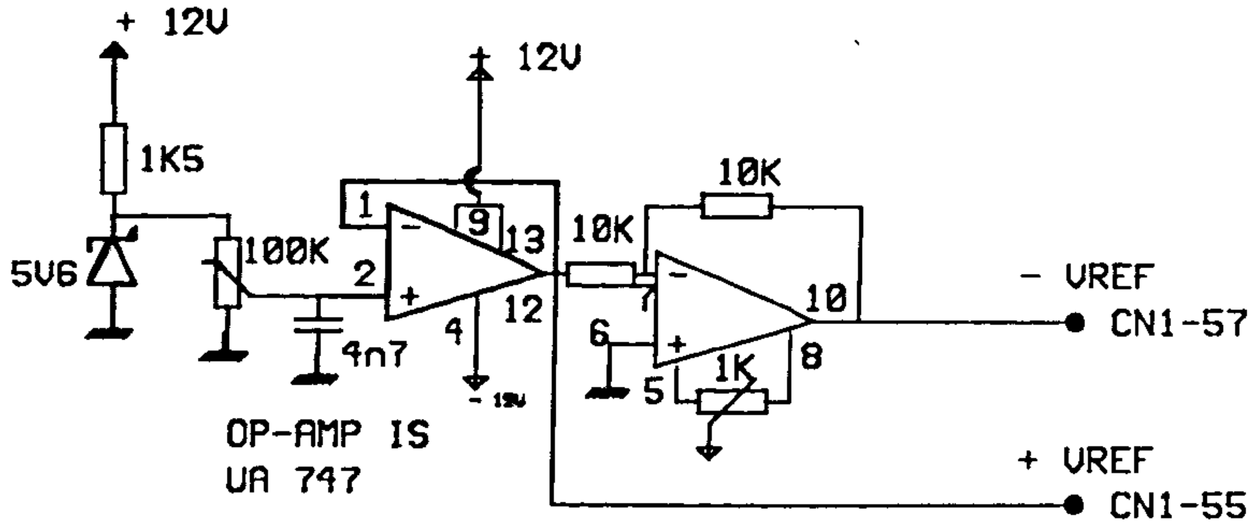

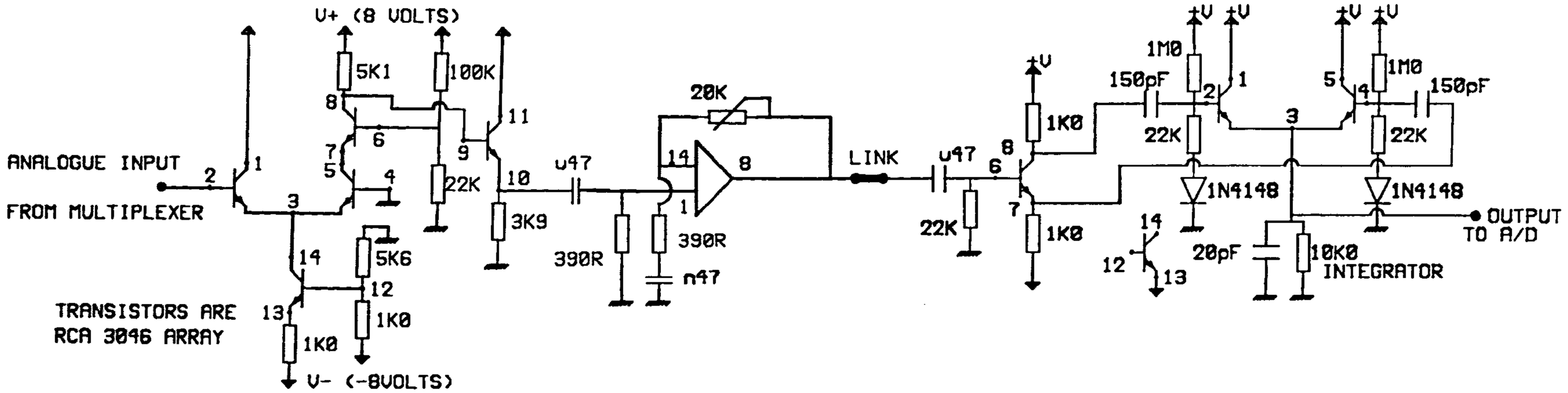

ISSUE	DESCRIPTION	APPD.	DATE

TITLE

DRAWN	TRACED	CHECKED	APPROVED	DATE

DRAWING No.

PART OF

DO NOT SCALE

SHEET OF

DRG. No.

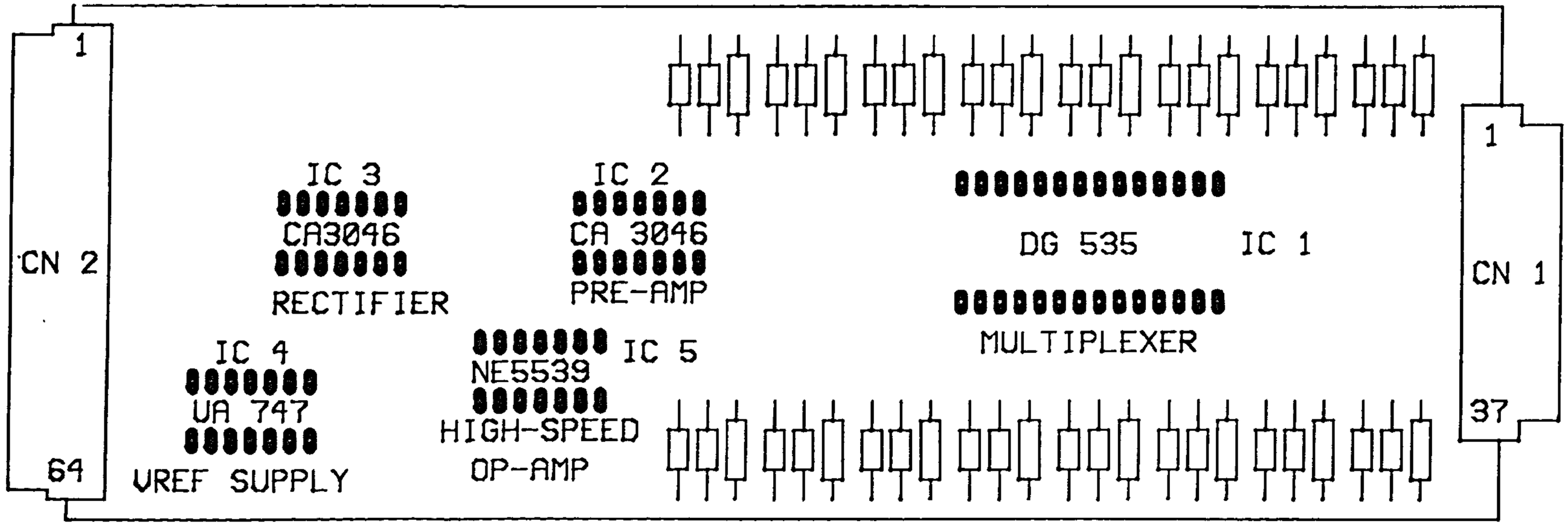

PVdF PROJECT RX MULTIPLEXER/PREAMPLIFIER BOARD 1-12-90

ISSUE	DESCRIPTION	APPD	DATE

TITLE

DRAWN	TRACED	CHECKED	APPROVED	DATE

DRAWING No.

210 x 297mm A4

PART OF

DO NOT SCALE

SHEET OF

DRG. No.

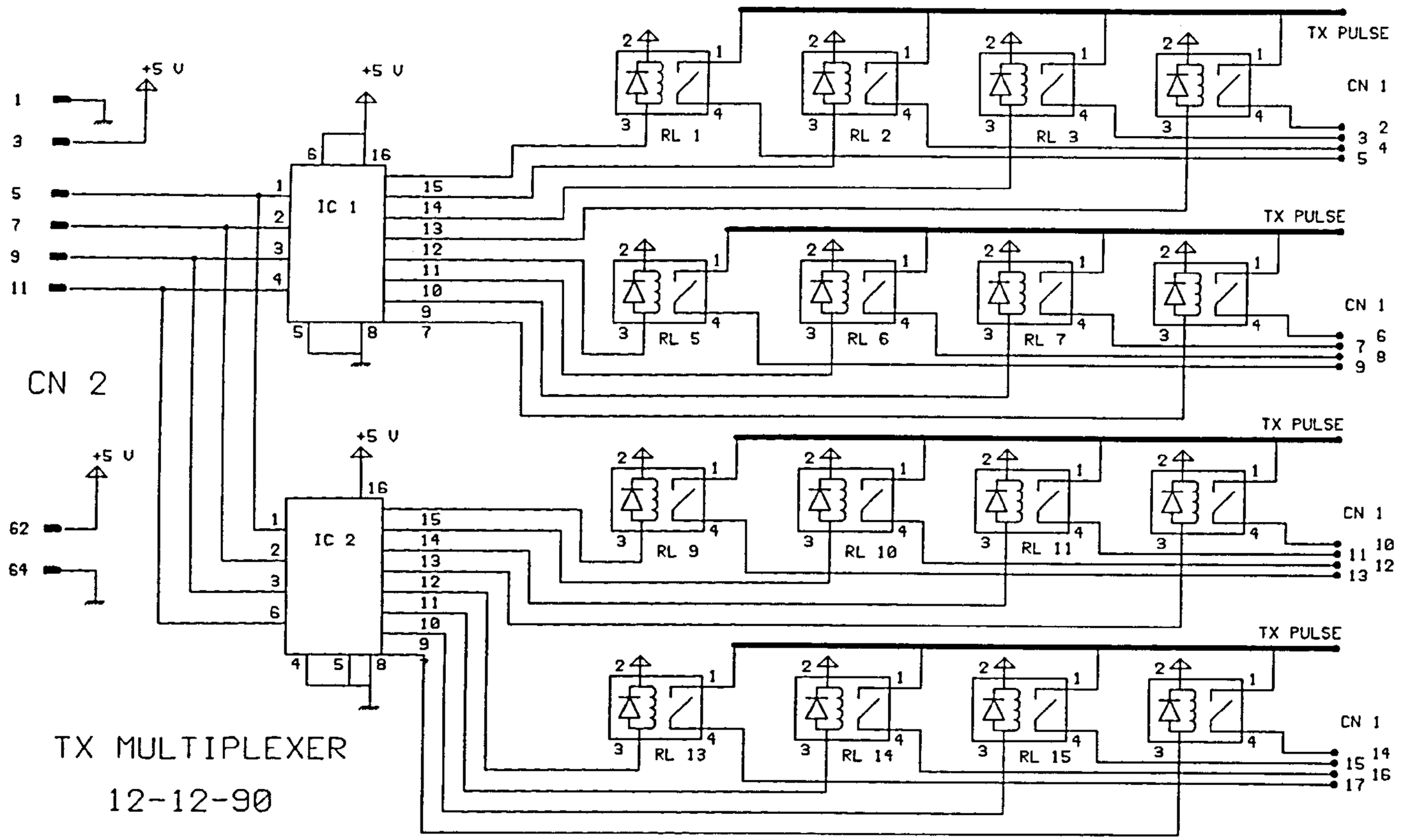

TX MULTIPLEXER

12-12-90

ISSUE	DESCRIPTION	APPD.	DATE

TITLE

DRAWN	TRACED	CHECKED	APPROVED	DATE

DRAWING No.

210 x 297mm A4

PART OF

DO NOT SCALE

SHEET OF

DRG. No.

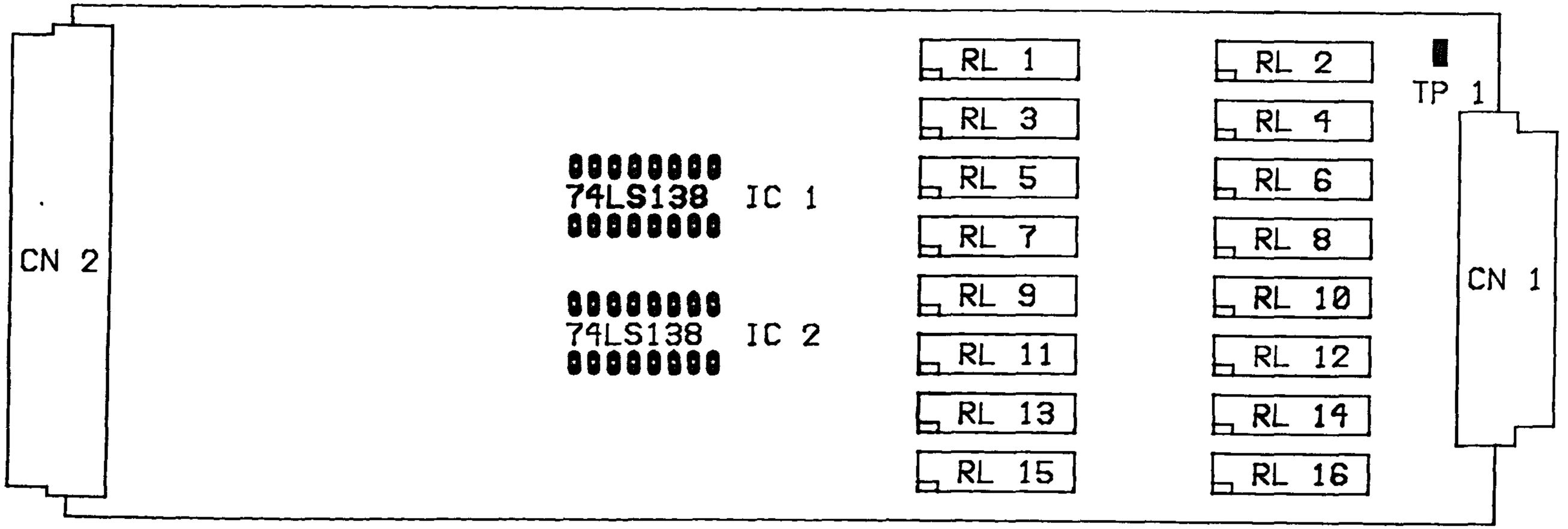

PVdF PROJECT

TX MULTIPLEXER BOARD

1-12-90

ISSUE	DESCRIPTION	APPD	DATE

TITLE

DRAWN	TRACED	CHECKED	APPROVED	DATE

DRAWING No.

210 x 297mm A4

PART OF

DO NOT SCALE

SHEET OF

DRG. No.

CN 1

PA0 … PA7

IC 1 74LS241

CN 2

ROW/COLUMN CONTROL

X0 3
X1 4
X2 5
X3 6
Y0 7
Y1 8
Y2 9
Y3 10

IC 2 … IC 9

PB0 … PB7

IC10 74LS241

CONTROL WORD LSB

11
12
13
14
15
16
17
18

MSB

IC11 … IC18

PC0 … PC7

IC19 … IC26

DATA LSB

20
21
22
23
24
25
26
27

MSB

IC27 74LS241

+5V 2,31

GND 1,32

49 PC +5V

50 PC GROUND

MSB							LSB
CLK3	CLK2	CLK1	$\overline{RST}$	$\overline{SET}$	X	X	$\overline{READ}$

CONTROL WORD FORMAT

ALL OPTOISOLATORS ARE HP 6N137

ISSUE	DESCRIPTION	APPD	DATE

TITLE

DRAWN	TRACED	CHECKED	APPROVED	DATE

DRAWING No.

APPENDIX 4:TRANSIENT RECORDER PROGRAM FOR ISOLATED SYSTEM

```
#include <dos.h>
#include <graphics.h>

#define base        0x300
#define port_a      0x304
#define port_b      0x305
#define data_port   0x306
#define control_port 0x307


int xsize,ysize;
int control_word=0x89;
int default_word=0x19;

float yplot,twopi;

int fifo_data[513];

main()
                {
    set_graphics();
                set_ports();

                do
                                {
                                clearviewport();
                                grid(400,200);
                                get_array();
                                draw_trace(fifo_data);
                                squares(fifo_data);
                                outtextxy(1,340,"Press <ESC> to quit or any other
key to repeat");
                                } while (getch() !=27);
                closegraph();
                }
```

```
set_graphics()
        {
        int g_driver, g_mode, g_error;
        detectgraph(&g_driver, &g_mode);

        initgraph(&g_driver, &g_mode, "C:\\TC");
        }

set_ports()
        {
        outportb(control_port,control_word);/*initialises the 8255 to a,b
                                output and port c input*/
        outportb(port_b,default_word);      /*sets 10MHz clock and
                                set,reset and read high*/
        outportb(port_a,0x44);              /*top 4 bits is tx multiplex
                                address bottom 4 is rx multiplex
                                address*/

        }

grid(xsize,ysize)
        {
        int xpos = 0;
        int ypos = 0;

        for(;xpos<=xsize;xpos+=xsize/10)
                {
                if (xpos==xsize/2) setcolor(11);/* light blue for
middle line*/
                else setcolor (9);
                line (xpos,0,xpos,ysize);
                }

        for ( ;ypos<=ysize; ypos+=ysize/10)
                {
                if (ypos==ysize/2) setcolor (11);/*light blue for
middle line*/
                else setcolor (9);
                line (0, ypos, xsize, ypos);
                }
moveto (0,ysize/2);
}
```

```
get_array()
        {
        int sample=0 ;
        outportb(port_b,0x29);
        outportb(port_b,default_word);/*reset the fifo*/
        delay(50);

        outportb(port_b,0x31);
outportb(port_b,default_word);/*and arm the trigger*/
delay(10);
for ( ;sample<=511; sample++)
                {
                outportb(port_b,0x38);/*toggle data read bit*/

                fifo_data[sample] = inportb (data_port)-32;

                outportb(port_b,default_word);/*and set it back
                                                again*/
                }
}
```

```
draw_trace(int fifo_data[])
        {
        int sample = 0;

        setcolor (10);
        for (sample=1 ;sample<=400; sample++)
                {
                yplot = 100 - (fifo_data[sample]);
                lineto (sample,yplot);
                }
        }
```

```
squares(int fifo_data[])
        {
        int sample=0;
        int x,z,ysum,xysum,xxysum;
        float a,b,c;

        setcolor(4);
        moveto(0,ysize/2);
for (sample=3;sample<400;sample++)
        {
        ysum=xysum=xxysum=0;
        for (x=-3;x<=3;x++)
                {

                ysum+= fifo_data[sample+x];
                xysum+=x*(fifo_data[sample+x]);
                xxysum+=x*x*(fifo_data[sample+x]);
                }
        a=(xxysum-4*ysum)/86;
        b=xysum/28          ;
        c=(99*ysum+14*xxysum)/301;

        lineto (sample, 90-(c));
        }
}
```

APPENDIX 5:FINAL C PROGRAM

```
/*************************************************************************
*                                                                        *
*          mat program to display color coded u-s depth                  *
*          on a 15x15 square array                                       *
*************************************************************************/

#include <dos.h>
#include <graphics.h>
#include <conio.h>

#define base        0x300
#define port_a      0x304
#define port_b      0x305
#define data_port   0x306
#define control_port 0x307
#define control_word 0x89
#define default_word 0x19

void initialise(void);
void set_up_screen(void);
void get_array(void);
void draw_array(void);
void draw_block(void);
void set_ports(void);
void set_mux(void);
int get_peaks(void);
int least_squares(void);
int get_depth(int);


int x,y,depth,speed,no_of_peaks;
int TRUE=1,FALSE=0;
int FIFO[512], PEAK[20],SEP[20], WEIGHT[20] [20];

char answer;
char cdepth[30];
```

```
main()
   {
   initialise();
   set_up_screen();
   set_ports();
   for (y=0; y<15; y++)
      {
      for (x=0; x<15; x++)
         {
         set_mux();
         get_array();
         no_of_peaks = least_squares(); /* algorithm to find peaks*/
         depth = get_depth(no_of_peaks);/* depth calculation */
         draw_array();                  /* put A-scan on screen*/
         draw_block();                  /*coloured square for depth*/
         if (( answer=getch())!= 'C')   /*user decides not to go on*/
            x--;                        /*so we redo this x value  */
         if (answer == 0x1b)            /* if user has got fed up  */          goto
exit;                    /* we allow him/her to quit*/
         }
      }
exit: outtextxy(200,340,"Finished-hit any key to clear");
      while (!kbhit() );
      closegraph();
   }

/************end of program, the rest is the subroutines************/
```

```
void initialise(void)
  {
  int gmode, gdriver;
  char speed_string[10];
  char keypress;                    /*temporary variable.*/
  char *this_char=speed_string;     /*set pointer to start adress*/
                                    /*of speed_string*/
  detectgraph(&gdriver,&gmode);
  initgraph(&gdriver,&gmode,"c:\\tc");
  settextjustify(LEFT_TEXT,BOTTOM_TEXT);/*set this to ensure the */
  moveto(200,175);                  /*Cursor position moves  */
outtext("Speed of Sound (M/S)?  " );  /*when outtext is called */
                                    /*to prompt user forspeed*/

          /* this next bit is a homegrown input routine */
  while (
    (keypress=getch())!= '\r'       /*is it carriage return?*/
    && (this_char - speed_string)<10 /*or more than 9 characters?*/
    )
    {
    (*this_char++) = keypress;      /*assign to (contents of)   */
    *this_char = 0;                 /*this_char, increment pointer*/
    outtext(this_char - 1);         /*terminate string and echo  */
    }                               /*last character only*/

speed = atoi(speed_string);         /*convert string to integer*/
clearviewport();                    /*clear screen and return*/
}
                /**********************************/
```

```
void set_up_screen(void)
   {
   int key_y;                          /* loop variable for colors  */
   char key_depth[5];                    /* string array for printing */
   for (key_y=0; key_y<16;key_y ++)  /* draw the color key (from  */
      {                                /* the top down.)            */
   itoa(16-key_y,key_depth,10);   /* convert key_y to string   */
   setfillstyle(SOLID_FILL,15-key_y);/* set color for key block*/
   bar(500,12*(key_y),515,12*(key_y+1)); /*draw color key block*/
   moveto(525,12*key_y);            /* put text cursor next to   */
   outtext(key_depth);              /* block, then print number. */
   if (key_y > 6)                   /* if only one digit...      */
      outtext(" ");                 /* add an extra space (Yuk)  */
   outtext (" mm");                 /* and print the units       */
   }
setfillstyle(EMPTY_FILL,MAGENTA);
bar3d(0,0,250,230,0,0);             /*draw large box for C-scan*/
bar3d(50,250,250,300,0,0);          /*draw small box for A-Scan*/
moveto(280,300);
outtext("Depth =        mm :  C-continue or R-redo");
}
/************************************/
```

```
void set_mux(void)
  {
  unsigned char mux_byte;
  mux_byte = 16*y+x;       /*receive multiplexer is top four bits*/
  outportb( port_a, mux_byte);
  }
                  /*********************************/
void get_array(void)
{
int sample,q,temp ;
int average_index=32;
for (q=0; q<average_index; q++)/*this is signal average for-loop*/
   {
   outportb(port_b,0x29);
   outportb(port_b,default_word);       /*reset the fifo*/
   delay(50);                           /*wait a bit */
   outportb(port_b,0x31);
   outportb(port_b,default_word);       /*and arm the trigger*/
   delay(10);                           /*wait for trigger event*/
   for (sample=0; sample<=511; sample++)
      {                                 /*then get the data*/
      outportb(port_b,0x38);                /*toggle data read bit*/
      if((temp = inportb (data_port)) > 64)  /*get A/D info*/
         temp = 64;                         /*check for overflow */
      outportb(port_b,default_word);    /*reset data read bit*/
      if (q==0)
         FIFO[sample]=temp;             /*put in array*/
      else
      FIFO[sample] += temp ;            /*or add to array*/
      if (q==average_index-1)           /*if this was last read*/
         FIFO[sample] /= average_index; /*divide by index*/
      }
   }
}
                  /*********************************/
```

```
int get_peaks(void)
                /**********************************
                * Old routine for detecting      *
                * peaks, uses test for up-slope *
                * on left, and down- on right   *
                **********************************/
{
int sample,n=0;

for (sample=100;sample<=300;sample++)
   {
   if (  FIFO[sample-1] <= FIFO[sample-2]
      || FIFO[sample+1] <= FIFO[sample+2]
      || FIFO[sample]   <= FIFO[sample-1]
      || FIFO[sample]   <  FIFO[sample+1]
      )
   continue;                  /* drop out if not a peak*/
   else
      PEAK[n++]=sample;       /* or store time coordinate of peak*/
   }
return n;
   }
                /**********************************/
void set_ports(void)
   {
   outportb(control_port,control_word);
                              /*initialises the 8255 for ports*/
                              /*a and b output and port c input*/
   outportb(port_b,default_word); /*sets 10MHz clock and set,reset */
                              /* and read high*/
   }
                /**********************************/
```

```
int get_depth(int n)
  {  int  most=0,best=0,tvalues=0,sum=0 ;
     int look, p, q;
     float bestave;

if (n<2)
     return -1;                  /*not enough peaks to calculate*/
                                 /*drop out of routine here*/
for (q=0;q<n;q++)
  SEP[q]=PEAK[q+1]-PEAK[q]; /*measure the sample space between*/
                                 /*successive peaks*/
for (q=0;q<=(n-2);q++)       /*compare all separations with each*/
  {                              /*other... if the difference is one*/
  for (look=0;look<=(n-2);look++)  /*sample count or less....*/
    if (abs(SEP[look]-SEP[q])<=1)
    WEIGHT[q][look]=TRUE;  /*set boolean array element TRUE*/
    else
    WEIGHT[q][look]=FALSE ;    /*otherwise set to FALSE*/
  }
for (p=0;p<=(n-2);p++)
  {
  for (q=0;q<=(n-2);q++)
    {
    tvalues += WEIGHT[p][q];      /*now we sum the booleans*/
    }                            /* along a separation row*/
  if (tvalues<most)                /* if this is not the most*/
                                 /* common separation, we */
    tvalues=0;                     /* reset 'true values' sum*/
  else                         /* if this is the most common*/
    most=tvalues;                /* separation, replace most with*/
  best=p;                       /*new value, store row value and*/
  tvalues=0;                     /* then reset 'true values'*/
  }
for (q=0;q<=(n-2);q++)         /* lastly we go through the best*/
  {                            /* row again, to make the average*/
  if (WEIGHT[best][q])         /* of the sample space in the most*/
     sum +=SEP[q];             /* common peak separation */
  }
bestave=sum/most;              /* average out the sample space   */
depth=(bestave*speed/20000); /* convert to millimetres (return */
return depth;                  /* trip) and send back the answer */
}
                /*********************************/
```

```
void draw_block(void)
   {
   setfillstyle(SOLID_FILL,depth);
   bar((16*x),(14*y),(16*(x+0.8)),(14*(y+0.8)) );/*draw the block*/
   itoa(depth,cdepth,10);      /*make a string to print the depth*/
   setfillstyle(EMPTY_FILL,WHITE); /*clear an area*/
   bar(340,250,380,300);
   outtextxy(350,300,cdepth);  /*and print the depth*/
   }
                  /*********************************/

void draw_array(void)
   {
   int left=51,top=251,right=249,bottom=299,clip=1;
   int sample,x,n=0;

   setviewport(left,top,right,bottom,clip);
   clearviewport();
   setcolor(YELLOW);

   for (sample=0;sample<300;sample++)
   {
   x=sample-100;
   lineto(x,(50-FIFO[sample]));
   if (sample == PEAK[n])
      {
      n+=1;
      setcolor(GREEN);
      line(x,(50-FIFO[sample]),x,(45-FIFO[sample]));
      setcolor(YELLOW);
      }
   }
setviewport(0,0,639,349,clip);
setcolor(WHITE);
}
                  /*********************************/
```

```
int least_squares(void)
  {  int x,sample=0;
     int n=0;                    /*no of peaks found, will be returned*/
     float temp;
     float a,b,c;
     int ysum,xysum,xxysum;
for (sample=100;sample<400;sample++)   /*run through the array */
  {
  ysum=xysum=xxysum=0;                  /*reset running sums    */
  for (x=-3;x<=3;x++)                  /*going from sample-3   */
    {                                  /*to sample+3           */
    ysum+= FIFO[sample+x];             /*make up running sums  */
    xysum+=x*(FIFO[sample+x]);         /* sum(y), sum (x*y) and*/
   xxysum+=x*x*(FIFO[sample+x]);       /* sum (x^2*y)           */
    }
  a=(xxysum-4*ysum)/86.0;    /*these factors arise from solving*/
  b=(xysum)/28.0 ;           /*simultaneous equations for      */
  c=(99*ysum-14*xxysum)/301.0;/*coefficients in ax^2+bx+c      */
     /******now we test for a maximum point******
     *      in ax^2 +bx+c this occurs when      *
     *      b/2a = 0.  we make the condition    *
     *      looser than that, because of the    *
     *      digitised nature of the signal      *
     ****************************************/
if ( a != 0  /* need this to avoid overflow in next statement*/
  &&n<20  /*and make sure we don't overflow the array PEAK[]*/
  )
  {
  temp = b/(2 * a);                    /* casts as int !?!!*/
  if ( (-0.5<temp<0.5)          /* within 1 sample of a peak?*/
       && a<0                  /* sure it is a maximum?*/
       && c>5                  /*is it above the noise level?*/
       && sample-PEAK[n-1]>2 /* and check not too close to*/
    )                          /*previous peak*/
                              /*if all this is satisfied then we*/
       PEAK[n++]=sample;   /*assign sample count to next peak*/
     }
  }
return n;
}
                  /*******************************/
```

APPENDIX 6:

COMPARISON OF PROPERTIES OF PZT-5H AND PVdF

	PZT-5H	PVdF
QUALITATIVE PROPERTIES	BRITTLE	FLEXIBLE
	STRONG RESONANCE	WIDE-BAND
	SMALL ELEMENTS	LARGE SHEETS
Density (ρ) kg/m^3	7500	1780
Speed of Sound (V_c) $mm/\mu S$	4.0	2.2
Stress Constant (d_{33}) $x10^{-12}$ m/Volt	593	33
Coupling Constant (k_{33})	0.75	0.29
Dielectric Permittivity (ε_r)	1200	12
Curie Temperature (T_c) °C	195	~85

(1) Data Supplied by Morgan Matroc (Vernitron) Ltd.

(2) Data Supplied By Atochem Sensors Ltd.